New Directions in Screen Printing and Related Fabrication Processes

A thesis submitted in partial fulfilment of the requirements of the Manchester Metropolitan University for the degree of Doctor of Philosophy

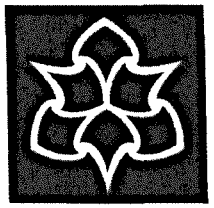

Manchester Metropolitan University

Nadeem Azram Choudhry

School of Science and the Environment
Division of Chemistry and Environmental Science
The Manchester Metropolitan University
John Dalton Building
Chester Street
Manchester M1 5GD, UK

2013

Twenty years from now you will be more disappointed by the things that you didn't do than by the ones you did do. So throw off the bowlines. Sail away from the safe harbor. Catch the trade winds in your sails. Explore. Dream. Discover.

- Mark Twain

Acknowledgements

First and foremost I would like to sincerely thank Dr Craig Banks for giving me the opportunity of a lifetime to work with him and on this pioneering research area. For his vision, direction and support throughout as a supervisor and as a friend made me get the most out of this adventure. It has been a true honour to have worked alongside one of the most dedicated and driven individuals I have come ever across in my academic life.

I would like to thank the guys in MMU, from lecturers to technical staff. I would like to thank Chris Rego, Dave Johnson, Aidan Doyle, Herman Potgieger, Megan Mclean, Lindsey Munro and Norman Allen for their moral support and "my door is always open" approach. The technical staff, in particular, Bill Ellison ("the Repair Man"), the guy who can fix anything, for always helping out with machines and equipment. Allen Blyth, Steve Wallwork, Norman Bridge, Norman Jenkinson, Jean and Dianne Holdsworth for always providing an excellent service in the labs.

I would also like the thank all the fellow colleagues, Maclom Kinnonmoth, Andy Jones, Don Carren, Ka Lun To, Karmele Teso, Itzia, Izaskun, Lucia, Fernando, Lik, Kinnan, Jay and Noredine for putting up with all the banter especially about 'Bury World Famous Market' talk (which is true by the way ha ha).

I should also mention 'The Banks Group', Sergant Dr Dimitrious Kampouris the greatest mentor, friend and brother one can ask for, I feel very privileged and honoured to have met Dimitrious, and I would like to take this opportunity to say Thank you for all his help, there are not enough words to express how deeply grateful I am to him. Also like to mention Dr Rashid Kadara, for his support and small talk conversations, Carlos Llorente for being the coolest Spaniard I have ever met and tolerating me when I laughed at his bad driving. Not to mention my fellow PhD collegues, Phill Hallam for his lady hunting tips, Dale Brownson for getting me into the joy of cycling and squash, Johnny 'BB' Metters for his daily updates on the train services and getting the sympathy vote for supporting Blackburn Rovers, Amit Patel for his cool dude approach to life, Yassin Mohammed for his funky scouse accent and his 'turning fringe players into superstars approach', Meerna El-Sayed for bringing young blood and freshness to the group, Said Hussein for his deep talks on life and politics, especially in the middle east.

Above all I would like to thank my beautiful family, for always encouraging and supporting me in my studies. Especially my dear mother, sisters and brother who have been very patient with me over the last few years and I'm very blessed to be surrounded by their love - none of this would have been possible without their blessings and wisdom.

I dedicate this thesis to my beloved and wonderful father, Mohammad Azram Choudhry (late) and to my son Sufiyan Choudhry.

Abstract

This thesis reports the development of screen printed electrodes and associated fabrication processes in order to develop and understand new electrochemical based sensors. There are three main sections to this thesis. In the first part, an overview of sensors, in particular electrochemical sensors, that are commercially available and their current problems and limitations with conventional electrodes and electrode materials is discussed. Second, an introduction into screen printing and their advantages are given. The full process by which these next generation electrodes are manufactured is thoroughly described followed by examples of screen printed-electrodes and their powerful application as well as their low detection limits which compare well to existing literature on the market.

The first example of a copper (II) oxide screen-printed electrode is reported, which is characterised with microscopy and its efficiency for the electrochemical sensing of glucose, maltose, sucrose and fructose is explored. It is shown that the non-enzymatic electrochemical sensing of glucose with cyclic voltammetry and amperometry is possible with low micro-molar up to milli-molar glucose readily detectable, which compares competitively with nano-catalyst modified electrodes. An additional benefit of this approach is that metal oxides with known oxidation states can be incorporated into the screen-printed electrodes allowing one to identify exactly the origin of the observed electro-catalytic response which is difficult when utilising metal oxide modified electrodes formed via electro-deposition techniques which result in a mixture of metal oxides/oxidation states. These next generation screen printed electrochemical sensing platforms provide a simplification offering a novel fabrication route for the mass production of electro-catalytic sensors for Analytical and Forensic applications. Other examples such as, bespoke screen printed electrodes which can be used as a template to produce randomly dispersed electro-catalytic micro-domains for analytical sensing purposes, are also shown to further demonstrate the applications and utility of screen printed electrodes.

The final section focuses on electrode design. It is demonstrated that the electron transfer properties of disposable screen-printed electrodes can be readily tailored via the introduction of a polymeric formulation into the ink used in their fabrication. This approach allows the role of the binder on the underpinning electrochemical properties to be explored and quantified for the first time, allowing the electrochemical reactivity of the screen-printed electrodes to be tailored from that of edge plane-like to basal plane-like reactivity of highly ordered pyrolytic graphite.

Building on this fundamental study of the origin of electron transfer at these novel electrodes, the first example of *"Cosmetic Electrochemistry"* is demonstrated where a commercially available cosmetic product, a deodorant, can be used to confer microelectrode behaviour on a macroelectrode. Proof-of-concept is shown that a graphite screen-printed electrode can be sprayed with an off-the-shelf cosmetic product and within seconds is ready to use. The polymer contained within the cosmetic product partially blocks the graphite screen-printed electrode surface leaving the underlying graphite electrode exposed in the form of graphite micron-sized sites which are randomly distributed across the electrode surface. The creation of microdomain sites enhance mass transport of the target analyte and it is shown that the electroanalytical performance of the cosmetically modified electrode, via the cathodic stripping of lead, could achieve a similar performance to current state-of-the-art methodologies. Further examples are also reported with the introduction of *plaster-trodes* where a commercially available plaster is electrolytically modified with electrocatalytic material and is used to detect various alcohols.

Table of Contents

Chapter 1: Introduction

1.1 Sensors

A sensor is a device which receives and responds to a signal. Sensors measure real-world conditions such as heat or light and converts this into a digital representation.[1,2]

Humans perceive senses through smell, taste, touch and hearing. There are many products one comes across on a daily basis such as cars, mobile phones and computers which contain sensors. Most common sensors like the temperature sensor, as well as pressure and light sensors are used significantly throughout the world. For example, when a person stands in front of an automatic door, the sensor detects an object and sends a signal and the door is opened. Similarly, the modern gaming machines offer wireless controllers in which sensors are used to track the motion movement of the person holding the controller and replicates this behaviour in the game mode without any buttons being pressed. More and more very cleverly designed products use a range of sensors in order to know what actions one wants to perform.

Sensors play an increasingly important role in our lives. They offer many benefits such as saving time, performing tasks consecutively without compromising on the quality and hence reduce human error. There are many types of sensors which can be categorised as:

- biosensors
- optical sensors
- pressure sensors, and
- chemical

1.2 Electrochemical Sensors

In this thesis, the focus is upon chemical sensors, in particular electrochemical sensors. Electrochemical sensors are considered to be amongst the largest group of chemical sensors.[3] Electrochemical sensors are devices which extract information about a sample from measurement of some electrical parameters. These sensors can be sub-categorised according to the measured electrical parameter, which can be explained by Ohm's law. Ohm's law states that the potential difference in a circuit is equal to the product of the current and the resistance. So let's consider an example, if a measurement of two potentials is taken (in volts), we are talking about potentiometric sensors and if the parameters of interest is current, we are talking about amperometric sensors.

Electrochemical sensors are electroanalytical devices that owe their popularity and success to the discipline of electrochemistry, which provides the strong scientific base on which they stand. Their purpose is to provide information about the chemical environment in which they are placed and the growing need for reliable sources of information guarantees their future. There is a strong engineering aspect of any sensor research and electrochemical sensors are no exception. The current trend in miniaturization of electronics and the rapid increase of the dedicated computational capacity leads to development of various electrochemical sensing arrays in which the information is obtained simultaneously through multiple sensing channels.

The journey of electrochemical sensors dates back to the 1930s. Prior to the release of these sensors, the majority of analysis was carried out on industrial machines. Miniaturised sensors became available on the market in the mid 1980s most notably the oxygen monitor.[5] Many important biomedical enzymatic sensors, including glucose sensors,

incorporate an enzymatic catalyst and an electrochemical sensing element. The Clark type of oxygen sensor is a well-known practical biomedical sensor based on electrochemical principles; an amperometric device.[5]

Sensors are an excellent choice for analysis as they are portable, reliable and exhibit good sensitivity and selectivity.[5, 6] Electrochemical sensors have been used extensively either as a whole or an integral part of a chemical and biomedical sensing element. For instance, blood gas (O_2, CO_2, and pH) sensing can be accomplished entirely by electrochemical means. Electrochemical sensors are essentially an electrochemical cell which employs either two or three-electrode arrangements. Electrochemical sensor measurement can be made at steady-state or under transient conditions. The applied current or potential for electrochemical sensors may vary according to the mode of operation, and the selection of the mode is often intended to enhance the sensitivity and selectivity of a particular sensor.[6]

Electrochemical sensors role has evolved in many applications. The police heavily relied on lab only analysis for the detection of alcohol content in a suspect's body.[7] A sample would be taken from the suspect and sent to a lab or police station to carry out the analysis, typically using a gas chromatography technique.[7] This was a time consuming and inconvienent exercise of conducting a test but also expensive as payment had to be made to third party for carrying out the analysis, who most likely was an expert analysis technician. Since then, enormous advances in breath-testing sensors have been made. These portable sensors are more or less completely automatic and are designed to be virtually operator proof to eliminate human error. Electrochemical breathalyzers are devices in which an electrical current is produced as a result of a chemical reaction taking place on the surface

of an electrode system.[8] The small electrical current produced by the alcohol in a person's breath reacting on the electrode within the machine can be used to give a digital display, move a needle or trigger certain lights on the device, depending on the amount of alcohol detected.

Fuel cell technology is particularly suitable for portable screening devices, due to the small size of the cells and the low power requirements of the technology.[9]

There are many benefits of the modern portable breathalyser in comparison to the conventional method of analysis. Such benefits include,

- cheap relatively to lab analysis,
- versatile, and
- on-site analysis

Other portable sensors which have evolved in recent years include; [10, 11, 12]

- glucose sensors,
- drug analysers,
- carbon monoxide sensors,
- gas sensors, and
- smoke detectors

1.3 Electrode Materials

The main drive for an electrochemist is to improve the electroanalytical response of a sensor towards the sensing of an analyte. For this to be feasible, we must turn our interests to electrode materials. As electrochemistry is concerned with the charge transfer between a solid (the electrode) and a molecule, which is usually in solution, the properties of the electrode itself may be important, particularly in the case of carbon surfaces, which is especially relevant in view of their widespread applications as electrode materials. Graphitic forms of carbon are plentiful, non-toxic and highly conductive, and have thus found uses as disposable electrode materials in electrochemical glucose sensing, or as continually-used substrates in energy storage and generation (*e.g.* lithium ion batteries, super-capacitors and fuel cells). In each of these roles, the interfacial properties, and particularly the charge transfer kinetics, of the carbon are essential. Such commercial electrochemical applications of carbon have traditionally used "screen-printed" or "activated" carbons, formed from micron-scale amorphous or graphitic particles, often mixed with a polymeric binder.[13] Particular attention will be directed into the electrode materials which have conventionally been employed and new electrode materials which are developing in the field of electrochemistry.

Historically, the electrode materials electrochemist's employed were, mercury (the hanging mercury drop electrode (HMDE) which famously won a Nobel Prize),[14] Noble metals such as gold and platinum, and more recently carbon-based electrodes such as, glassy carbon electrode (GCE), boron doped diamond electrode (BDDE) and carbon nanotubes. More recently we have had carbon nanotubes being widely used as electrode material.[15] Hence, we can say the fundamental element for the effective development of an electrochemical

sensor is the working electrode. As the electrochemical processes take place at the working electrode surface, it is essential we choose the optimum electrode materials to enhance the electrocatalytic behaviour of the sensor towards detecting electroactive species. The evolution of the electrode materials has brought us to this point of refinement where electrodes are designed for specific analyte sensing.

Next, it is relevant to provide a discussion into the various forms of carbon. Carbon-based electrodes are nearly ubiquitous in the laboratory today because of their availability in various forms, shapes and usefulness over a wide potential range. There are various compositions of carbon ranging from highly ordered pyrolytic graphite to less ordered glassy carbon to boron doped diamond through to carbon-paste to exquisitely small carbon nanotubes.

Carbon is considered to be a popular choice as an electrode material mainly due to it being cheap, readily available, easily modifiable and chemically inert properties.[16,17] The properties of carbon such as high flexibility, high tensile strength, low weight, high temperature and low thermal expansion makes it a very popular material to utilise amongst the electrochemists. Carbon exists in many forms, most famously as a diamond which is considered to be the strongest material.

In this thesis, there were many forms of carbon which were utilised, most notably the BDDE, the GCE (glassy carbon electrode) and pyrolytic graphite.

Boron Doped Diamond Electrode (BDDE)

The boron doped diamond electrode dates back to one of electrochemistry's early fortunes and has played a key role in building strong foundations within the electrochemistry

world.[16] The BDDE has become a basic necessity in an electrochemist's laboratory. The BDDE is a very hard, versatile and robust material and therefore is widely adopted as an electrode surface.[17] The significant advantage of BDDE lies with its wide potential window which can be applied on the electrode for the particular analysis under consideration. Other benefits include low background currents and corrosion stability in aggressive media.[17,18] Figure 1 below shows the design of BDDE.

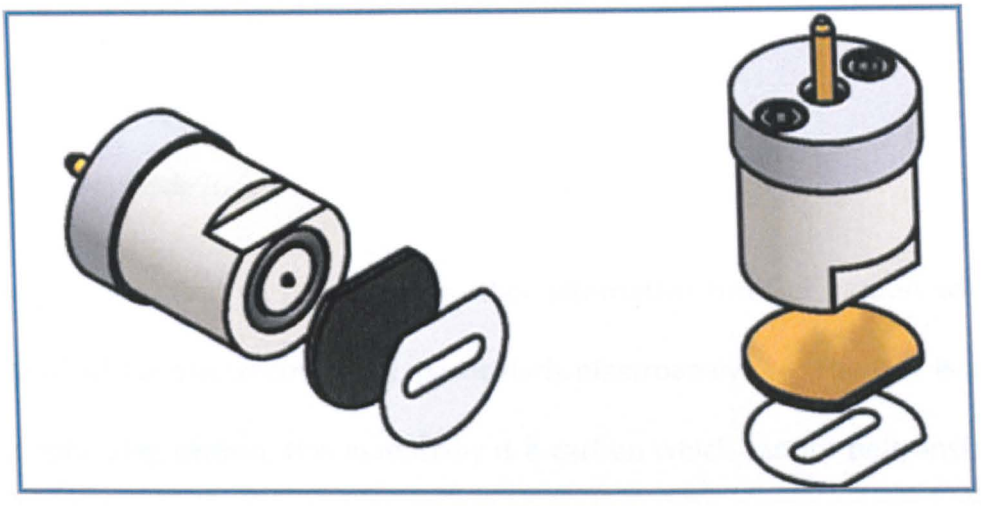

Figure 1. Represents the thin film design of the BDDE.[21]

Typically, the boron-doping levels can be in the range of 500 – 10,000 ppm.[19] Boron doping can lead to a p-type semiconductor.[19] The fascinating properties of diamond and why it is truly the hardest naturally occurring material and highest atom-number density of any material however, diamond exhibits an sp^3 orbital structure which makes it inert and therefore is unsuitable to utilise as a working electrode. Boron is by far the most widely used dopant to produce diamond conducting electrodes.[19] The reason for this is due to boron acquiring low charge carrier activation energy.[20] Together the boron-doped diamond structure gives the following electron configureuration: $1s^2$ and four $2sp^3$ (hybrid orbitals). This electron configureuration results in the formation of four strong-covalent bonds with

four other carbon atoms (each sharing a pair of electrons). Furthermore, a regular tetrahedron configureuration is achieved.

Since the BDDE is a high purity and high performance material, a common technique used for producing it is known as the method of chemical vapour deposition (CVD). Typically, the CVD process involves the substrate being exposed to a volatile precursor, which reacts and decomposes on the substrate surface to produce the desired deposit (in this case boron). It is common to be left with volatile by-products, however these can be removed by gas flow through the reaction chamber.

Glassy Carbon Electrode (GCE)

Next, attention is turned to consider a further alternative form of carbon which is also widely utilised within electrochemistry, particularly electroanalysis.[22] The GCE is an example of a non-graphitizing carbon, this essentially is a carbon which cannot be transformed into crystalline graphite even at temperature in excess of 3000 °C.[23] Its notably distinguished properties such as extreme resistance to chemical attack makes it a suitable material for chemists to utilise.[24] Furthermore, it has been demonstrated that the rates of oxidation of glassy carbon in oxygen, carbon dioxide or water vapour are lower than those of any other carbon.[25] As we are well aware, normal graphite can be reduced to a powder by a mixture of sulphuric acid and nitric acids at room temperatures, GC is however unaffected by such treatment, thus making it highly resistant to attack by acids. This particular property makes the GC a useful electrode material that can be used widely in the field of electrochemistry. The structure of GC bears some resemblance to that of a polymer, in which the 'fibrils' are very narrow, curved and twisted ribbons of graphite carbon.[21]

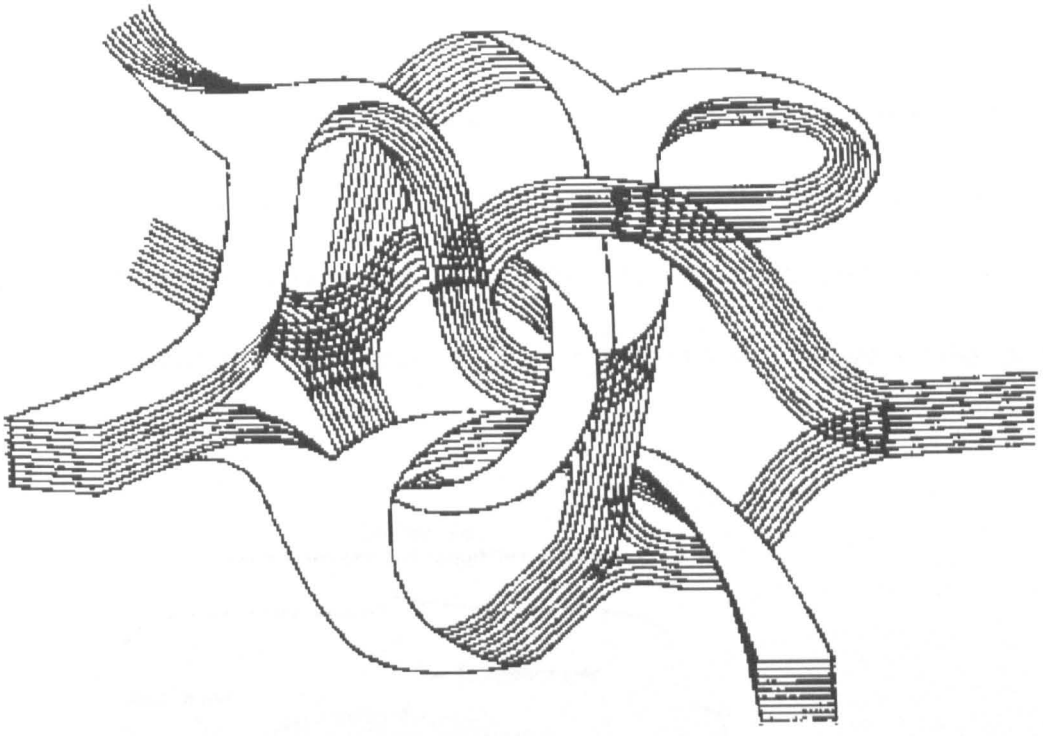

Figure 2. Represents the structure of the GCE.[21]

GC is produced by pyrolyzing a carbon polymer, under carefully controlled conditions, to a high temperature like 2000 °C.[23] An intertwining ribbon-like material results with retention of high conductivity, hardness and inertness. Figure 2 shows a typical GCE structure. The electrochemistry is affected greatly by its surface chemistry of carbon-oxygen functionalities and its cleanliness, *i.e.* absence of adsorbed impurities.

Pyrolytic Graphite

Edge-plane pyrolytic graphite (EPPG) is one kind of pyrolytic graphite. The pyrolytic graphite material can be cut and modified on the electrode by facing its surface from either the basal-plane (BPPG) or its edge-plane (EPPG). The BPPG electrode contains graphite layers parallel to the working surface. Figure 3 shows the comparison between edge plane basal plane.

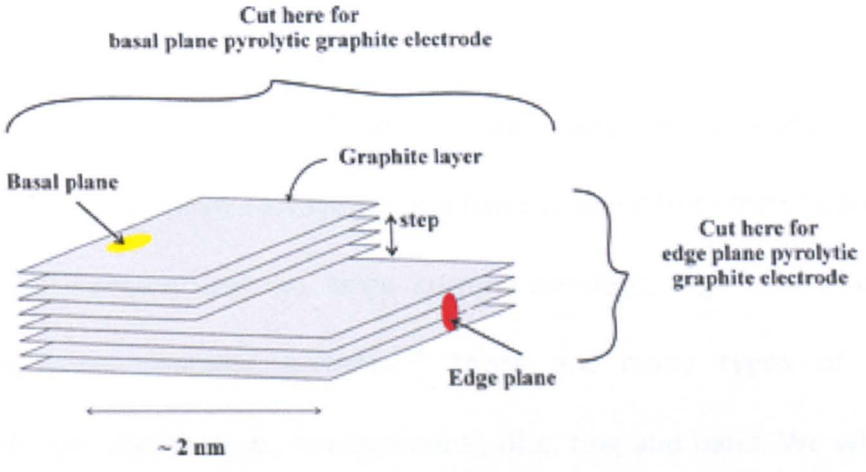

Figure 3. Represents the different orientations between edge plane and basal plane.[59]

Edge-plane pyrolytic graphite (EPPG) electrodes are more advantageous in comparison to basal plane pyrolytic graphite (BPPG) electrodes due to its enhanced electrocatalytic properties, as the highly reactive edge plane 'defects' of the EPPG electrode allows low detection limits, high sensitivities, improved signal to noise characteristics and low potentials.[60, 61, 62] The BPPG electrode is the same material as the EPPG electrode, however the different orientation of the EPPG gives it a distinct advantage over the BPPG electrode. Figure 3 shows the difference in orientation between the EPPG and BPPG electrode.[59] The basal plane site is smaller and the interlayer spacing is greater compared to the EPPG form. A BPPG electrode is typically used on a compound that increase the electrocatalytic

response of the working electrode surface. The compound is deposited on the BPPG and the electrochemical sensing of the analyte is tested. Once the response of the modified BPPG is greater compared to the bare BPPG, this indicates that the compound is increasing the electrocatalytic behaviour of the working electrode surface (thus the BPPG has slow electrocatalytic behaviour).

Microelectrodes

Microelectrodes or multi-microelectrodes arrays play an important role to an electrochemist. Microelectrodes arrays are at a fixed distance from their nearest neighbour. They offer many benefits such as, large current densities, high spacial resolution and reduced capacitative charging currents.[26] There are many types of geometries a microelectrode can offer such as, hemispherical, disc, ring and band. We will focus on the disc since this is the most widely used microelectrode for this project. Micro-disc electrodes offer a smaller surface area. Therefore, the current is small (in the pico or nano amps range). In comparison to microelectrodes, macroelectrodes are also widely used as they offer a linear diffusion profile. The surface area of macroelectrodes are much larger hence giving larger current densities (micro amps range). Macroelectrodes are cheaper to manufacture however they are not as powerful as microelectrodes which instead offer the small size that allows them to be inserted in places where other electrodes are not easily accessed.[27] Another benefit is the low total current, microelectrodes pass tiny amounts of current therefore, induce small amounts of electrolysis.[28] Microelectrode diffusion layers are very thin (micrometres), thus the concentration gradients across the diffusion layer will be high. As a result of this, the rate of mass transport to microelectrodes is much higher than for

macroelectrodes. Furthermore, microelectrodes offer high current density, which in effect leads to a good signal resolution and hence low detection limits are achieved.[27] Microelectrodes are employed in many areas of electrochemistry, some of the applications are listed below:

- analytical sensing,
- trace electrochemical analysis,
- electrochemical reaction mechanism and kinetics,
- electrochemical reactions in solutions of high resistance,
- detection in flowing liquids,
- scanning electrochemical microscopy (SECM),
- cell-based biosensors, drug discovery and safety pharmacology, and
- in-vivo electrochemistry

Typically microelectrodes are fabricated by:[27, 28]

- employing lithography,
- sealing thousands of microelectrodes in epoxy resin,
- injection of liquid conductors into porous insulators,
- attaching polymeric membrane onto the electrode surface, and
- ion beam milling

Microelectrode behaviour is represented by a sigmoidal shaped voltammogram, in comparison to a macroelectrode which represents a quasi-reversible numerical simulations were presented by Guo and Linder[29] who showed the responses obtained from different microelectrode arrays. The simulations represent many different scenarios which can be

achieved depending on the experimental parameters.[29] For example, if hemispherical diffusion is evident on each microelectrode and the diffusion profiles are completely independent (not overlapping) then the resulting behaviour can be expected to achieve a sigmoidal shaped response, thus microelectrode behaviour. In reality, this behaviour is difficult to reproduce however we can expect a similar response. Figure 4 shows the comparison of diffusion layers of microelectrode verses macroelectrode. This concept is further discussed later in this thesis, chapter 6.

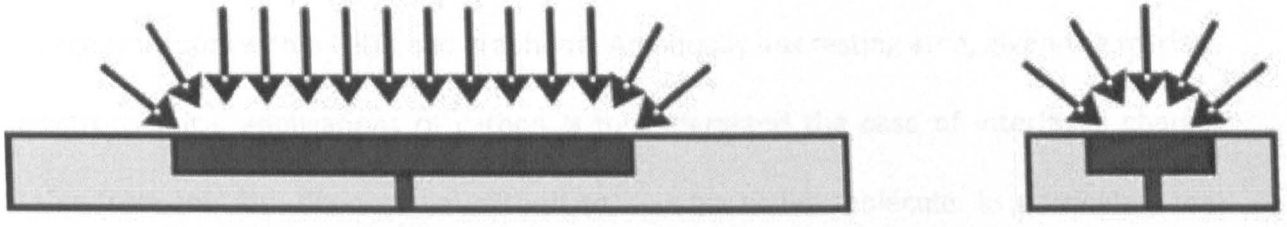

Figure 4. Represents the diffusion layers of (linear) microelectrode (right) and (hemispherical) macroelectrode (left).

Carbon Nanotubes (CNTs) and Graphene

Carbon nanotubes (CNTs) consist of rolled up 1-dimensional sheets of carbon atoms.

Recently 2-dimensional carbon in the form of single graphite sheets, known as graphene, has been isolated. [76, 77, 78, 79] These analogues of graphite have attracted much interest because of their unique electronic properties, not least the exceptionally high carrier mobility, and atomically well-defined structure. Figure 5 shows a typical CNT structure.

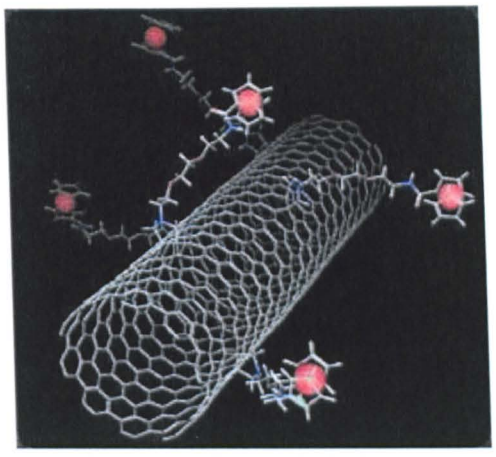

Figure 5. Represents a typical CNT structure.[30]

These properties have stimulated enormous interest in theoretical and experimental studies of charge transport within CNTs and graphene. An equally interesting area, given the myriad of electrochemical applications of carbon is to understand the case of interfacial charge transfer from the low dimensional carbon to a redox-active molecule. In particular, the structure of mono- and bi-layer graphene provides an ideal model system with which fundamental questions about charge transfer to/from carbon's can be answered.

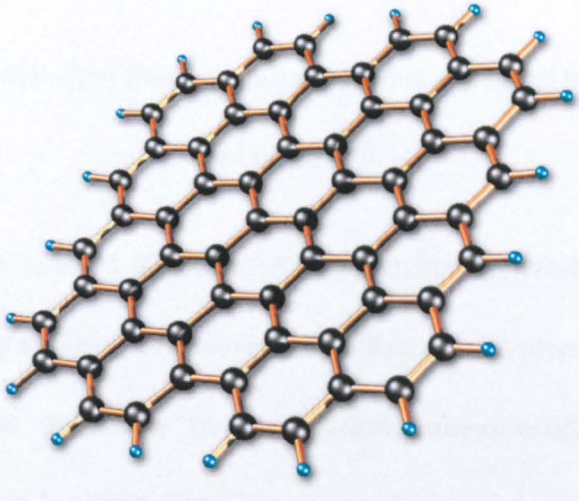

Figure 6. Represents the structure of graphene.[31]

The recent discovery of graphene has triggered enormous interest both in fundamental and applied science communities. So far, the studies have focused on the physical properties of graphene, in particular its electronic transport behaviour under applied electric and magnetic fields. Figure 6 and 7 show structure and ultra thin properties of graphene.

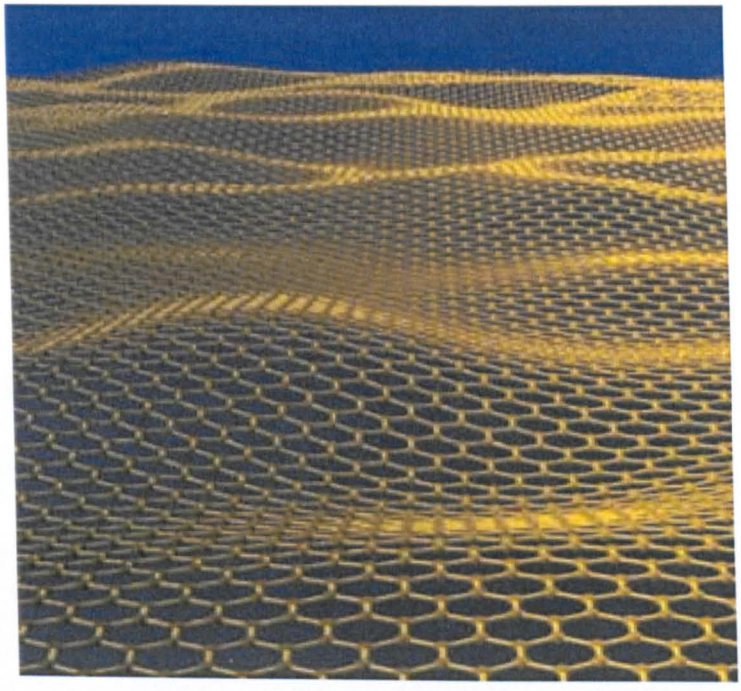

Figure 7. Represents the ultra thin graphene which is expected to develop super fast electronics.[32]

Transistors and chemical sensors of extraordinary sensitivity, which demonstrate the high application potential of graphene.[35] However, in contrast to its physical characterization, the chemical modification of graphene remains largely unexplored, despite the intriguing properties anticipated for functionalized graphene. Specifically, chemical functionalization of the edges of graphene is predicted to enable tailoring its electronic properties.[33]

Graphene has most recently become one of the 'hottest' topics in materials science. This breakthrough was due to the pioneering work by Professor Konstantin Novoselov and Professor Andre Geim, who won a Nobel prize for their outstanding research on the world's thinnest material. Novoselov's development involved using a simple piece of adhesive tape to obtain a flake of graphene one atom thick from a piece of ordinary graphite, such as that used in pencils.[33, 34] Furthermore, the Nobel prize winners demonstrated that such sheets of graphene were stable, despite predictions to the contrary.[35] In the current climate, where technology is the engine of the economy, and science is the petrol to keep this engine running, graphene is considered to be the most important scientific advancements in recent times.

Graphene electrochemistry is continually being developed in the Banks' Group and further discoveries are expected to be reported in the foreseeable future.

Nanoparticles

In recent years nanoparticles have been extensively developed and used for the effective modification of an electrode surface, thus improving the electrocatalytic response of the working electrode.[36] Typically, metal nanoparticles will have dimensions less than 100 nanometres. The increase in large surface area to volume ratio, which is a gradual progression as the particle gets smaller, leads to an increasing dominance of the behaviour of atoms on the surface of a particle over that of those in the interior of the particle. This affects both the properties of the particle in isolation and its interaction with other materials.[36] Its surface area is a critical factor in the performance of catalysis and structures

such as electrodes, allowing improvements in performance of such technologies as fuel cells[37] and batteries.[38] The large surface area of nanoparticles also results in a lot of interactions between the intermixed materials and in nanocomposites, leading to special properties such as increased strength and increased heat resistance. Furthermore, the fact that nanoparticles have dimensions below the critical wavelength of light renders them transparent, a property which makes them very useful for applications in packaging, cosmetics and coatings.[39]

1.4 Drawbacks in the current market

The development of powerful portable sensors have significantly improved the quality of life as they are convenient and easy to operate yet highly sensitive and offer instant on the spot results. However, all the sensors mentioned above such as the oxygen, glucose and breath testing sensors are generally expensive to produce. Although relatively reproducible, these sensors can be compromised by many parameters resulting to inaccurate analysis. Conditions such as changes in sensitivity, which may be due to changes in temperature or humidity, brings doubt on the reproducibility.

Obviously these devices cannot be used by law enforcement agencies. Although they can produce reliable results in the right conditions depending on the quality of the device in question. The mass production of very poor quality novelty devices use this technology.

Another drawback to these conventional electrodes is the cleaning aspect, many electrodes such as the BDDE, GCE and gold electrodes require extensive cleaning using a pad

containing alumia before, during and after analysis. Furthermore, such electrodes are highly expensive in comparison to the 'next generation' of electrodes which are mentioned below.

Electrochemists strive on the prospect of being able to find ways to improve the electro-analytical performance of electrochemical sensors. One such way is utilising the technique of screen-printed electrodes, which will evaluated in the following chapter.

Chapter 2:

Screen-Printed Sensors

2.0 Screen-Printed Sensors

One prominent commercialisation of a screen-printed sensor was the glucose biosensor used by those suffering with diabetes,[40] which is a billion dollar per annum global market. Society is in a constant state of growth and development and it is inevitable that demands for sensing devices related to clinical and industrial applications will increase; this is particularly true in the former case within the UK where the recent budget cuts in the NHS[41] are pushing the onus onto individual self-monitoring. In order to achieve this, inexpensive and disposable, yet highly accurate and rapid, devices are greatly sought. Additionally the portability of such devices is of fundamental importance. Decentralised sensing is ever more necessary and thus traditional techniques utilising highly expensive, immovable analytical equipment such as gas chromatography-mass spectrometers are not feasible for sensing outside the realms of standard laboratories. Examples of cases where portable, economical and sensitive sensors are highly desirable include: utilisation in hospitals where there is a suspected drug over-dose,[42] the personal monitoring of diseases such as diabetes,[43] the detection of potential pollutants or toxins within environmental samples such as river water,[44] the screening of drinking water at different sources,[45] and also the rapid determination of naturally occurring biomolecules.[46] Screen-printed sensors not only address the issue of cost effectiveness but they also satisfy the previously much sought after criterion of highly reproducible and sensitive methods of detection towards target analytes, whilst maintaining the low cost production through scales of economy. The adaptability of screen-printed sensors is also of great benefit in areas of research, which will be discussed in this chapter of this thesis.

2.1 Screen Printing

Screen printing has been used for thousands of years to generate designs. The development of screen printing can be traced from two separate sources, the oldest is concerned with stencil making while the more recent involves ink and fabric technology.[47,48] The earliest evidence of screen printing was witnessed in the middle ages when tar was painted onto stretched plain cloth and allowed to dry, forming a negative stencil.[47] Paint was then forced with a stiff brush through the area free from tar on to the banners or uniforms.[47]

It was in the mid-nineteenth century when the second and more orthodox historical development began in screen printing.[49] The ability to attach stencils to a fixed mesh meant that fancy designs could now be registered and painted with a brush.[49] Shortly after this, the squeegee was invented, enabling a more consistent deposit of ink to be printed than had been with the brush.[49] Nowadays screen printing is considered to be the simplest forms of print making available. It involves the use of a stencil applied to a fabric mesh stretched over a rigid frame. Ink poured into the frame is forced with a squeegee through the open areas of the stencil. This produces an image when the underside of the screen comes in contact with the substrate.

2.2 Screen-Printed Electrodes

Screen-printed electrodes are a next generation of electrodes offering wide applications in the field of electrochemistry, in particular electroanalysis. Electrochemists turned to screen-printed electrodes as cheaper alternative to conventional electrodes which are highly expensive and require extensive cleaning. Screen-printing technology is a well-established technique for the fabrication of both chemical and biosensors. The adaptability of screen-

printed electrodes is also of great benefit in areas of research. The ability to modify the electrodes with ease, through differing inks commercially available for the reference, counter, and working electrodes, allows for highly specific and finely calibrated electrodes to be produced for specific target analytes.

The uniqueness of these screen-printed electrodes is containing a reference and a counter electrode as well as the working electrode. This simply makes this the complete sensor, which can be printed in a single sheet, therefore reducing the cost of the working electrode materials as well as the costs for the reference and counter. The ink used to produce screen-printed electrodes is carbon based, which is relatively cheap and therefore the overall cost of a complete screen-printed electrode is inexpensive. Figure 8 depicts a typical commercial screen-printed electrode.

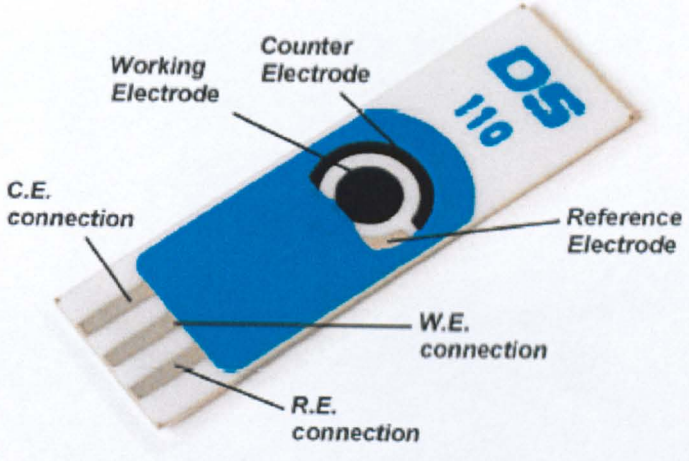

Figure 8. Represents a typical commercial Screen-Printed Electrode.[50,51]

Screen-printed electrodes can be manufactured in-house using a screen printing machine (DEK 248) and the process involves using a stencil to print the desired shape and design of

the electrode. To produce screen-printed electrodes, a printing technique which uses a woven mesh to support an ink blocking stencil. The stencil forms open areas of mesh that transfers ink onto the substrate. The screen is made of a porous, finely woven fabric called a mesh which is stretched over a steel frame. The mesh can be made up of polymer fibre, stainless steel or nylon. Areas of the screen are blocked off with a non-permeable material to form a stencil, which is negative of the image to be printed. Next, the ink is placed on the mesh and is spread across the screen using a squeegee, this forces the ink to pass through the holes of the mesh, leaving an image to be deposited on the substrate. The final step involves the substrate to be removed and placed in an oven to be dried and this will bind the ink to the substrate. Figure 9 shows an example of the above principle.

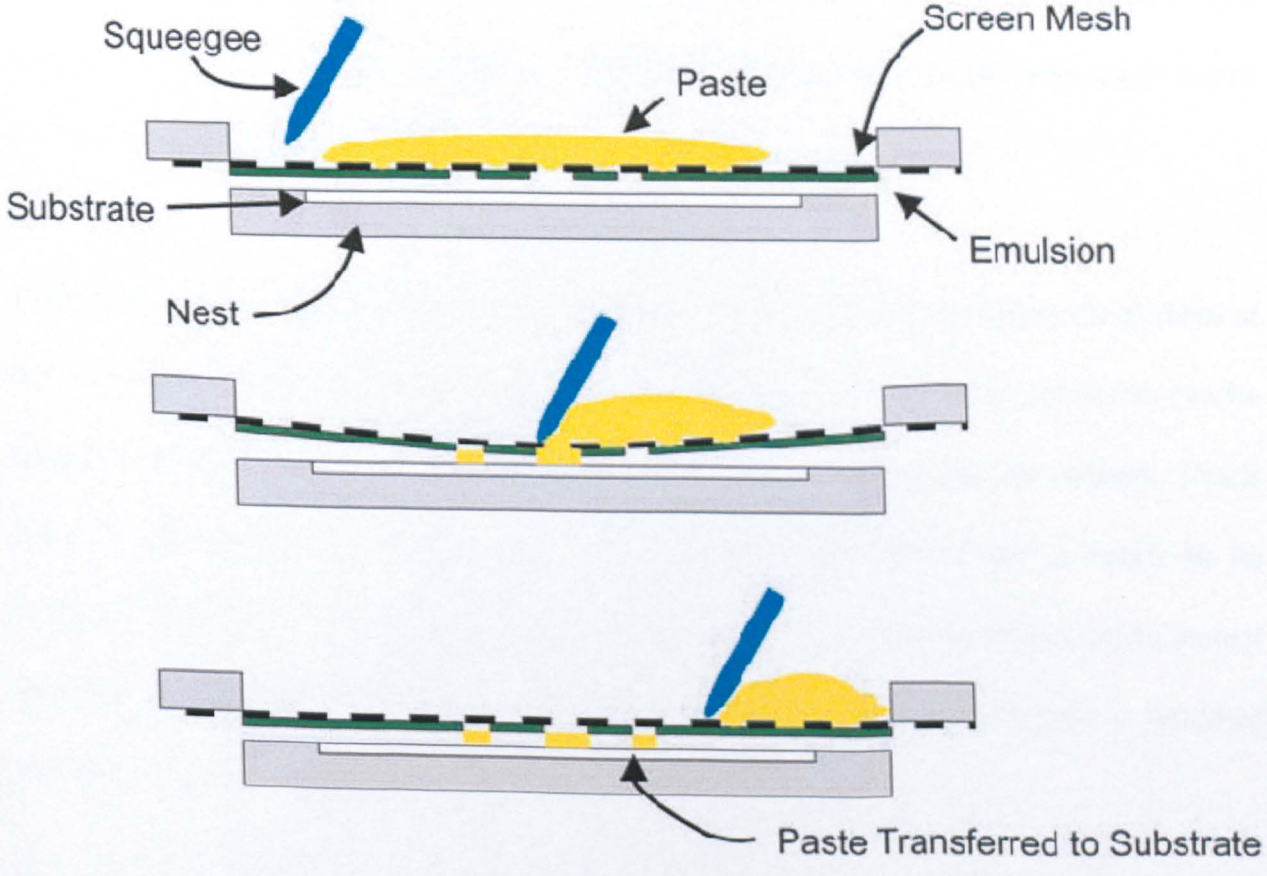

Figure 9. Represents the principle method to produce screen-printed electrodes.[52]

In ancient China, silk was one of the first materials used as a mesh.[53] A pattern was created in the silk using pitch or similar materials to block out unwanted areas, and dye was forced through the pattern by hand to cloth or other surfaces to create colored patterns. By performing several sequential screenings with different colors and patterns, complex decorative patterns could be formed.[53] This continues to be one of the most common applications of the screen-printing process.

Silk continued to be one of the most common materials used until the development of synthetic materials,[53] and the term "silk screening" is still commonly used to describe the screen-printing process.[54] The development of synthetic fibers, such as nylon, made possible greater control of the mesh materials, and the added development of photosensitive materials used for creating the patterns allowed screen printing to become much more precise, repeatable, and controllable.[53]

The distinct advantage of screen-printed electrodes is the simplicity to which the surface of the working electrode can be modified. The carbon ink used to print the electrodes can be incorporated or mixed with a compound in order detect the analyte in the solution. This is done by thoroughly mixing the compound within the ink mixture and is ready to be printed.[53] This ultimately leaves an electrochemist with an easy to manufacture sensor which is reproducible and only costs tens of pence to produce. Furthermore, a modified working electrode significantly improves the response.[55]

As mentioned previously, inks consist of graphite particles, polymer binder and other additives which are utilised for dispersion, printing and adhesion tasks. The exact ink

formulation is regarded by the manufacturer as proprietary information and it has been shown that differences in ink composition *e.g.* type, size or loading of graphite particles and in the printing and curing conditions can strongly affect the electron transfer reactivity and the overall analytical performance of the resulting carbon sensors. Screen-printed electrochemical sensors provide excellent platforms for modification with a variety of nanoparticles and structurally related materials requiring no pre-treatment such as electrode polishing or electrochemical pre-treatment *via* electrodeposition, as is common with other electrode materials.[53]

In many cases there will be many target molecules for which it is electrochemically challenging or near impossible to obtain a useful voltammetric signal. In such an instance, a common approach is to employ an electro-catalytic mediator, and methodologies to immobilise the chosen mediator onto the screen-printed sensor include drop casting, physical attachment (the use of polymer coatings), covalent bonds sorption (physisorption and chemisorption), or mixing into a carbon paste, which are all viable approaches.[53, 54]

2.3. Process of production of screen-printed electrodes

Today, in the electrochemistry industry, the primary mesh material is stainless steel, which adds an additional degree of control and precision over nylon in addition to added resistance to wear and stretching. The crude hand methods of printing have evolved to sophisticated, microprocessor-controlled machines that are self-aligning, have the ability to measure the thickness of the film and also to adjust the printing parameters to compensate for variations in the properties of the thick-film paste.

Still, of all the processes used to manufacture electronic circuits, the screen printing process is the least analytical. It is not possible to measure the parameters of the paste and convert them to the proper printer settings needed to produce the desired results due to the large number of variables involved. Many of the variables are not in the direct control of the process engineer and may change as the printing proceeds. For example, the viscosity of the paste may change during a print run as a result of evaporation of the solvent used to thin the paste. Screen printing will remain one of the processes where the skill of the process engineer cannot be replaced by a computer. Although it is possible to screen very viscous pastes or pastes with large particles using a coarse screen, a stencil — with openings created by etching, laser, or electroforming, is the preferred method of application for these types of pastes. The screen wires interfere with the transfer of the paste to the substrate, leaving voids in the printed film.

Chapter 3

Screen-Printed Electrodes

3.1 Production of Screen-Printed Electrodes

3.1.1 The Screen

The screen mesh is manufactured by weaving stainless steel wires to form a long sheet. The direction along the length of the sheet is referred to as the "warp" direction, whereas the direction across the width of the sheet is referred to as the "weft" direction. The vast majority of meshes used in thick film screen printing are woven in the so-called plain weave pattern, as shown in figure 10, formed by routing one wire over and under only one wire at a time. In the twilled weave pattern, each wire is routed over and under two wires at a time. The plain weave has more open area for a given mesh count and wire size, whereas the twilled weave is stiffer and is less likely to stretch.

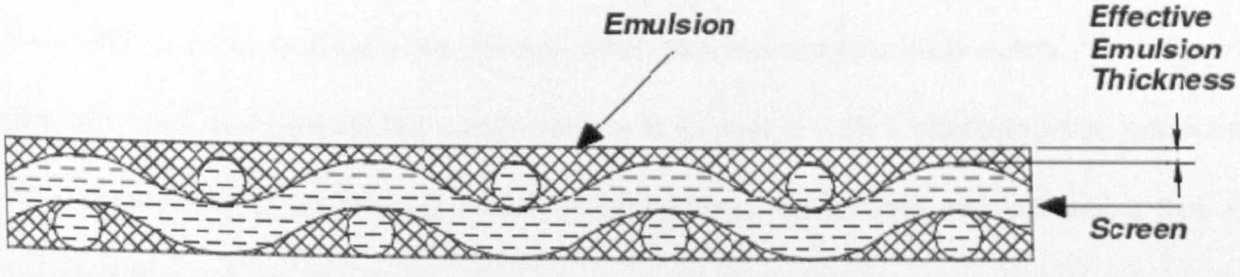

Figure *10. Represents wave pattern which can be achieved from using thick film screen mesh.*[56]

One of the most important parameters of the screen is the mesh count, or the number of wires per unit length. In general, the mesh count is the same for both the warp and weft directions, as is the wire size. In practice, the mesh count may vary from 80 wires per inch for coarse screening, such as solder paste, to 400 wires per inch for fine-line printing. Another important parameter is the size of the opening in the screen, which strongly

influences the amount of paste that can be transferred during the printing process, and limits the maximum particle size of the material used to manufacture the paste.

3.1.2 Production of Screen

The screen frame is usually made from cast aluminium. With these specifications, the screen will be parallel to the substrate mounting platform and will have the same reference point with respect to the substrate. This precaution will greatly improve the quality and reproducibility of the print as well as minimizing the setup time.

The screen is prepared for use by stretching the mesh by pneumatic or mechanical methods over a large frame capable of accommodating several smaller screen frames. The mesh is attached to the small frames with epoxy that cures at room temperature. After curing, the mesh is trimmed away around the periphery of the epoxy, simultaneously separating the individual screen frames. A screen manufactured in this manner can be expected to last for thousands of prints without losing tension when handled and treated properly.

The final step in preparing the screen for use is to coat it with a photosensitive emulsion. The so-called direct emulsion is initially in liquid form. To sensitize the screens, a dam or mould is formed around the periphery of the screen with cellophane tape or similar material to control the thickness. The top of the screen mesh is placed on a flat surface exactly the size of the inside of the frame. The emulsion is poured on the mesh and smoothed with a straight edge to coat the screen evenly and fill the mesh. The thickness may be built up, if desired, by allowing the initial coating to dry and repeating the process with a second dam.

The quality of the screen is critical to the screen-printing process. The wire mesh should initially be inspected for uniformity of wire size and the size of the opening. The screen must

be cleaned with detergent to remove any oils and dirt prior to sensitization, and all photoprocesses must be performed under yellow light. The emulsions used for screen printing are not ultrasensitive to light, but the exposure time even to yellow light should be minimized

3.1.3 The Stencil

Stencils can be formed by photoetching a pattern through a thin sheet of brass or stainless steel from both sides of the metal. The opening created in this manner has a characteristic hourglass shape, narrower in the middle than at the top and bottom. There is also a limitation in the minimum size of the opening owing to the fact that the etching process proceeds laterally, and at the same, time, it is etching vertically through the metal as illustrated in Figure 9.[52] This not only limits the pitch of the devices that can be mounted in surface mount technology (SMT) applications, but also necessitates complicated correction factors that vary with the size and thickness of the metal. The so-called hourglass effect can be minimized by electropolishing the stencil. This process is accomplished by attaching the stencil to electrodes and immersing it in an acid bath. The electric field lines concentrate at the sharp edges, causing these areas to etch faster than smoother surfaces. The sharp edges become rounded, resulting in better paste transfer.

3.1.4 The Ink

The composition and characteristics of the paste are critical factors in screen printing. The cermet (combination of ceramic and metal) pastes commonly used in the thick-film technology have four major ingredients:[53, 54]

(1) an active element that establishes the function of the film,

(2) an adhesion element that provides the adhesion to the substrate;

(3) an organic binder a matrix that holds the active particles in suspension and which provides the proper fluid properties for screen printing, and

(4) a solvent or thinner that establishes the viscosity of the vehicle phase.

There are three critical parameters of the ink that relate to screen printing:[53, 55]

(1) the ratio of the solids content,

(2) the particle size distribution, and

(3) the viscosity.

3.1.5 The Squeegee

The purpose of the squeegee is to force the paste through the open areas of the mesh and onto the substrate. There are three types of squeegees in common use which come in various sizes to suit the purpose. These can be termed as, the hand squeegee, the one-arm and the composite.

The hand squeegee is made up from a flexible blade inserted into a groove of a wooden handle. The squeegee is used to cut the surface of the ink cleanly, using the minimum

pressure to produce a good quality image. It should not be used to force ink through the screen under excessive pressure.

The one-arm squeegee is attached to the back of the printing table and runs along a rail parallel to the front of it. This type of squeegee has the advantage of being easier to control than is the hand squeegee. Hand squeegees should not be used with one-arm units, as the extra pressure will distort them.

The composite squeegee can be used for either hand or one-arm units as the blade is held in metal grippers along its entire length. The composite squeegee can be taken apart for cleaning. The advantage of the composite squeegee is that it can have a number of small blades attached to it, thereby enabling the user to print different colours on the same print stroke.

3.1.6 The Blade

The squeegee blade is made up of either rubber, which is inexpensive but becomes blunt very quickly, or polyurethane, which maintains its sharp edge for more printings.[53] Both types of blades come in three different grades: hard, medium and soft. Hard blades are used for printing on shiny flat surfaces that are non-absorbent, such as glass, plastic or ceramic, where the minimum of spreading can be tolerated. Medium flexibility squeegees are used for printing on all absorbent surfaces, where a higher pressure is used for printing, as when using a one-arm squeegee or an automatic machine. Soft blades are ideal for hand printing since they flex to accommodate undulations in the printing stock and are sensitive to fluctuations in pressure, allowing difficult areas to be printed. It is formed of a flexible

material such as polyurethane or neoprene and comes in two basic shapes, diamond, and trailing edge, as lowering the substrate or raising the screen. Figure 11 shows the comparison of type of blades typically used during screen-printing electrodes.

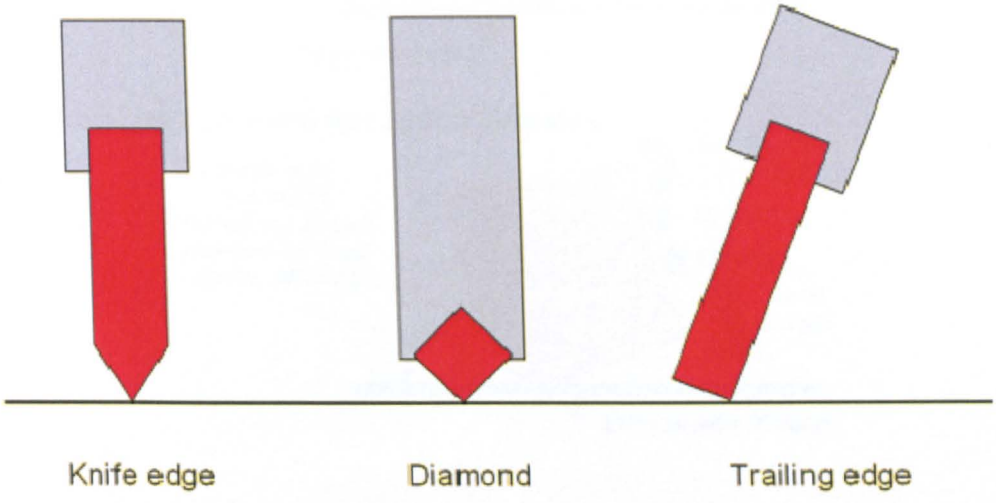

Figure 11. Represents three types of blades which can be utilised for screen-printed electrodes.[57]

3.1.7 Angle of squeegee

The angle at which the squeegee is held determines the thickness of the ink deposit. The more upright the blade the thinner the deposit, the lower the blade the thicker the ink will print. Figure 12 below shows some of the distinguishable influential components that are present whilst the printing process is performed.

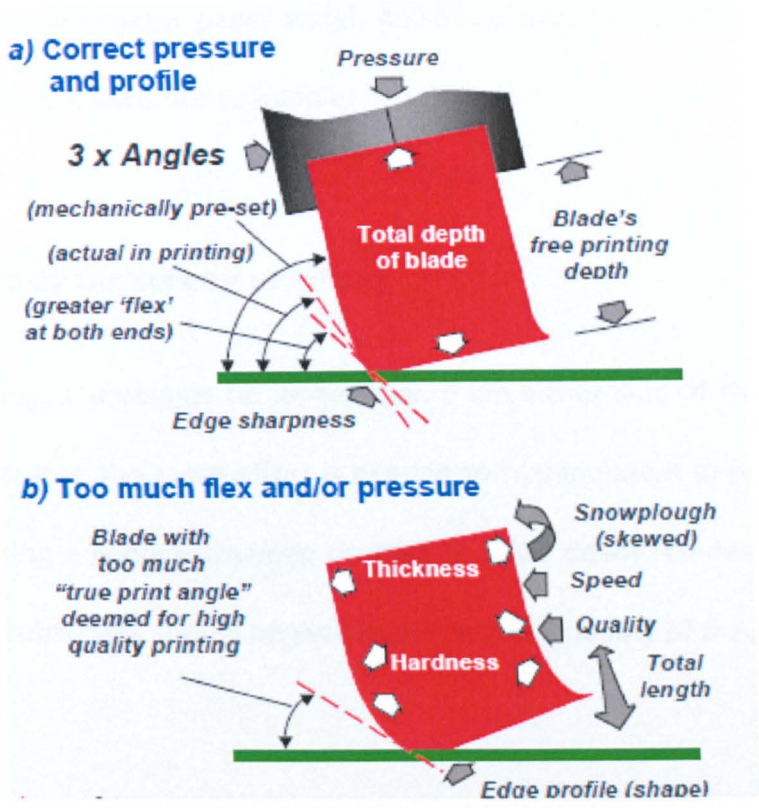

Figure 12. Represents the essential components during the screen printing process.[58]

It is important to understand that the right mechanical combination of printing integrity (frame size/type, fabric, tension, stencil/emulsion thickness/application, clarity of image, off-contact, peel-off, squeegee issues, press set-up/make-ready, etc.) interacting against the substrate that begets a successful print.

3.1.8 Weight and size of substrates

The weight of the substrate should be taken into account when screen printing is performed. If the substrate is large, it also needs to be heavy to enable it to be handled successfully. For example, the weight of paper, which is expressed in grams per square metre. This is calculated by weighing 1,000 sheets of meter square paper, thus 1,000 sheets

of 400 grams per square meter paper weigh 400 kilograms. Note, the heavier the weight gets, the more difficult it becomes to handle.

3.1.9 Getting ready for screen printing

To facilitate printing, a squeegee no longer than 5 cm either side of the image should be used, as the longer it is, the more effort is needed to manipulate it in printing. All surfaces must be clean, using a general cleaning product to wipe down remove any contaminates present. A pile of substrates should be available to test the quality of the print.

3.1.10 Drying process

The drying of the finished screen-printed electrodes differ depending on what type of ink or substrate is being utilised. In this thesis, the substrate being used remained the same throughout. On the other hand, the ink composition differs from one analysis to another as different ink compositions are used depending on what the target analyte is. An oven is used to dry the screen-printed electrodes which is typically set to 60 °C for thirty minutes.

3.1.11 Cleaning up

There are a number of general-purpose cleaning products available to remove ink from the screen or if a colour needs to be changed in between printing layers. The compatibility of these cleaners with the printing ink should be established by reading the manufacturer's instructions. The cleaning up is one of the most difficult aspects of screen printing. However, following a set procedure each time can make this process fairly quick and easy. The ink is

collected by the squeegee and brought to the front of the screen, where it is collected on to the blade against the front inside edge of the frame. The ink can be scrapped off the squeegee into a disposable waste bin using a wooden spatula. The small quantity of ink remaining in the screen can be removed by washing with a volatile solvent such as acetone. This process is continued until the screen is clean. The screen should be thoroughly inspected after cleaning to make sure no ink or contaminates are present. This can be achieved using a light and carefully inspecting the screen, in particular the holes of the screen where the ink is passed through.

3.2 Print Quality

Poor print resolution simply means that the printed film does not match the layout in terms of dimensions or shape. It can be because of spreading of the print because of improper rheology, or a flaw in the screen. Figure 13 shows smooth screen separation behaviour during the screen-printing process. These factors help to improve resolution of the pattern;

- Emulsion thickness — thinner emulsion is better.
- Pattern alignment to wire mesh — 45° is optimum.
- Attack angle — shallow attack angle is better.
- Durometer — softer durometer is better.
- Speed — slower speed is better.
- Downstop — smaller downstop is better.
- Alignment — tighter alignment is better.
- Rheology — high viscosity is better.
- Pressure — lower pressure is better.
- Screen tension — degrading of tension worsens resolution.

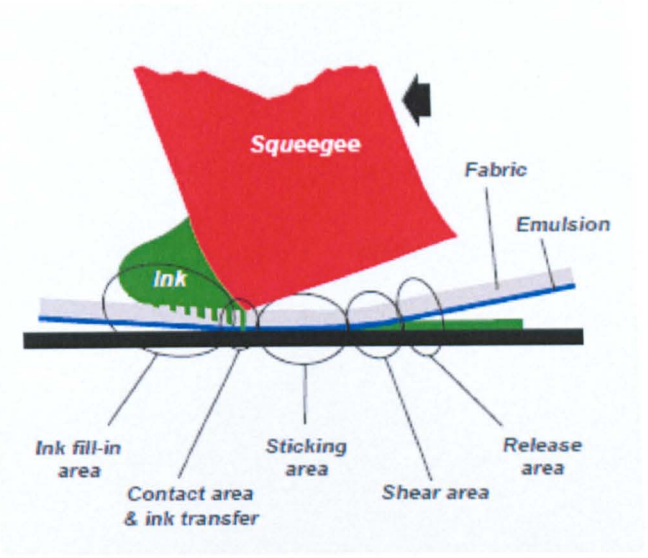

Figure 13. The rheology of screen printing: the ideal profile of a squeegee and substrate whilst printing, showing smooth screen separation behaviour.[58]

3.3 Good Practice

Some good practices to follow in a printing environment are to avoid excessive wiping of the screen. This will stretch the screen and may introduce contaminants into the ink. A few drops of solvent can lower the viscosity by several orders of magnitude. The essential key ingredient to successful screen printing is cleanliness. Another point to remember is to avoid to overworking paste as this will cause the solvent to evaporate, increasing the viscosity, and causing the paste to dry out. Furthermore, excessively working the paste without allowing time for the viscosity to recover will lower the viscosity.

Chapter 4

Other Fabrication Processes

4.1 Other fabrication methods

Screen printing was the dominant fabrication process used throughout this thesis. However plating and sputtering methods were used in addition to the screen-printed electrodes. In both cases, screen printing is done first in order to produce a conducting carbon surface and later plating or sputtering can be performed.

4.2 Plating

Plating or electroplating is a deposition process of a metal to coat an electrode. An example (figure 14 below) will be given to explain this process. In this particular case, an electrolytic cell is being used to silver plate the spoon. The power supply is used to force the electrons from the left (anode) to the right (cathode). The cell contains a salt solution (silver nitrate) of the metal to be plated. As the spoon is negatively charged, it attracts the positively charged silver ions that are floating around in the solution, thus plating the spoon with silver. The amount of silver that is deposited is directly proportional to the number of electrons that the battery provides.

Electroplating offers many benefits. In particular, electrochemists utilise this fabrication process since it is corrosion resistant. Once a material has been electroplated with a metal, it forms a protective layer of oxide on the surface and no longer reacts with oxygen. Furthermore, durability is increased and can provide insulation to the electrode. Later in this thesis (chapter 9) an example is given where fabrication of the screen-printed electrode is done *via* plating.

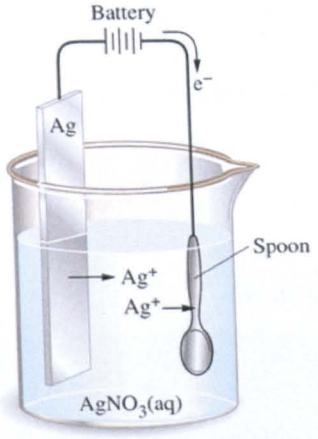

Anode oxidation

$Ag \rightarrow Ag^{+} + e^{-}$

Cathode Reduction

$Ag^{+} + e^{-} \rightarrow Ag$

Overall reaction:

$Ag \rightarrow Ag^{+} + e^{-} \rightarrow Ag$

Figure 14. Shows the electroplating process whereby a spoon is plated by the silver ions in the solution.[63]

4.3 Sputtering

Sputtering is a physical-vapour deposition. A process which is used in order to deposit very thin films on to a substrate. Sputtering occurs when an ionised gas molecule is used to displace atoms of a specific material. These atoms then go onto bond at the atomic level to a substrate and create a thin film. Figure 15 below represents how this process is performed. There are many types of sputtering procedures available on the market. The most common are ion beam, diode and magnetron sputtering. The high voltage is achieved across a low pressure gas (usually argon) in order to create a high-energy plasma. The energised plasma ions strike a target, which consists of the desired coating material. This force releases the atoms from the target material and they subsequently bond with those of the substrate. As sputtering is undergone in a high-energy environment, it forms an unbreakable bond between the film and the substrate (at the atomic level), thus creating a

thin, uniform and cost-effective film. Sputtering is a cheap method for scientist to employ as the target material is relatively cheap and is available for many demanding metals.

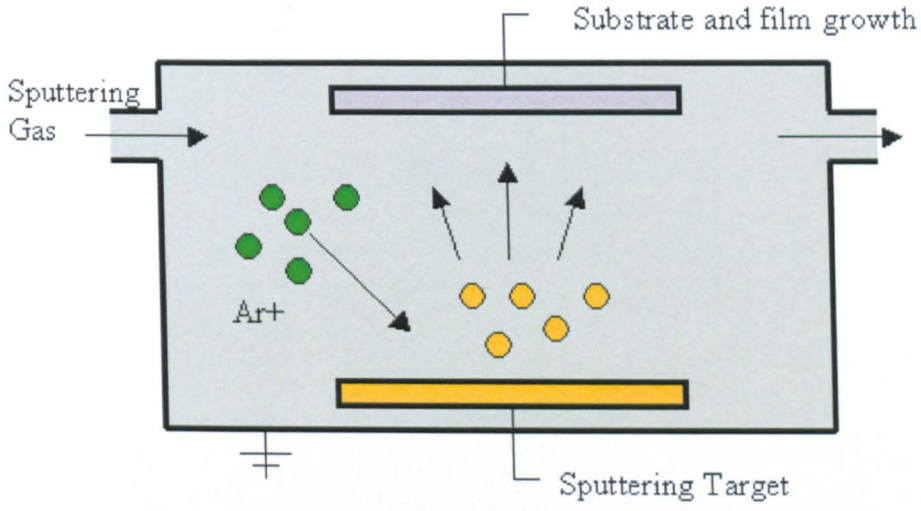

Figure 15. Shows the process of sputtering.[64]

Sputtering is heavily employed in the semi-conductor industry to deposit thin films of various materials in integrated circuit processing. The fabrication of CD's and DVD's also involves sputtering for the deposition of the metal (aluminium) layer. A distinct advantage of sputtering is it can easily deposit materials with very high melting points. On the other hand, it is difficult to achieve layer by layer growth. Later in this thesis (chapter 13), an example is demonstrate where the fabrication of metallic microdomains can be simplified by sputter coating screen-printed electrodes.

Chapter 5

Electrochemistry

5.1 Electrochemistry

In order to fully understand and develop the complete sensor (or electrochemical sensor), electrochemistry must be employed. Electrochemistry sets the principles applied on the electrochemical sensors. Electrochemistry lies in the cross-field of analytical and physical chemistry. Electrochemistry is the study of chemical reactions which take place in a solution by applying a potential difference between the electrode and electrolyte and recording the current that is induced to flow. This is represented by a voltammogram from plotting current, I, as a function of the applied potential, *E*.

5.2 Electrochemical Techniques

Electrochemical techniques provide analytical information on the processes taking place, in particular the study of interactions between the electrode and the solution containing the analyte.

5.3 Equilibrium Electrochemistry

Electrochemical techniques can be sub-categorised as equilibrium and dynamic electrochemistry. The first technique of equilibrium electrochemistry is where the electrochemical potential remains constant (in equilibrium) across the chemical system, therefore eliminating the chemical reaction stated by Gibbs law (equation 5.1):

$$\Delta G = \Delta H - T\,\Delta S \qquad (5.1)$$

Gibbs developed a theory to predict whether a chemical reaction is spontaneous or not, based on free energy.

The Nernst equation[80] (equation 5.2) can be used to determine the equilibrium potential of a half cell in the solution. The potential applied at the electrode is proportional to that applied from the analyte in the electrochemical cell.

$$E_{electrode} = E^{o}_{red} - RT/nF \ln (a_{red}/a_{ox}) \qquad (5.2)$$

To help understand this electrochemical process, a well known system can be given. The ion selective electrode, which can be measured using a volt meter, contains two electrodes which are the same (Ag/AgCl), are immersed into an aqueous solution containing the ions to be measured, together with a separate, external reference electrode. A potential difference is developed across the ion-selective electrode membrane when the target ions diffuse through the high concentration side to the lower concentration side.

5.4 Mass Transport

There are three forms of mass transport that can influence an electrolysis reaction: migration, convection and diffusion.

5.4.1 Migration

Migration consists of the movement of ionic specices in the liquid phase towards the oppositely-charged electrode (figure 16 below). This is essentially an electrostatic effect which arises due to the application of a voltage on the electrodes. This in effect creates a charged interface (thus the electrodes). Any charge ions or partially charged ions in the

solution coming near that interface will either be attracted or repelled from it by electrostatic forces.

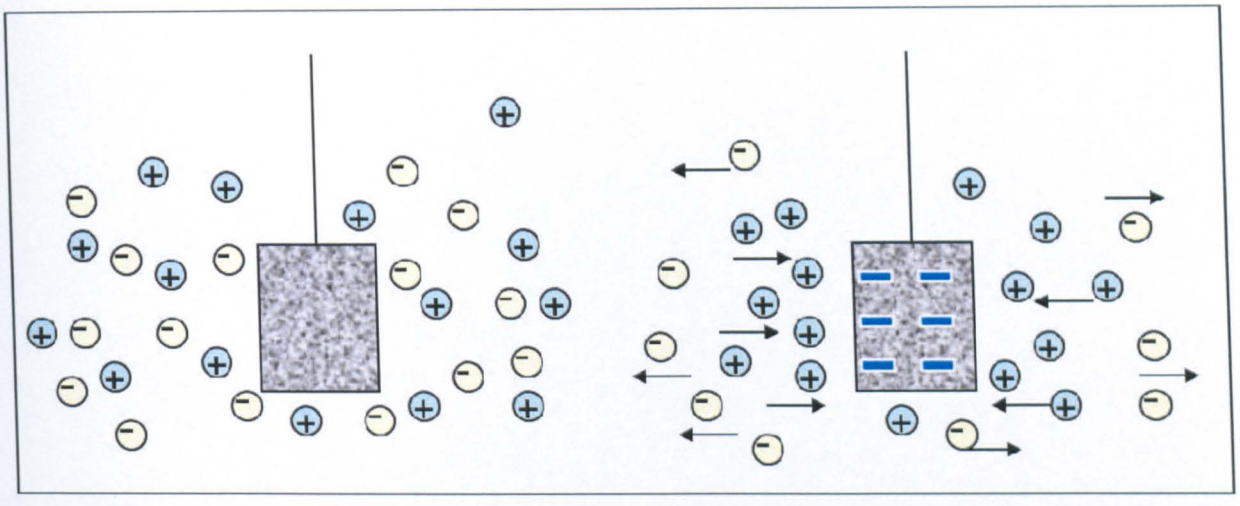

Figure 16. Change in the applied potential to a solid electrode in a solution containing ions affects charge migration for increasing negative charge at the electrode surface.[65] *Applying a negative charge at electrode surface when in solution affects the charge migration of ions.*

The migration flux, J_m induced can be described mathematically using:

$$J_m = -\frac{zF}{RT} D\,[x]\frac{\partial \varphi}{\partial x} \qquad (5.3)$$

where J_m is dependent on the concentration of the ions, x and their charges z, R is the molar gas constant, F is Faraday's constant 96485 C/mol, T is the absolute temperature, $\partial\varphi$ is the galvanic potential and ∂x is the distance from the electrode.

5.4.2 Convection

Convection results from the forced movement of solution species by mechanical forces. This can be a pump, a flow of gas, stirring or even gravity. There are two types of convection, the first is known as natural convection and is present in any solution. Natural convection is generated by small thermal or density differences and acts to mix the solution in a random and therefore unpredictable fashion. The other form of convection is termed forced convection. It is typically several orders of magnitude greater than any natural convection effects and therefore effectively removes the random aspect from the experimental measurement.

5.4.3 Diffusion

Diffusion occurs in all solutions and is the random movement of molecules from a region of higher concentration to regions of lower concentration (figure 17 below). The rate at which a molecule diffuses is dependent upon the difference in concentration between two points in solution, known as the concentration gradient and diffusion coefficient. The movement of a chemical species under the influence of a concentration gradient can be described by Fick's First law [81]:

$$J = -D\frac{\partial[A]}{\partial x} \qquad (5.4)$$

where J is the flux in mol cm^{-2} s^{-1}, D represents the diffusion coefficient in cm^2 s^{-1} and [A] expresses the concentration of the species in mol cm^{-2}.

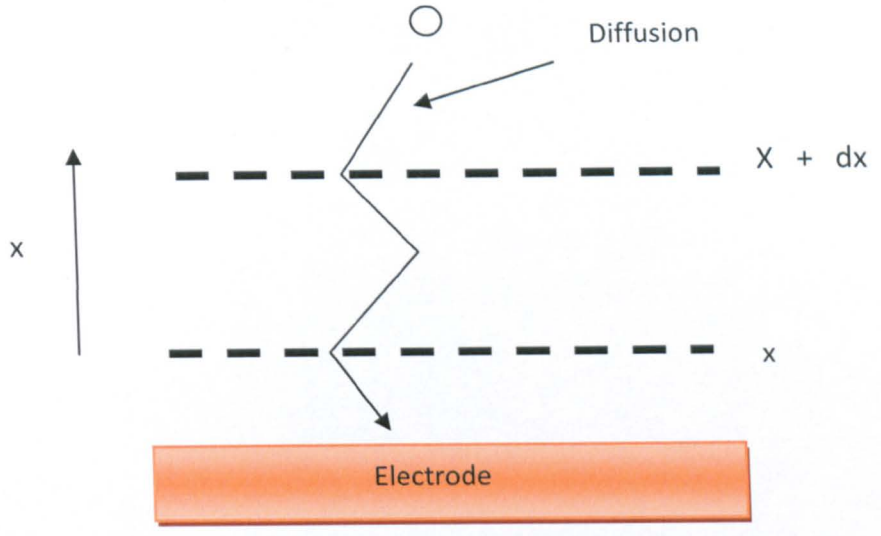

Figure 17: Represents the redox reactions which occur on the electrode surface

5.5 Voltammetric Techniques

The two main techniques which were utilised during this thesis are linear sweep and cyclic voltammetry. Both techniques are very similar, the only difference being that in cyclic voltammetry, when a desired potential is reached, the experiment reverses. In comparison, linear sweep voltammetry (LSV) method measures the current at the working electrode while the potential between the working electrode and reference electrode is swept linearly in time. Consider a general *n*-electron reduction:

$$A_{ox} + ne^{-} \Leftrightarrow A_{red} \qquad (5.5)$$

Using the Nernst equation, we can understand how the potential of the working electrode changes during the course of the experimental procedure. The experiment will begin at a potential value, E_1. A powerful electrochemical machine known as a potentiostat is used for

these dynamic electrochemical techniques. The general purpose of a potentiostat is to control the voltage whilst measuring the potential or vice versa.

5.5.1 Cyclic Voltammetry

Cyclic voltammetry is a fundamental electrochemical technique which can be used to study redox behaviour of compounds. Cyclic voltammetry is very similar to LSV. However in this case, the voltage is swept between two values at a fixed rate. When the voltage reaches E_2, the scan is reversed and the voltage is swept back to E_1. During analysis, the potential is varied between two potential limits to cause electroactive chemical species to be reduced or oxidised at the electrode. The resultant current is proportional to the concentration of the chemical species. Triangular waveform of the potential in potential sweep techniques (figure 18).

$$(0 < t \leq \lambda) \quad E = E_i + v\,t \qquad (5.6)$$

$$(\lambda < t \leq 2\lambda) \quad E = E_i + 2v\lambda - v\,t \qquad (5.7)$$

where t is the time of the potential sweep, λ is the time corresponding to the switching potential, E_λ, E_i is the initial potential and v is the scan rate in $v\ s^{-1}$.

Cyclic voltammetry is a very versatile electrochemical technique which allows to probe the mechanics of redox and transport properties of a system in solution. This is accomplished with a three-electrode arrangement whereby the potential relative to some *reference* electrode is scanned at a *working* electrode while the resulting current flowing through a *counter* (or *auxiliary*) electrode is monitored in a quiescent solution. The technique is ideally

suited for a quick search of redox couples present in a system; once located, a couple may be characterized by more careful analysis of the cyclic voltammogram. More precisely, the controlling electronics are designed such that the potential between the reference and the working electrodes can be adjusted. The big impedance between these two components effectively forces any resulting current to flow through the auxiliary electrode. When the potential of the working electrode is more positive than that of a redox couple present in the solution, the corresponding species may be oxidized (*i.e.* electrons going from the solution to the electrode) and produce an *anodic* current. Similarly, on the return scan, as the working electrode potential becomes more negative than the reduction potential of a redox couple, reduction (*i.e.* electrons flowing away from the electrode) may occur to cause a *cathodic* current. By IUPAC convention, anodic currents are positive and cathodic currents are negative.

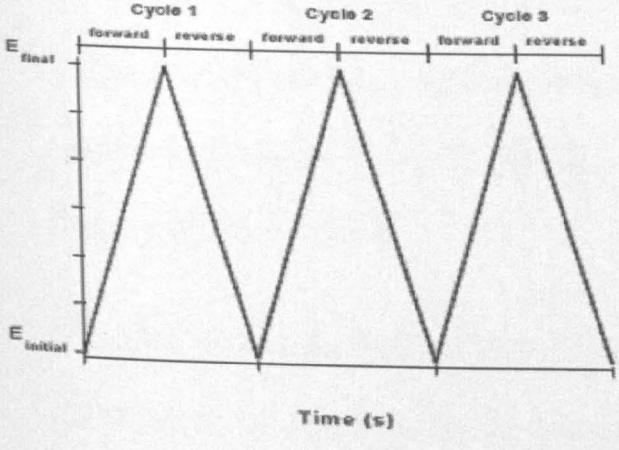

Figure 18. A cyclic voltammetry potential waveform with switching potentials.[82]

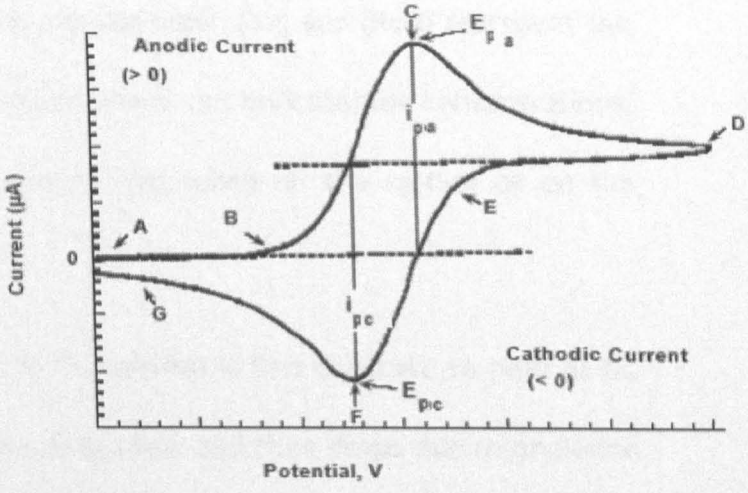

Figure.19 The expected response of a reversible redox couple during a single potential cycle.[82]

The magnitude of the observed Faradaic current can provide information on the overall rate of the many processes occurring at the working electrode surface. As is the case for any multi–step process, the overall rate is determined by the slowest step. For a redox reaction induced at a working electrode, the rate determining step may be any one of the following individual step depending on the system: rate of *mass transport* of the electro-active species, rate of adsorption or de-sorption at the electrode surface, rate of the electron transfer between the electro-active species and the electrode, or rates of the individual chemical reactions which are part of the overall reaction scheme.

For the oxidation reaction involving *n* electrons the Nernst Equation gives the relationship between the potential and the concentrations of the oxidized and reduced form of the redox couple *at equilibrium* (at 298 K):

$$E = Eo' + \frac{0.059}{n} \log_{10} \frac{[Ox]}{[Red]} \qquad (5.8)$$

where E is the applied potential and $E^{0'}$ the formal potential; [ox] and [Red] represent the surface concentrations at the electrode/solution interface, *not* bulk solution concentrations. The Nernst equation may or may not be obeyed depending on the system or on the experimental conditions.

A typical voltammogram is shown in figure 19. The current is first observed to peak at E_{pa} (with value i_{pa}) indicating that an oxidation is taking place and then drops due to depletion of the reducing species from the diffusion layer. During the return scan the processes are reversed (reduction is now occurring) and a peak current is observed at E_{pc} (corresponding value, i_{pc}).

Providing that the charge-transfer reaction is reversible, that there is no surface interaction between the electrode and the reagents, and that the redox products are stable (at least in the timeframe of the experiment), the ratio of the reverse and the forward current i_{pr}/i_{pf} = 1.0 (in *Figure*. 19 $i_{pa} = i_{pf}$ and $i_{pc} = i_{pr}$). In addition, for such a system it can be shown that:

- The corresponding peak potentials E_{pa} and E_{pc} are independent of scan rate and concentration,
- The formal potential for a reversible couple $E^{0'}$ is centered between E_{pa} and E_{pc}: $E^{0'} = (E_{pa} + E_{pc})/2$
- The separation between peaks is given by $\Delta E_p = E_{pa} - E_{pc} = 57/n$ mV (for an n electron transfer reaction) at all scan rates. (The measured value for a reversible process would generally be higher due to uncompensated solution resistance and non-linear diffusion. Larger values of ΔE_p, which increase with increasing scan rate, are characteristic of slow electron-transfer kinetics).

To distinguish between reversible (diffusion-controlled) and irreversible (charge-transfer controlled) kinetics of electrode process potential, the scan rate is used as diagnostic tool. The rate of reagent transport is proportional to the square root of the scan-rate. Thus, in one experimental set, a shift in reversibility might be executed and analysis of ΔE_p *vs.* $v^{1/2}$ gives information on reversibility and applicability of further calculations.

In simple terms, the working electrode may be regarded as a "reagent" of adjustable oxidizing or reducing strength. However, this is a purely conceptual image. In actual fact, the electrochemical processes are occurring at the interface of two different phases, the electrode and the electro-active species in solution. In other words, the processes under studies are heterogeneous in nature. For the electron transfer to occur, the molecules in

solution have to approach the electrode. In a cyclic voltammetry experiment, the solution is kept unstirred; in this situation, mass transport can occur only by diffusion due to concentration gradients created around the electrode surface. Such concentration–distance profiles at different steps of a cyclic voltammogram scan are illustrated in Figure. 18. The magnitude of the observed signal will be very much a function of these diffusional properties of the system. Intuitively, the current intensity (*i.e.* the flow of electrons) is expected to depend on the surface area of the working electrode and the concentration of the electro-active species. Also, one can expect the voltage scanning rate to affect the concentration profile around the electrode which in turn directly affects the rate of charge transport, and for this matter the diffusion coefficient appears explicitly. The expression of the peak current (I_p) for the forward sweep in a reversible system at 298 K is given by the Randles–Sevcik equation:

$$I_p = 0.4463\, n\, F\, A\, C\, (n\, F\, v\, D / R\, T)^{½} \qquad (5.9)$$

Where n is the number of electron equivalent exchanged during the redox process, A (cm^2) the active area of the working electrode, D ($cm^2\ s^{-1}$) and C ($mol\ cm^{-3}$) the diffusion coefficient and the bulk concentration of the electroactive species, and v is the voltage scan rate ($V\ s^{-1}$). In the present experiment, the dependence of I_p on scan rate and concentration will be examined.

5.5.1.1 Irreversible and Quasi-reversible Systems

For irreversible processes (those with sluggish electron exchange), the individual peaks are reduced in size and widely separated. Totally irreversible systems are characterized by a shift of the peak potential with the scan rate:[66]

$$E_p = E^\circ - (RT/\alpha n_a F)[0.78 - \ln(k^\circ/(D)^{1/2} + \ln(\alpha n F v/RT)^{1/2}] \qquad (5.10)$$

where α is the transfer coefficient and n is the number of electrons involved in the charge-transfer step. Thus, E_p occurs at potentials higher than E°, with the overpotential related to k° (standard rate constant) and α. Independent of the value k°, such peak displacement can be compensated by an appropriate change of the scan rate. The peak potential and the half-peak potential (at 25°C) will differ by $48/\alpha n$ mV. Hence, the voltammogram becomes more drawn-out as αn decreases

The peak current, given by:

$$I_p = (2.98 \times 10^5)\, n(\alpha^2 n)^{1/2}\, A\, D^{1/2}\, C\, V^{1/2} \qquad (5.11)$$

where the constant is understood to have units (*i.e.* 2.98 x 10^5 C mol^{-1} $V^{-½}$). Assuming α = 0.5, the ratio of the reversible-to-irreversible current peaks is 1.27 (*i.e.* the peak current for the irreversible process is about 80% of the peak for a reversible one). For quasi-reversible systems (with $10^{-1} > k^\circ > 10^{-5}$ cm/s) the current is controlled by both the charge transfer and mass transport. Overall, the voltammograms of a quasi-reversible system are more drawn out compared to a reversible system and exhibits a larger separation in peak potentials.

For quasi-reversible systems (with $10^{-1} > k^\circ > 10^{-5}$ cm/s) the current is controlled by both the charge transfer and mass transport. For a quasi-reversible reaction (ΔEp up to 200 mV) a numerical approach brings values of function Ψ:[83]

ΔEp / mV	64	68	72	84	92	105	121	141	212
Ψ	6	3	2	1	0.75	0.5	0.35	0.25	0.1

to calculate the rate constant, using following equation:[83]

$$\Psi = k^0 (D_{ox}/D_{red})^{\alpha/2} / [D_{ox}\pi(nF/RT)]^{1/2} \qquad (5.12)$$

One of the problems an electrochemist is faced with in cyclic voltammetry, is it can only be used empirically, since little theory existed for relating quantitatively the shapes of the curves to the mechanism of the electrochemical reaction. This is when Robert Nicholson[68] introduced a numerical approach for solving integral equations derived from the appropriate boundary value problems. New correlations make it possible to characterise unknown systems by studying the variation of peak current, half-peak potential, or ratio of anodic to cathodic peak currents as a function of rate of voltage scan.[68, 69]

5.5.2 Chronoamperometry

The method of chronoamperometry may be applied for measuring the oxidation or reduction currents of analytes at the working electrode. The Faradaic current under diffusion-controlled conditions is related directly to the concentration gradient. Thus, since the slope of the concentration profile for oxidation decreases with time following the potential step, so will the observed current.

Chronoamperometry experiments are most commonly either single potential step, in which only the current resulting from the forward step, or double potential step, in which the potential is returned to a final value. The most useful equation for this technique is the Cottrell equation, which describes the observed current at any time following a large forward potential step in a reversible redox reaction, as a function of $t^{1/2}$.

$$ip = \frac{n\,F\,A\,D_0\,C_0}{\pi t½} \qquad (5.13)$$

where n is the stoichiometric number of electrons involved in the reaction, D_o is the diffusion constant for the electroactive species, C_o is the concentration of the electroactive species and A is the electrode area.

Chapter 6

Electrode Design on Electrochemical sensors

6.1Electrode Design

One of the most fundamental aspects which effects the electrochemical response of an electrochemical sensor is the working electrode material. Furthermore, to improve the electrochemical response, the diffusion of the electroactive analyte towards the working electrode surface must be controlled. Discussion about the diffusion profiles has previously been mentioned in this thesis (chapter 1). In particular the diffusion profile of a compound towards the working electrode surface affects the diffusion limited current value and thus the overall response of the sensor.

The peak height in this case is well defined (due to an increase to the current value). In comparison, a macroelectrode response represents a Gaussian shaped peak, where the peak area measurement gives more precise results compared to measuring the peak heights, unless the redox peak of the macroelectrode is very sharp.[67]

Microelectrodes are far more favourable for an electrochemist to utilise because they offer a response of a mixture of electroactive species, which is better to interpret, since the peak heights and peak potentials are well separated and observed. Furthermore, the limitations of the small peak current values obtained from the microelectrodes were soon turned around by the development of multimicroelectrodes. In multimicroelectrodes, there is no overlapping of their diffusion profiles (microelectrodes are independent) and each microelectrode equally contributes to the overall electrochemical response of the sensor therefore a bigger response is achieved.

A simulation approach was developed by Guo and Linder.[67] Figure 20 below shows this representation in which a sigmoidal shaped response is commonly associated with microelectrodes.

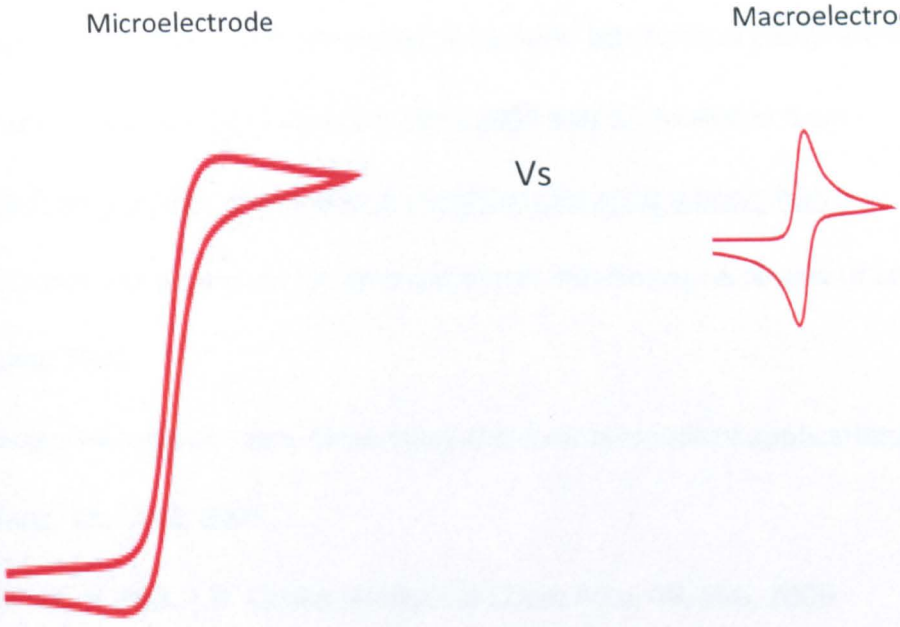

Figure 20. Represents the typical response obtained from microelectrodes and macroelectrodes and the difference in current value and peak measurement.[66]

The design of an electrode is therefore fundamental in terms of diffusion profile of the analyte. Simply adding more microelectrodes in a specific region in order to achieve the behaviour stated above and increase the current values is not necessarily the best approach since there is a limit factor, where the diffusion profiles of each of the microelectrodes could interfere with another electrode.

6.2 References:

1. Sensorland.com [internet]. Portal website: Sensors, The information centre for sensors and data systems; [updated 2011 May 1; cited 2011 September 4]. Available from http://www.sensorland.com
2. Engineershandbook.com [internet]. New York: Mechanical components: Introduction to sensors; [updated 2011 June 21; cited 2011 July 5]. Available from http://www.engineershandbook.com/Components/sensors.htm
3. Electrochemical sensors for environmental monitoring: A review of recent technology, J. Wang, 2003
4. Electrochemical sensors, biosensors and their biomedical applications, X.Zhang, H.Ju, J. Wang, **12**, 1141, 2007,
5. S. Park, H. Boo, T.D. Chung, Analytical Chem Acta, **46**, 556, 2006.
6. E.Bakker, Analytical Chemistry, **76**, 3285, 2004
7. Blood alcohol: Understanding quantitative blood alcohol testing in drunk driving cases, Michigan Bar Journal, 2003
8. Breathalyzeracloholtester.com [internet]. New Jersey: AlcoMeters: [updated 2011 June 1; cited 2011 June 25]. Available from http://www.breathalyzeralcoholtester.com/alcotector-fuel-cell-breathalyzer.html
9. M. Liu, J.J. Hu, T. Ma, S. Wang, H. Ding, Analytical Sciences, **27**, 839, 2011
10. I.M Vergas-Sansalvador, C. Fay, T. Phelan, M.D. Benito-Lopez, Analytical Chemica Acta, **216**, 699, 2011
11. Dynament.com [internet]. London: Gas sensor technology; [updated 2011 May 13; cited 2011 July 8]. Available from http://www.dynament.com/

12. Goindustrial.co.nz [internet]. New Zealand: Easy to operate alcohol and drug detectors: [updated 2011 April 26; cited 2011 June 3]. Available from http://www.goindustrial.co.nz/c/Draeger-Safety-Pacific-326851/Draeger-Alcohol-and-Drug-Detectors-p25230

13. N.A. Choudhry, D.K. Kampouris, R.O. Kadara, C.E Banks, Electrochem Comm. **6**, 12, 2010

14. J. Barek, J.C. Moreira, J. Zima, Sensors, **5**, 148, 2005

15. K.Y. Dong, J. Lee, D.J. Ham, J. Choi, I.S. Hwang, J.H. Lee, H.H. Choi, B.K. Ju, Inec 3rd International nanoelectronics conference, 2010

16. K. Peckova, J. Bareck, Current Organic Chem. **15**, 3014, 2011

17. J.H.T Luong, K.B. Male, J.D. Glennon, Analyst, **135**, 3008, 2010

18. P. Forsberg, E.O. Jorge, L. Nyholm, F. Nikolajeff, M. Karlsson, Diamond and related materials, **20**, 1121, 2011

19. A. Kraft, International journal of Electrochemical Science, **2**, 355, 2007

20. R.S. Balmer, J.R. Brandon, S.L. Clewes, H.K. Dhillon, J.M. Dodson, I. Friel, P.N. Inglis, T.D. Madgwick, M.L. Markham, T.P. Mollart, N. Perkins, G.A. Scarsbrack, D.J. Twitchen, A.J. Whitehead, J.J. Wilman, S.M. Wollard, Journal of Physics-Condensed Matter, **21**, 36422, 2009

21. Esainc.com [internet]. Sunnyvale, USA: ECD Innovations. [updated 2008 April 15; cited 2011 June 21]. Available at http://www.esainc.com/femtogram/spring08/ecdinnovations.shtml

22. Als-Japan.com [internet]. Tokyo: ALS – Electrochemical electrodes professional. [updated 2011 May 25; Cited 2011 June 11]. Available at http://www.als-japan.com/1037.html

23. A. Noorbakhsh, A. Salimi, Biosensors and Bioelectronics, **30**, 188, 2011

24. Y. Zhang, G.Y. Jin, W.X. Cheng, S.P. Li, Frontiers in Bioscience, **10**, 23, 2005

25. M. Noked, A. Soffer, D. Aurbach, Journal of Solid State Electrochemistry, **15**, 1563, 2011

26. K. Peckova, J. Barek, Current Organic Chemistry, **15**, 3014, 2011

27. T. Fofonoff, S. Martel, C. Wiseman, R. Dyer, I. Hunter, N. Hatsopoulos, J. Donoghue, 24th Annual International Conference of the Engineering in Medicine and Biology Society, 2002

28. B. Zhang, B. Stewart, Cold Spring Harbor Protocols, **201**, 5490, 2010

29. J.D. Guo, E. Linder, Anal. Chem. **81**, 130, 2009

30. Nanoshel.com [internet]. Delaware, USA: Nanotechnology company. [Updated 2011 July 2; cited 2011 July 23]. Available at http://www.nanoshel.com/buy-nanotubes.php

31. Craigbanksresearch.com [internet]. Manchester: Graphene electrochemistry. [Updated 2011 June 11; cited 2011 July 2]. Available at http://craigbanksresearch.com/page3.html

32. Dailymail.com [internet]. London: Online news resource. [Updated 2011 July 25; cited 2011 July 25]. Available at http://www.dailymail.co.uk/sciencetech/article-2018440/Worlds-thinnest-substance-graphene-power-generation-computers.html

33. S.V. Morozov, K.S. Novoselov, A.K. Geim, Physics-USPEKHI, **51**,744, 2008

34. K.S. Novoselov, A.K. Geim, Materials Technology, **22**, 178, 2007

35. K.S. Novoselov, A.K. Geim, Nature Materials, **6**, 183, 2007

36. X.L. Luo, A. Morrin, A.J. Killard, M.R. Smyth, Electroanalysis, **18**,319, 2006

37. Y. Yuan, J. Ahmed, L.H. Zhao, B. Zhao, S. Kim, Biosensors and Bioelectronics, **27**, 106, 2011

38. S.C. Nagure, S.S. Babu, B. Bhushan, A. Kumar, M. Mills, Acta Materialia, **59**, 6917, 2011

39. D. Papakostas, F. Rancan, W. Sterry, A. Vogt, Archives of Dermalogical Research, **303**, 533, 2011

40. S.K. Vashist, D. Zheng, K. Al-Rubeaan, J.H.T. Luong, F.S. Sheu, Analytica Chem. Acta, **703**, 124, 2011

41. Guardian.com [internet]. London: online news resource. [Updated 2011 October 17; cited 2011 October 17]. Available at http://www.guardian.co.uk/society/2011/oct/17/nhs-cuts-impact-on-patients-revealed

42. K.Peterson, J. Zapletalova, P. Kudlova, V. Matuskova, J. Bartek, D. Novotny, R. Chlup, Biomedical Papers – Olomouc, **153**, 47, 2009

43. I. Kusumi, K. Ito, K. Uemura, M. Honda, T. Hayashishita, K. Miyamato, Y. Kako, S. Tsuchida, N. Hashimoto, T. Koyama, Progress in neuro-psychopharmacology and biological psychiatry, **35**, 1922, 2011

44. H.Y. Cao, W.B. Shi, J.X. Xie, Y.M. Huang, Anal.Methods. **3**, 2102, 2011

45. Z.H. Rivera, E. Oosterink, L. Rietveld, F. Schoutson, L. Stolker, Anal. Meths. Acta. **700**, 114, 2011

46. W. Wang, W.Y. Wu, X.Q. Zhong, W. Wang, Q.A. Miao, J.J. Zhu, Biosensors and Bioelectronics, **26**, 3110, 2011

47. J.F. Jing, P.F. Li, J. Wang, Applied Mechanics and Mechanical Engineering, **29**, 896, 2010

48. I. Locher, G. Trosler, Textile Research Journal, **77**, 837, 2007

49. M. Mikuz, S.S. Turk, P.F. Traveer, Coloration Technology, **126**, 249, 2010

50. Dropsens.com [internet]. London: Screen-printed electrodes inc. [updated 2011 May 27; cited 2011 June 21]. Available at http://www.dropsens.com/en/screen_printed_electrodes_pag.html

51. Edaq.com [internet]. London: Kanichi Research Bismuth oxide electrodes. [updated 2011 June 12; cited 2011 June 27]. Available at http://www.edaq.com/product_details_page.php?product_no=ET095-20

52. London-displays [internet]. London: Advanced graphic design for science and technology. [Updated 2011 July 16; cited 2011 August 13]. Available at http://www.london-displays.com/screen-printing.htm

53. Pneac.org [internet]. London: National environmental assistance centre. [Updated 2011 August 21; cited 2011 August 31]. Available at http://www.pneac.org/printprocesses/screen/

54. K. Cao, K. Cheng, Z.L. Wang, 7th International Conference on Electronics Pacaging Technology, 320, 2006

55. C.J. Quintana, F. Arduini, A. Amine, F. Punzo, G. Destri, C. Bianchini, D. Moscone, Anal. Chem. Acta, **707**, 171, 2011

56. Defelsko [internet]. Fairfax, USA: Advanced screen printing through education and research. [updated 2011 June 14; cited 2011 September 2] Available at http://www.defelsko.com/applications/screen_printing/Screen-Printing.htm

57. T-shirtforums.com [internet]. Birmingham: Squeegee blade shapes and designs. [Updated 2011 August 21; cited 2011 September 7]. Available at http://www.t-shirtforums.com/screen-printing/t30727.html

58. M. Young, The influence of squeegee angle and its edge profile, Imagetek, 2001

59. C.E. Banks, R.G. Compton, Analyst, **15**, 131, 2006

60. C.E. Banks, R.G Compton, Anal. Sci. **21**, 1263, 2005

61. C. E. Banks, A. Crossley, C. Salter, S.J. Wilkins, R.G. Compton, Angew.Chem. Int.Ed. **45**, 2533, 2006

62. C.E. Banks, R.R. Moore, T.J. Davies, R.G. Compton, Chem.Commun. **16**, 1804, 2004

63. Newworldencyclopedia.org [internet]. Online article: Research group. [updated 2011 August 22; cited 2011 September 5]. Available at http://www.newworldencyclopedia.org/entry/Electroplating

64. Wikipedia.com [internet]. Online resource. [updated 2011 August 18; cited 2011 August 22]. Available at http://en.wikipedia.org/wiki/File:Sputtering.gif

65. Asdlib.org [internet]. Online resource: Analytical electrochemistry – the basic concepts. [updated 2011 June 20; cited 2011 August 7]. Available at http://www.asdlib.org/onlineArticles/ecourseware/Kelly_Potentiometry/PDF-5-MassTransport.pdf

66. F.Gao, L.Viry, M.Maugey, P.Poulin, N.Mano, *Nature. Commun.* **2,** 1032, 20102

67. S.J.Hood, D.K.Kampouris, R.O.Kadara, N.Jenkinson, F.J.Campo, F.Munoz, C.E.Banks, *Analyst*, **134,** 2301, 2009

68. R.S. Nicholson, I. Shain, Analytical Chemistry, **4,** 36, 1963

69. S. Griese, D.K. Kampouris, R.O. Kadara, C.E. Banks, Electrochem Commun, **10**, 1633, 2008

70. P.M. Hallam, C.E. Banks, Phys.Chem.Chem.Phys. **13**, 1210, 2011

71. C.V. Rao, B. Viswanathan, Journal of Colloid and Interface Science, **367**, 337, 2012

72. P.M. Hallam, B.L. Riehl, B.D. Riehl, C.E. Banks, RSC Advances, **1,** 93, 2011

73. X.B. Ji, C.E. Banks, G.Hu, A.Crossley, R.G. Compton, Electroanalysis, **18**, 2141, 2006

74. G.G. Wildgoose, C.E. Banks, H.C. Leventis, R.G. Compton, Microchimica Acta, **152,** 187, 2006

75. K. Zaghib, G. Nadeau, K. Kinishita, Journal of Power Sources, **97,** 103, 2001

76. D.A.C. Brownson, C.E. Banks, Phys.Chem.Chem. Phys. **13** 15825, 2011

77. D.A.C. Brownson, D.K. Kampouris, C.E. Banks, Journal of Power Sources, **196**, 4873, 2011

78. D.A.C. Brownson, C.E. Banks, Analyst, **136,** 2084, 2011

79. D.A.C. Brownson, C.E. Banks, Analyst, **44**, 2768, 2010

80. M.Eric, S. Richard, M. Donald, J. Cannon, Analytical Chemistry, **2**, 7, 2011

81. A.M. Maxam, W. Gilbert, Proc. Acad. Sci, **74**, 560, 1977

82. Basins.com [internet]. Online resource: Advanced linear sweep voltammetry systems. [updated 2011 July 26; cited 2011 August 11]. Available at http://www.basinc.com/mans/EC_epsilon/Techniques/CycVolt/cv.html

83. J. O'Mara, K.N. Amulya, Modern Electrochemistry, **2**, 1533, 2008

Chapter 7

Examples of Screen-Printed Electrodes

7.0 Next Generation Screen-Printed Electrochemical Platforms: Non-Enzymatic Sensing of Carbohydrates using Copper (II) Oxide Screen-Printed Electrodes

7.1 Abstract

In this chapter, the first example of a copper (II) oxide screen-printed electrode is presented which is characterised with microscopy and explored towards the electrochemical sensing of glucose, maltose, sucrose and fructose. It is shown that the non-enzymatic electrochemical sensing of glucose with cyclic voltammetry and amperometry is possible with low micro-molar up to milli-molar glucose concentrations readily detectable which compares competitively with nano-catalyst modified electrodes. The sensing of glucose shows a modest selectivity over maltose and sucrose while fructose is not detectable. An additional benefit of this approach is that metal oxides with known oxidation states can be incorporated into the screen-printed electrodes allowing one to identify exactly the origin of the observed electro-catalytic response which is difficult when utilising metal oxide modified electrodes formed via electro-deposition techniques which result in a mixture of metal oxides/oxidation states. These next generation screen-printed electrochemical sensing platforms provide a simplification over previous copper oxide systems offering a novel fabrication route for the mass production of electro-catalytic sensors for analytical and forensic applications. This work was published in *Analytical Methods* **1**, 183, 2009 and included contributions from Dimitrios Kampouris, Rashid O' Kadara, and Craig E. Banks.

7.2 Introduction

The pursuit of non-enzymatic glucose sensing is a vigorous and competitive area of research due to efficiencies. The development and fabrication of cost effective, simple, accurate, portable and rapid sensors for glucose are socially important, aiding diabetics who represent ~5% of the world population.[1] Additionally glucose sensing has applications in medical and food industries, biochemistry and glucose-oxygen fuel cells.[2, 3] A Related topic to this is the sensing of carbohydrates which finds widespread exploitation in analytical and forensic applications.[4] For example, carbohydrate content of tobaccos can distinguish between varieties which would enable, for example, the matching of an unknown tobacco found at a crime scene.[4, 5] Chromatography coupled with electrochemical detection is widely used and reported for carbohydrate sensing,[4] particularly in foodstuffs and determining food adulteration. The electrochemical oxidation of glucose is highly dependent on the chosen electrode and copper finds wide interest for the analysis of glucose, carbohydrates and amino acids.[6, 7] A range of electrode materials have been reported such as platinum, nickel, gold and silver for the sensing of carbohydrates but using these can be problematic due to poisoning/fouling of the electrode surface, especially at gold and platinum electrodes.[8] Additionally the cost of these precious metals needs to be considered. In comparison, cobalt and copper electrodes are reported to provide enhanced stability, with low detection limits and wide analytical ranges achievable.[9]

A range of advantageous approaches have been reported such as flower-shaped copper oxide nanostructures[10] and nanospheres[11] which are immobilised onto suitable electrode surfaces. In these cases and others where catalytic materials are simply immobilised onto an electrode surface, consideration needs to be given to surface stability. Other approaches

have reported amperometric glucose biosensors based on the dispersion of glucose oxidase (GOx) and copper oxide within a graphite paste composite.[12] A variant on paste electrodes are screen-printed electrodes. Screen-printed electrodes are produced by spreading a thixotropic fluid evenly across a mesh screen which defines the geometry of the desired electrode. The thixotropic fluid or ink contains a variety of substances such as graphite, carbon black, solvents and polymeric binder. The mesh screen is a negative of the desired shape or electrode and various screens are used to build up the desired designs. Copper-plated screen-printed electrodes have been reported for various analytes,[13, 14, 15] and in particular Jumar and Zen have reported Cu plated screen-printed carbon electrodes for the amperometric detection of hydrogen peroxide where glucose oxidase was immobilized on to the copper layer.[16]

In this thesis, we report the first example of a copper-oxide screen-printed electrode where micron-sized copper (II) oxide is incorporated within the surface of the screen-printed electrode. Such an electrode precludes the need for copper plating, greatly simplifying the electrode fabrication and provides a strategy for fabricating electrodes in large quantities. Copper (II) oxide screen-printed electrochemical sensing platforms have been tested for the non-enzymatic detection of carbohydrates, in particular, glucose sensing.

7.3 Experimental Section

All chemicals used were of analytical grade and were used as received without any further purification from Sigma Aldrich. These were: copper(II) oxide powder (<5 mm, 98%), glucose, sucrose, maltose, fructose (all ACS reagents), potassium chloride (>99.0%), potassium phosphate monobasic (>99%) and sodium hydroxide (> 99%). All solutions were prepared with deionised water of resistivity not less than 18.2 MΩ cm. A fresh solution of the chosen carbohydrate was prepared daily. Voltammetric measurements were carried out using a m-Autolab III (Eco Chemie, The Netherlands) potentiostat/galvanostat and controlled by Autolab GPES software version 4.9 for Windows XP. All measurements were conducted using a three electrode configureuration with a large surface area platinum wire as a counter and a saturated calomel electrode as the reference electrode. Connectors for the efficient coupling of the screen-printed electrochemical sensors were purchased from Kanichi Research Services Ltd (http://kanichi-research.com/). In amperometric experiments, convection was applied via the use of a stirrer plate and a magnetic stirring bar rotating at 6000 rpm. Screen-printed carbon electrodes were fabricated in-house with appropriate stencil designs using a microDEK 1760RS screen printing machine (DEK, Weymouth, UK). The surface topography was studied by surface profilometry (Dektak). The surface topography of each screen-printed electrode was measured by a Dektak ST stylus surface profilometer which has the capability of measuring step height down to a few nm. The Dektak is controlled by a PC running Windows with software offering several data processing functions as well as image capturing and storage. Scanning electron microscopy (SEM) images were obtained using a JEOL JSM-5600LV model.

7.4 Results and Discussion

7.4.1 Characterisation of the copper oxide screen-printed electrodes

Previously the fabrication of screen-printed electrodes[17, 18] has been reported and in this case, commercially purchased copper (II) oxide was mixed into the ink formulation prior to screen printing. This adversely affects the rheology of the ink which needs to be modified with organic solvents and the standard printing parameters that were previously used,[17, 18] need to be tailored to ensure an efficient printing process. Parameters that need to be monitored/tailored from adding in the copper (II) oxide are printing pressure, viscosity of the ink, dispersion of the metal oxide, time of drying and so on. Increasing amounts of copper (II) oxide were incorporated into the screen-printed electrodes over the range of 0 – 10% (M_P/M_I), where M_P is the mass of particulate and M_I is the mass of ink formulation used in the printing process. Figure. 7.1 depicts SEM images of the bespoke copper (II) oxide screen-printed electrochemical sensing platform where a 'webbed' appearance is evident.

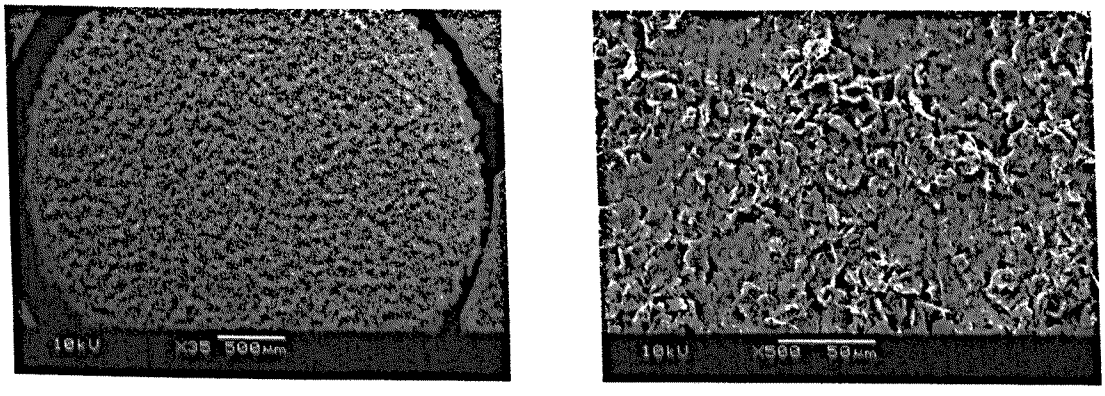

Figure 7.1: SEM images of a 5% copper-oxide screen-printed electrochemical sensing platforms

Analysis of the electrode surfaces was explored with profilometric analysis where R_a values, which are the arithmetical mean surface roughness (in microns), were measured for the 2, 5 and 10% (M_P/M_I) copper (II) oxide screen-printed electrode and found to correspond to 1.2, 1.8 and 2.5, respectively. In the absence of copper (II) oxide, the screen-printed electrodes have a *R*a value between 1–1.317 and clearly the introduction of the copper (II) oxide results in the electrode surface becoming more 'coarse' as the amount of copper (II) oxide is increased in the ink. It should be noticed that this surface roughness is critical since it defines the inherent reproducibility and electrochemical performance of the sensors. An additional benefit of using screen-printing technology is that the oxidation state of the copper can be readily controlled and changed, allowing users to easily identify exactly which oxidation states are responsible for their observed electrochemical response; this can sometimes be time consuming and not straight forward when metals and their inherent oxides are produced *in-situ* via electro-deposition. It has been reported that copper (or copper oxide) electrodes provide superior and enhanced sensitivity for carbohydrates. [19] In particular, Kano *et al.*[19] have shown for the electrochemical oxidation of glucose in sodium hydroxide, that copper(II) oxide modified electrodes are superior over copper (I) oxide modified electrodes; consequently we have focused on fabricating copper (II) oxide screen-printed electrodes and exploring their use towards glucose and associated compounds.

7.4.2 Electro-catalytic sensing of carbohydrates

Emphasis is turned to exploring the electrochemical sensing of carbohydrates using the copper(II) oxide screen-printed electrodes, with Figure. 7.2A depicting the voltammetric profiles resulting from the addition of glucose where a quantifiable peak is observed at ~ +0.6 V (vs. Ag/AgCl). Analysis of the peak height from glucose additions is shown in Figure. 2B where a linear response is observed over the range 100 mM to 500 mM, beyond which, the plot is observed to plateau. Based on this linear range (3 sigma) a limit of detection was found to correspond to 27 (±2) mM (I_H/A = 0.08 A M + 3.83 x 10^{-6} A; R^2 = 0.992).

The insert of Figure. 7.2A depicts the voltammetric response of the copper oxide screen-printed electrode in sodium hydroxide only, which is likely due to the electrochemical oxidation of copper(II) to copper(III).[20] The electrochemical performance of the copper oxide screen-printed electrode was explored in pH 7 for glucose detection but no significant response was observed supporting the inference that the copper(III) oxide serves as a catalyst in the electrochemical oxidation.[19]

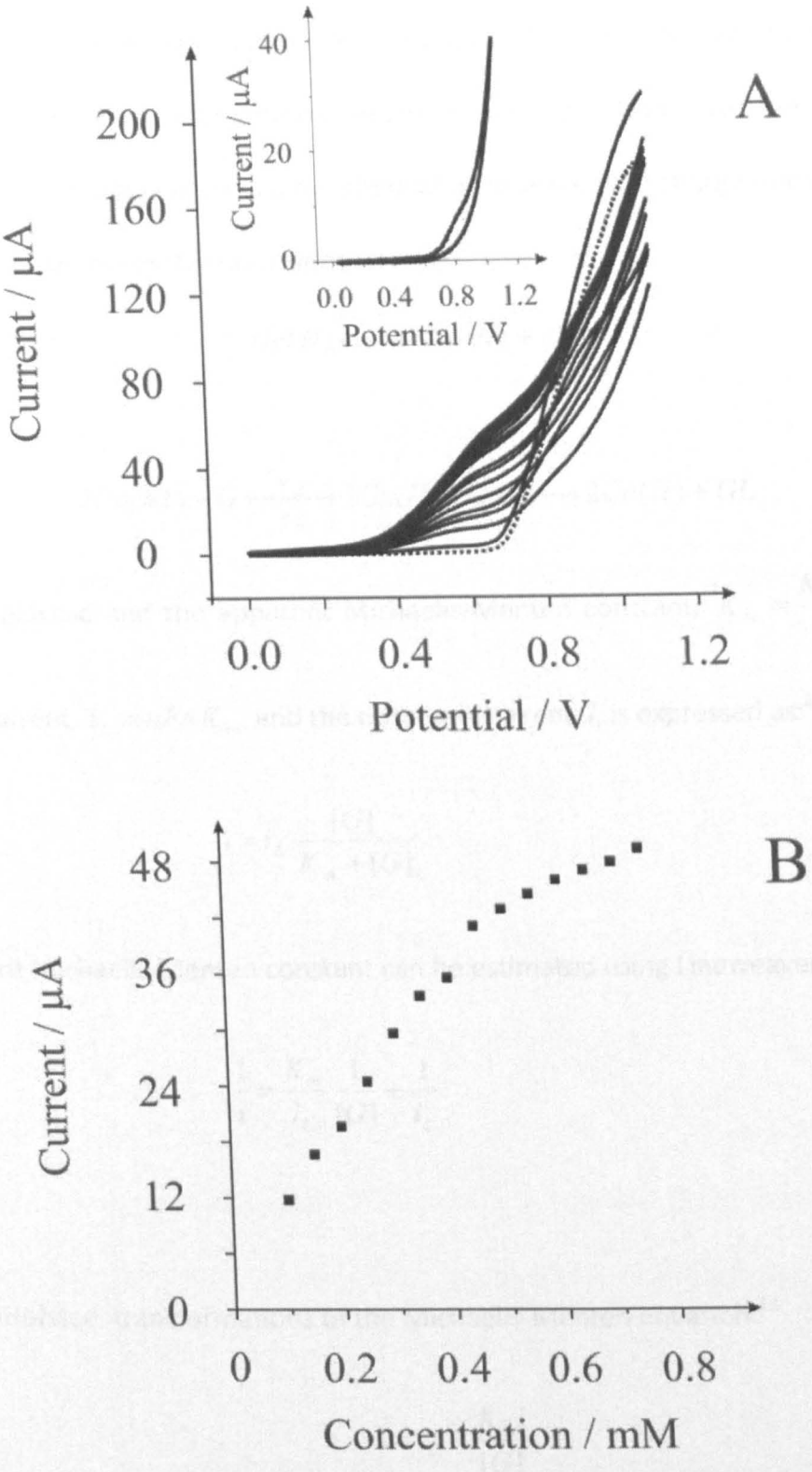

Figure 7.2. Cyclic voltammetric profiles (A) resulting from the addition of glucose into a 0.1 M NaOH solution using a 2% copper (II) oxide screen-printed electrochemical sensing platform. The insert of (A) is the response of the copper (II) oxide screen-printed electrode in 0.1 M NaOH. All scans recorded at 50 mVs^{-1}. The analysis of the peak height versus glucose additions is shown in (B).

Figure. 7.2B shows that at high glucose concentrations a Michaelis–Menten type[22] response is observed. The catalytic reaction for the electrochemical oxidation of glucose may be described by the formation and decomposition of an intermediate charge transfer complex, similar to that of Michaelis–Menten kinetics:

$$Cu(II) \longleftrightarrow Cu(III) + e^-$$

$$2Cu(III) + G \underset{K_{-1}}{\overset{K_{+1}}{\longleftrightarrow}} 2Cu(II)GL \xrightarrow{K_{+2}} 2Cu(II) + GL$$

Where G is glucose and the apparent Michaelis-Menten constant, $K_M = \frac{K_{-1} + K_{+2}}{K'_{+1}}$ .The maximum current, $i_L = nFAK_{+2}$ and the observed current, *i*, is expressed as:[21]

$$i = i_L \frac{[G]}{K_m + [G]}$$

The apparent Michaelis-Menten constant can be estimated using Lineweaver-Burke:[22]

$$\frac{1}{i} = \frac{K_m}{i_L}\frac{1}{[G]} + \frac{1}{i_L}$$

and Eadie-Hofstee transformations of the Michaelis-Menten equation:[23]

$$i = i_L - \frac{K_m i}{[G]}$$

where *i* is the observed current, i_L is the maximum current observed at high glucose concentration, [G] is the concentration of glucose, and K_m is the Michaelis-Menten rate constant. The average K_m was estimated to be 0.33 mM. The low value indicates a good

affinity of the copper (II) oxide microdomains and the glucose substrate. This value is comparable to those previously reported, such as zinc oxide nanowires modified with glucose oxidase[22] and with the reported value of 0.022 mM for a glassy carbon electrode modified with single walled carbon nanotubes, which in turn is modified with an ionic liquid, gold nanoparticles and glucose oxidase.[23]

The mechanism of the electrochemical oxidation of carbohydrates at copper (II) oxide electrodes according to Xie and Huber[24] involves the chemisorption of hydroxide ions on CuO surface lattices followed by oxidation of the hydroxide to a hydroxyl radical:

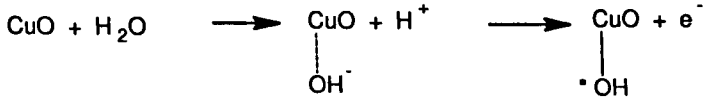

At adjacent lattice sites, the target analyte adsorbs onto the copper oxide surface:

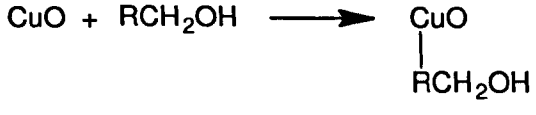

The rate determining step involves the formation of a bridge cyclic intermediate and the abstraction of a hydrogen atom from the carbon in the alpha position to the functional group:

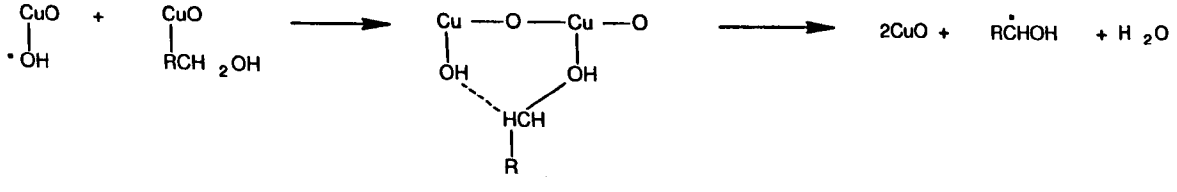

After abstraction, the analyte radical is rapidly oxidised to a carboxylate or other product [24].

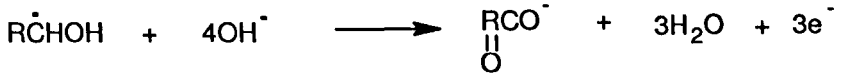

An alternative mechanism for the electrocatalytic oxidation of glucose at a copper oxide surface was later proposed by Kano *et al.*[19] as:

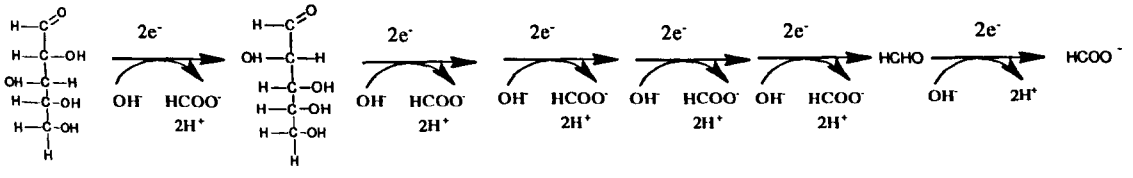

7.4.3 Amperometric detection of carbohydrates

Next, attention was turned to exploring the amperometric determination of glucose using the copper (II) oxide screen-printed electrodes. Figure 7.3 depicts the amperometric response obtained using a 5% copper (II) oxide screen-printed electrode from glucose additions over the range 50 μM up to 1200 μM. Two linear portions are clearly evident. The first is from 50 to 600 μM (I_H / A = 3.2 x 10^{-4} A/M + 3.3 x 10^{-8} A ; R^2 = 0.997) and the second from 650 to 1200 μM (I_H / A = 2.4 x 10^{-4} A/M + 7.5 x 10^{-8} A ; R^2 = 0.998). Based on the first linear part, the limit of detection (based on three sigma) was found to correspond to 4 μM.

This limit of detection is analytically competitive and compares to recent reports utilising dimethylglycoxime functionalized copper nanoparticles,[25] flower-shaped copper oxide nanostructures,[10] CuO nanorod modified electrodes,[26] and is superior over nickel

hydroxide modified carbon ionic liquid electrodes.[27] Since microdomains of copper (II) oxide are utilised, they comparable favourably to recent reports using nano-catalysts.

The amperometric detection of glucose was repeated using 2% and 10% copper oxide screen-printed electrodes. The response of the 10% copper oxide screen-printed electrode was observed to be highly un-reproducible with no stable response achievable. This is likely due to the reduction in the number of conductive pathways. Figure 7.4 depicts the response obtainable at a 2% copper (II) oxide screen-printed electrode where a linear response was obtained over the range 0.5 mM to 6 mM ($I_H / A = 3.2 \times 10^{-5} A/M + 3.3 \times 10^{-8} A$; $R^2 = 0.997$).

Clearly these approaches have potential for determining glucose levels in the range concerned with identifying hydroglycemia. While the 2% has a reduced sensitivity to glucose, this analytical response appears useful for extending the sensing range to higher glucose concentrations.

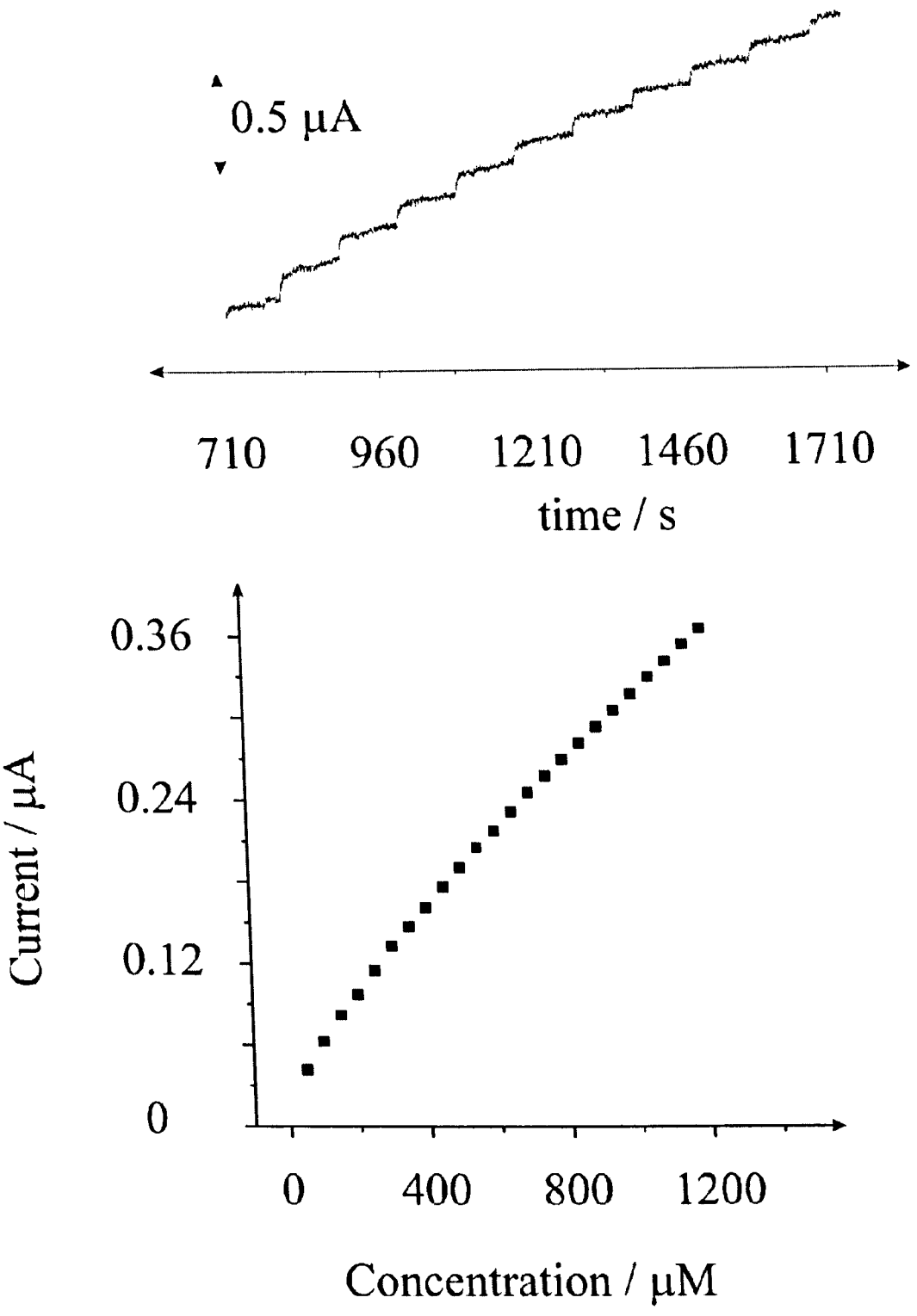

Figure 7.3: A typical amperometric response obtained at a 5% copper (II) oxide screen-printed electrochemical sensing platform resulting from 50 µM additions of glucose into a 0.1 M NaOH solution. The potential was held at + 0.6 V (vs. SCE). Also shown is the analysis of the current from the glucose additions.

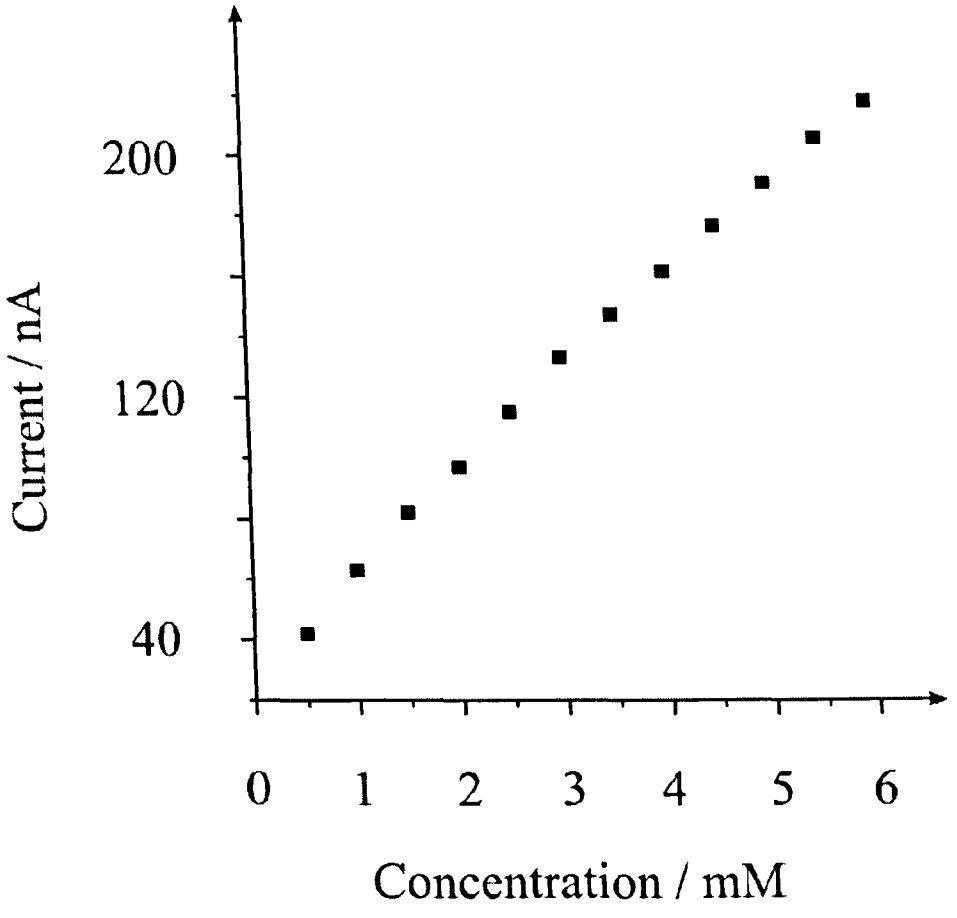

Figure 7.4. Calibration plot resulting from amperometry using a 2 % copper oxide screen-printed electrochemical sensing platform resulting from additions of glucose into a 0.1 M NaOH solution. The potential was held at + 0.6 V (vs. SCE).

Next, we turn to exploring the copper (II) oxide screen-printed electrode towards the sensing of other carbohydrates. Figure 7.5A depicts the cyclic voltammetric profiles obtained at the copper oxide screen-printed electrodes from the electrochemical oxidation of sucrose, maltose and fructose. No significant voltammetric response was observed for fructose while voltammetric profiles were observed at + 0.99 V and + 1.06 V for the maltose and sucrose (vs. SCE) respectively.

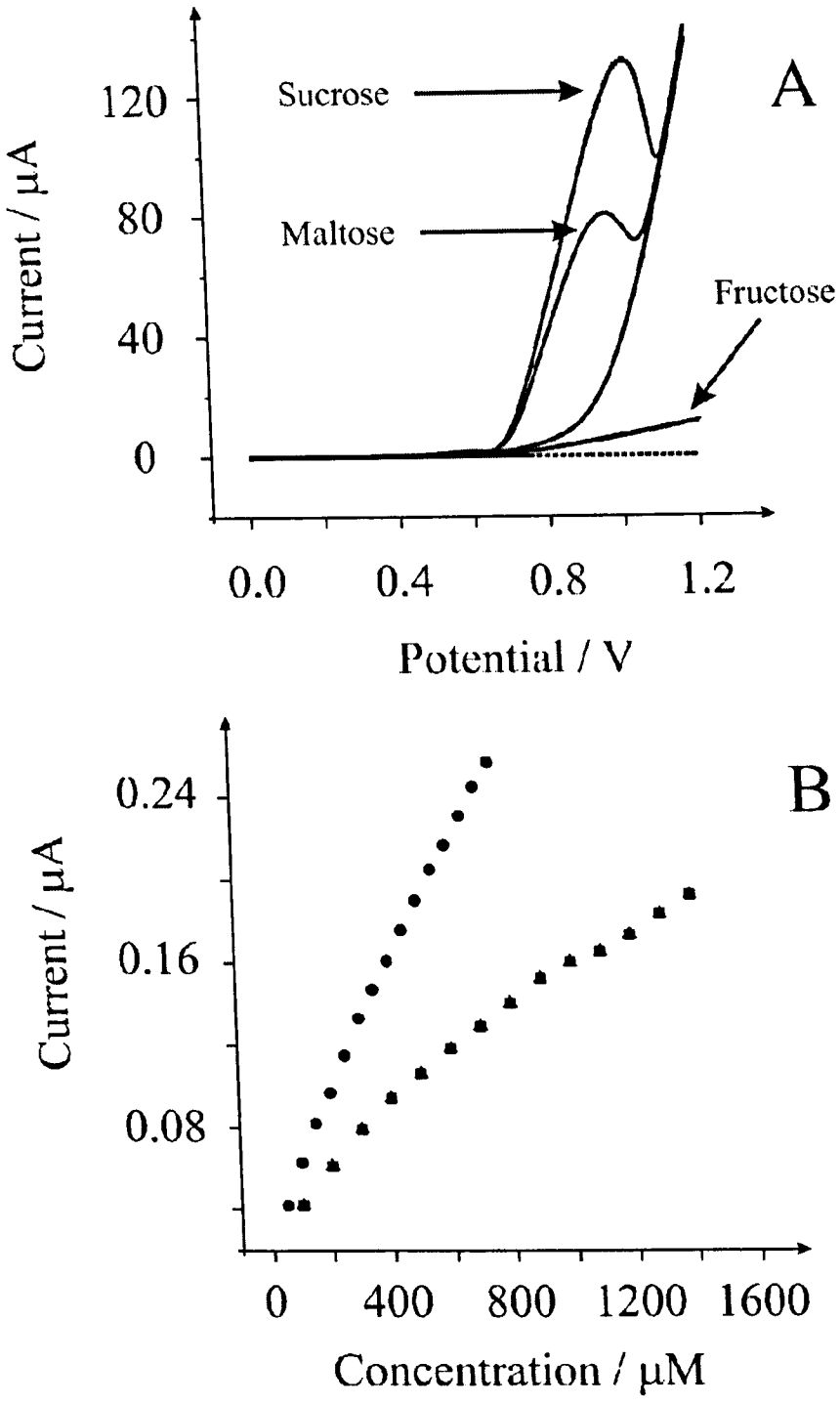

Figure 7.5A: Cyclic voltammetric profiles obtained using a 2% copper oxide screen-printed electrochemical sensing platform recorded in 0.1 M NaOH solution containing 1mM glucose, 1mM fructose, 1mM, maltose and 1mM sucrose. The dotted line is the screen-printed electrode in the absence of any carbohydrates. All scans recorded at 50 mVs^{-1}. Part (B) compares the amperometric response obtained for glucose (circles), sucrose (triangles) and maltose (diamonds). The potential was held at + 0.6 V (vs. SCE).

Figure 5B depicts the analysis from the amperometric measurements of glucose from holding the potential at +0.6 V. This was repeated for the case of sucrose and maltose which is found to have a reduced activity using the copper (II) oxide screen-printed electrode. Maltose, a disaccharide of two α -1,4- limited glucose units has been shown that the number of electrons transferred during the oxidation is surface oxide dependant where 'one unit' is easy to oxidise where to increase the number of electrons, a significant amount of oxide required.[20] While glucose is unaffected by the level of oxide, this suggests that disaccharides are sensitive to the micron sized copper (II) oxide domains. Based on this response the copper oxide domains allow a modest selective sensing of glucose over other carbohydrates.

7.5 Conclusions

The first example of a copper (II) oxide screen-printed electrode is reported which has been characterised with microscopy and explored towards the non-enzymatic sensing of glucose. This next generation screen-printed electrochemical sensing platform provides a simplification over previous copper oxide systems and provides a novel fabrication route for producing inexpensive, sensitive sensors which can be readily mass-produced. In comparison to other analytical systems, the screen-printed electrodes which contain micron-sized copper (II) oxide particles compares favourably with electrode modified with nano-catalysts allowing low micro-molar up to milli-molar glucose to be readily detected. Additionally, we envisage that the use of such an electrode can be used in conjugation with chromatography precluding the need for electrode polishing/re-generation between measurements.

This approach is beneficial over systems where the electro-deposition of copper is undertaken as this can result in differing copper oxidation states and the underlying catalytic mechanism may not be easily de-convoluted. In contrast, screen-printed electrodes can be readily fabricated with copper (II) oxide and copper (I) oxide and explored with the analytical target to fully understand the underlying (electro) chemical processes.

We note that copper oxide finds use in other areas such as supercapacitors,[27] cyclohexanol oxidation,[28] lithium-ion batteries,[29] nitrite,[30] , amikacin[31] and sulfite detection[32] and we expect that our copper oxide screen-printed electrochemical sensing platforms can be beneficially utilised in such areas.

7.6 References

1. Heller, A. and B. Feldman, Electrochemical glucose sensors and their applications in diabetes management. Chemical Reviews, **108**, 2482, 2008.
2. Lin, J.H., C. Zhao, Y. Zhang,S., Sens.Actuators B, **137**, 768, 2009..
3. Tominaga, M., Y. Taema, and I. Taniguchi, Electrocatalytic glucose oxidation at bimetallic gold-copper nanoparticle-modified carbon electrodes in alkaline solution. Journal of Electroanalytical Chemistry, **624**, 8, 2008.
4. Oshea, T.J., S.M. Lunte, and W.R. Lacourse, detection of carbohydrates by capillary electrophoresis with pulsed amperometric detection. Analytical Chemistry, **65**, 948, 1993..
5. Zook, C.M., Characterization of tobacco products by high-performance anion exchange chromatography-pulsed amperometric detection. Journal of Agricultural and Food Chemistry, **44**, 1773, 1996.
6. Luo, P.F., F.Z. Zhang, and R.P. Baldwin, constant potential amperomtric detection of underivatised amino-acids and peptides at a copper electrode. Analytical Chemistry, **63**, 1702, 1991.
7. Nagy, L., G. Nagy, and P. Hajos, Copper electrode based amperometric detector cell for sugar and organic acid measurements. *Sensors and Actuators B-Chemical*, **76**, 494, 2001.
8. LaCourse, W.R., Grushka, E., and Grinberg, N., Advances in Pulsed Electrochemical Detection for Carbohydrates, Advances in Chromatography, Taylor & Francis Group: Boca Raton. **47**, 247, 2009.

9. Male, K.B., Electrochemical detection of carbohydrates using copper nanoparticles and carbon nanotubes. Analytica Chimica Acta, **516**, 35, 2004.

10. Umar, A., Enzymatic glucose biosensor based on flower-shaped copper oxide nanostructures composed of thin nanosheets. Electrochemistry Communications, **11**, 278, 2009..

11. Reitz, E., CuO Nanospheres Based Nonenzymatic Glucose Sensor. Electroanalysis, **20**, 2482, 2008.

12. Luque, G.L., M.C. Rodriguez, and G.A. Rivas, Glucose biosensors based on the immobilization of copper oxide and glucose oxidase within a carbon paste matrix. Talanta, **66**, 467, 2005.

13. Zen, J.M., H.H. Chung, and A.S. Kumar, Flow injection analysis of hydrogen peroxide on copper-plated screen-printed carbon electrodes. Analyst, **125**, 1633, 2000.

14. Zen, J.M., Photoelectrochernical oxygen copper-plated screen-printed sensor using carbon electrodes. Analytical Chemistry, **74**, 6126, 2002.

15. Tsai, D.M., A capillary electrophoresis end-column amperometric detection system incorporating disposable copper-plated screen-printed carbon electrodes. Journal of the Chinese Chemical Society, **52**, 773, 2005.

16. Kumar, A.S. and J.M. Zen, Electrochemical investigation of glucose sensor fabricated at copper-plated screen-printed carbon electrodes. Electroanalysis, **14**, 671, 2002..

17. Kadara, R.O., N. Jenkinson, and C.E. Banks, Characterisation of commercially available electrochemical sensing platforms. Sensors and Actuators B-Chemical, **138**, 556, 2009.

18. Kadara, R.O., R.O., N. Jenkinson, and C.E. Banks, Manufacturing electrochemical platforms: Direct-write dispensing versus screen printing. Electrochemistry Communications, **10**, 1517, 2008.

19. Kano, K, Electrocatalytic oxidation of carbohydrates at copper(II)-modified electrodes and its application to to flow-through detection. Journal of Electroanalytical Chemistry, **372**, 137, 1994.

20. Torto, N., T. Ruzgas, and L. Gorton, Electrochemical oxidation of mono- and disaccharides at fresh as well as oxidized copper electrodes in alkaline media. Journal of Electroanalytical Chemistry, **464**, 252, 1999.

21. Ju, H.X. and D. Leech, Os(bpy)(2)(PVI)(10)Cl Cl polymer-modified carbon fiber electrodes for the electrocatalytic oxidation of NADH. Analytica Chimica Acta, **345**, 51, 1997.

22. Zang, J.F., Tailoring zinc oxide nanowires for high performance amperometric glucose sensor. Electroanalysis, **19**, 1008, 2007.

23. Gao, R.F. and J.B. Zheng, Amine-terminated ionic liquid functionalized carbon nanotube-gold nanoparticles for investigating the direct electron transfer of glucose oxidase. Electrochemistry Communications, **11**, 608, 2009.

24. Xie, Y.Q. and C.O. Huber, electrocatalysis and amperometric detection using an electrode made of copper-oxide and carbon paste. Analytical Chemistry, **63**, 1714, 1991.

25. Xu, J.Z., Nano-sized copper oxide modified carbon paste electrodes as an amperometric sensor for amikacin. Analytical Letters, **36**, 2723, 2003.

26. Safavi, A., N. Maleki, and E. Farjami, Fabrication of a glucose sensor based on a novel nanocomposite electrode. Biosensors & Bioelectronics, **24**, 1655, 2009.

27. Patake, V.D., Electrodeposited porous and amorphous copper oxide film for application in supercapacitor. Materials Chemistry and Physics, **114**, 6, 2009.

28. Hasanzadeh, M., A study of the electrocatalytic oxidation of cyclohexanol on copper electrode. Catalysis Communications, **10**, 295, 2008.

29. Gao, S.Y., Green Fabrication of Hierarchical CuO Hollow Micro/Nanostructures and Enhanced Performance as Electrode Materials for Lithium-ion Batteries. Journal of Physical Chemistry C, **112**, 19324, 2008.

30. Sljukic, B., Copper oxide - Graphite composite electrodes: Application to nitrite sensing. Electroanalysis, **19**, 79, 2007.

31. Xu, Q., Preparation of functionalized copper nanoparticles and fabrication of a glucose sensor. Sensors and Actuators B-Chemical, **114**, 379, 2006.

32. Kiattipoomchai, M., Measurement of sulfite at oxide-coated copper electrodes. Analyst, **123**, 2017, 1998.

Chapter 8

8.0 Disposables Highly Ordered Pyrolytic Graphite-Like Electrodes: Tailoring the Electrochemical Reactivity of Screen-Printed Electrodes

8.1 Abstract

In this chapter, it has been demonstrated that the electron transfer properties of disposable screen-printed electrodes can be readily tailored via the introduction of a polymeric formulation into the ink used to fabricate these electrochemical platforms. This approach allows the role of the binder on the underpinning electrochemical properties to be explored and allows the electrochemical reactivity of the screen-printed electrodes to be tailored from that of edge plane to basal plane of highly ordered pyrolytic graphite. *This work was published in Electrochemistry Communications* ***12****, 6, 2010* and included contributions from Dimitros Kampouris and Craig E. Banks.

8.2 Introduction

Carbon-based materials are extensively used in electrochemistry and are used in a plethora of applications [1, 2, 3, 4]. Understanding the underpinning electrochemical properties of these materials is widely recognised[5] but are largely overlooked. The available carbon materials are characterised by the dimensions of the crystallites comprising the material and have key structural factors which is the average graphite crystallite size (or lateral grain size), L_a, and L_c, which is the interplanar crystallite size perpendicular to the graphene planes. Highly ordered pyrolytic graphite (HOPG) has the largest L_a value of the order of ~ 1 μm with an L_c value of 10 μm. Different graphite materials have differing values of L_a and L_c which are the smallest for amorphous carbon, glassy carbon and carbon black[5]. To understand the

reactivity of carbon electrodes, well defined and controllable graphite surfaces are employed such as that of HOPG. These graphitic materials consist of atomically flat basal plane graphite terraces separated by steps and defects exposing the edge of the graphite layers which have an interlayer spacing of 0.335 nm [2, 5, 6, 7]. Through applying the use of edge plane and basal plane pyrolytic graphite electrodes the electrochemical reactivity of the ever popular carbon nanotubes was shown to be due to edge plane like defects/sites which occur at the ends and along the axis of the tubes[7]. HOPG has the advantage that by cleaving the electrode surface, the proportion of edge plane sites can be increased or decreased.[7] This is a significant advantage as it is useful for extracting mechanistic information and by using an HOPG with a low proportion of edge plane like – sites/defects, the electrode can be modified with electro-catalytic materials such as carbon nanotubes and nano-particles precluding the contribution of the underlying electrode to the observed voltammetric response.[7, 8, 9, 10] Elegant work by Compton and co-workers has shown by covering basal plane terraces of HOPG with a passivating polymer that the contribution to the voltammetric response is negligible with electrochemical reactions at edge plane graphite being anomalously fast[6]. Extreme situations can occur when this is not the case and it has been shown that by slowing the rate of diffusion by applying a Nafion coating to HOPG, electron transfer at basal plane terraces of HOPG can become significant[11]. Another carbon-based electrode that is often used in a range of electroanalytical situations is screen-printed electrodes[12]. The screen printing of electrochemical sensing platforms is alluring due to its reproducibility, simplicity and ability to produce large volumes at an economical cost. Screen-printed electrochemical platforms provide excellent platforms for modification with various nano-particles and materials and require no pre-treatment such as electrode polishing or electrode pre-treatment as is common with other electrode materials. While

these electrodes find widespread usage,[13, 14, 15, 16, 17] the fundamental understanding of the electrochemical reactivity at these electrodes is seldom studied. For the work reported herein, we identify the role of edge plane like – sites/defects in screen-printed electrodes with cyclic voltammetry and show for the first time how the heterogeneous transfer rate can be readily tailored allowing the electrochemical reactivity to be controlled.

8.3 Experimental Section

All chemicals used were of analytical grade and were used as received without any further purification from Sigma–Aldrich. All solutions were prepared with deionised water of resistivity not less than 18.2 MΩ cm. Voltammetric measurements were carried out using a l-Autolab III (Eco Chemie, The Netherlands) potentiostat/galvanostat and controlled by Autolab GPES software version 4.9 for Windows XP. All measurements were conducted using a three electrode configureuration with a platinum wire as the counter and a SCE as the reference electrode. Screen-printed carbon electrodes were fabricated in-house with appropriate stencil designs using a microDEK 1760RS screen printing machine (DEK, Weymouth, UK). A carbon–graphite ink formulation previously utilised [18] was first screen-printed onto a polyester flexible film (Autostat, 250 lm thickness). This layer was cured in a fan oven at 60°C for 30 min. Next a silver/silver chloride reference electrode was included by screen printing Ag/AgCl paste (Gwent Electronic Materials Ltd., UK) on to the plastic substrate. Last a dielectric paste ink (Gwent Electronic Materials Ltd., UK) was printed to cover the connection and define the 3 mm diameter graphite working electrode. After curing at 60°C for 30 min the screen-printed electrode is ready to use. This procedure was repeated with the initial carbon–graphite ink formation modified with increasing

proportions of a polymeric binder[19], poly(vinyl chloride), which is mixed into the ink formulation over the range of 0–80% (M_B/M_I), where M_B is the Mass of the polymeric binder and M_I is the Mass of ink formulation used in the printing process. Scanning electron microscopy (SEM) images were obtained using a JEOL JSM-5600LV model.

8.4 Results and Discussion

Figure 8.1A and C depicts SEM images of a standard electrode surface which has a 'webbed' aspect. In these electrodes, powdered graphite which has values between 100 and 1000 Å for both L_a and L_c is used along with a small proportion of carbon black and the polymeric formulation which is used to bind the components together.

The graphite used has L_a and L_c values similar to that of pyrolytic graphite but due to the other components, a slower electron transfer rate is observed compared to an electrode material comprised solely of pyrolytic graphite. Shown in Figure 8.1B and D is a 40% (M_B/M_I) modified electrode. Instantly one can observe that the electrodes surface consists of discrete domains of graphite and polymeric binder, the latter is observed in the top and bottom of Figure 8.1D. It is found that increasing the amount of binder introduced into the ink formulation greatly increases the proportion of polymeric domains. Additionally this 'fills' in the gaps between the graphite which is observed on comparison of Figure 8.1C and E which will reduce the number of conductive pathways through the electrode surface (see later). Note that the white spots in Figure 8.1E are artefacts from electrolyte (salt) deposits which are from using the electrodes in the test redox system, which we now turn to exploring. The voltammetric performance of these screen-printed electrochemical platforms

were explored in 1 mM $[Ru(NH_3)_6]^{3+}$/1 M KCl. Figure. 8.2 illustrates five cyclic voltammograms recorded at 0.5 V s^{-1}.

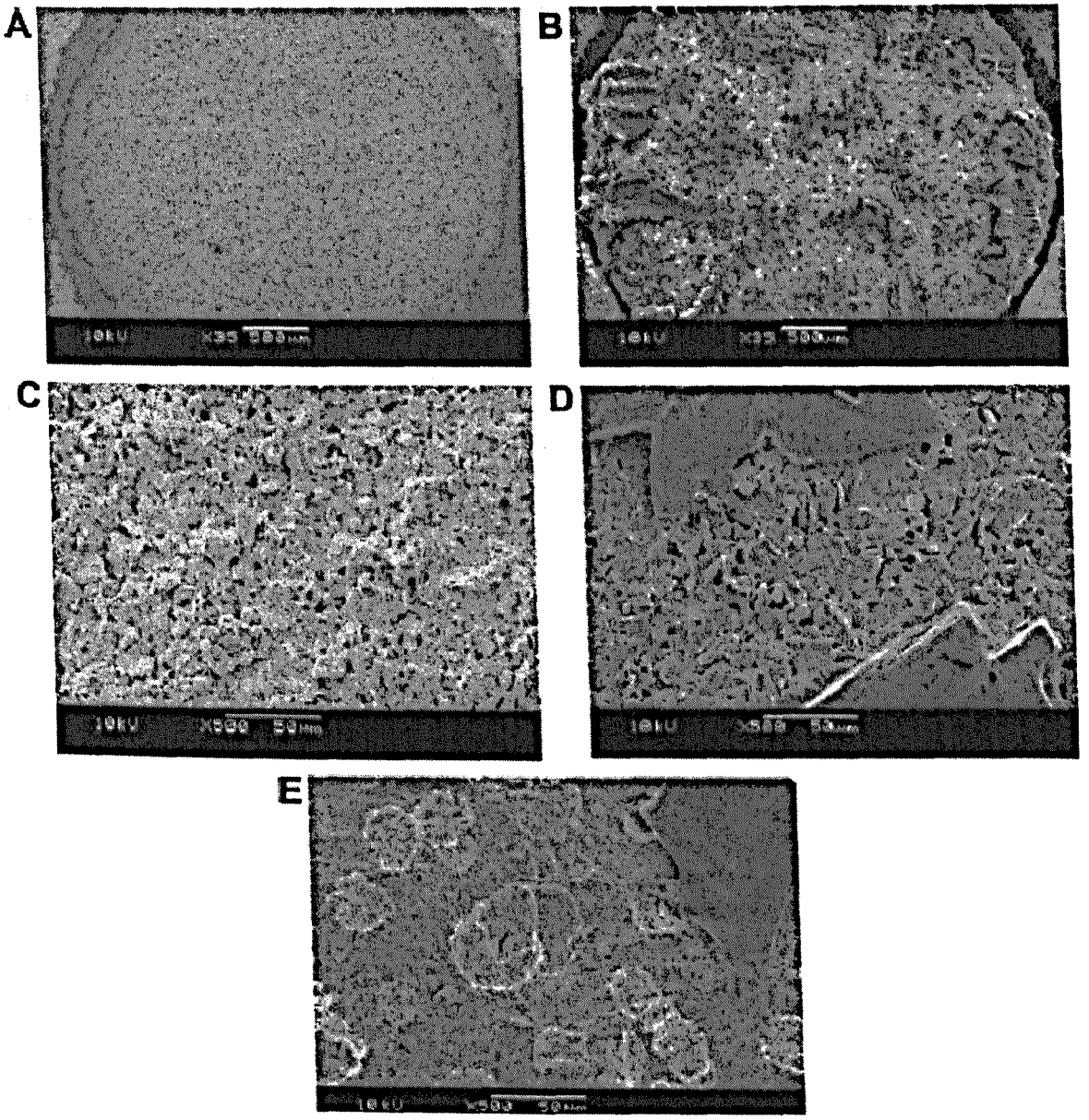

Figure 8.1. SEM images of the screen-printed electrochemical platforms of the bare unmodified (A and C) with that of a 40% (M_B/M_I) modified (B and D) and 80% (M_B/M_I) (E) electrochemical platform.

Due to the difference in surface area between the electrochemical platforms, which is due to the change in surface geometry through introducing the polymeric binder, the y axis is represented by *I/Ip* for comparative purposes. Clearly in Figure 8.2, introducing the polymeric binder has a profound affect on the cyclic voltammetric profiles. As the binder is introduced, the resistance of the electrodes is slightly increased as evidenced in the non-faradaic currents on the cyclic voltammetry.

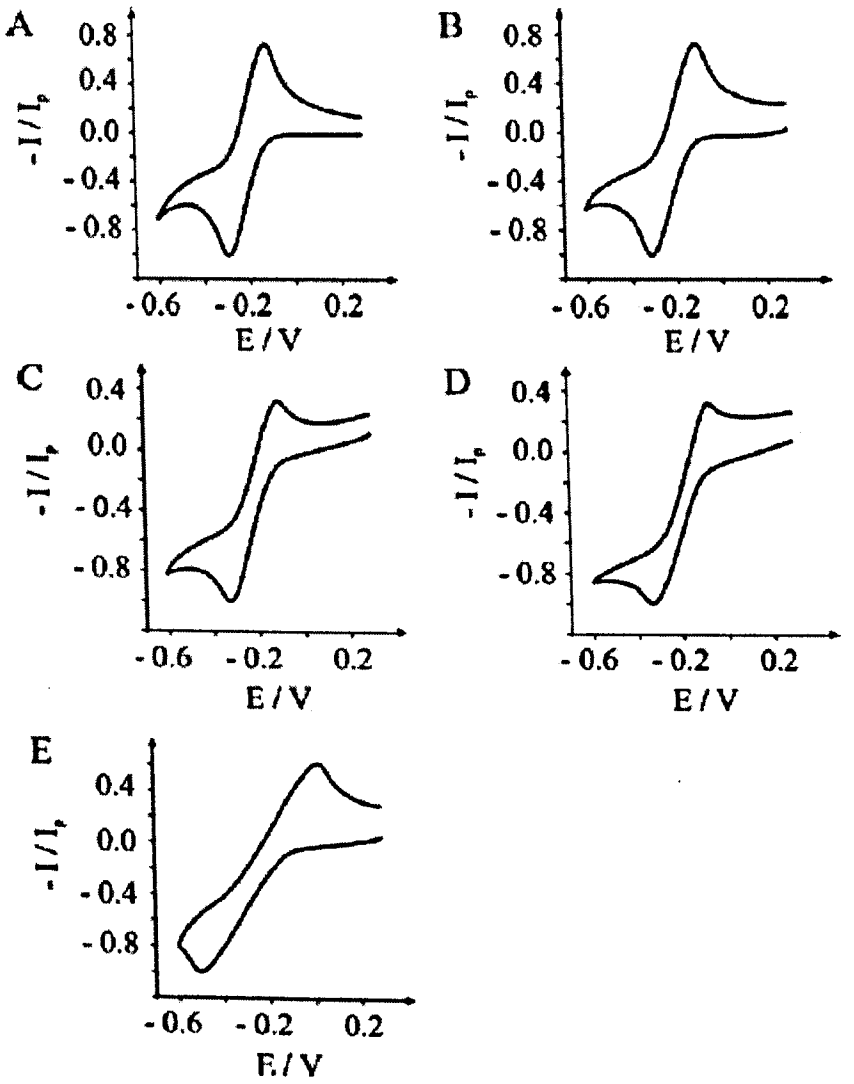

Figure 8.2. Cyclic voltammetric profiles for the reduction of 1 mM $[Ru(NH_3)_6]^{3+}$/1 M KCl at differing % (M_B/M_I) screen-printed electrodes: (A) 0%, (B) 20%, (C) 40%, (D) 60%, and (E) 80%. All scans recorded at 0.5 V s^{-1} vs. SCE.

The corresponding fit of the electrochemical platforms with a numerical simulation package allows the effective electron transfer rate constant, k^0_{eff} to be deduced. Note that no compensation ohmic drop was applied in accordance with previous studies.[20] Figure. 8.3 depicts the effect of increasing the amount of polymeric formulation in the ink on the effective electron transfer rate constant; this term is used since the screen-printed electrode consists of basal plane, edge plane and polymeric domains.

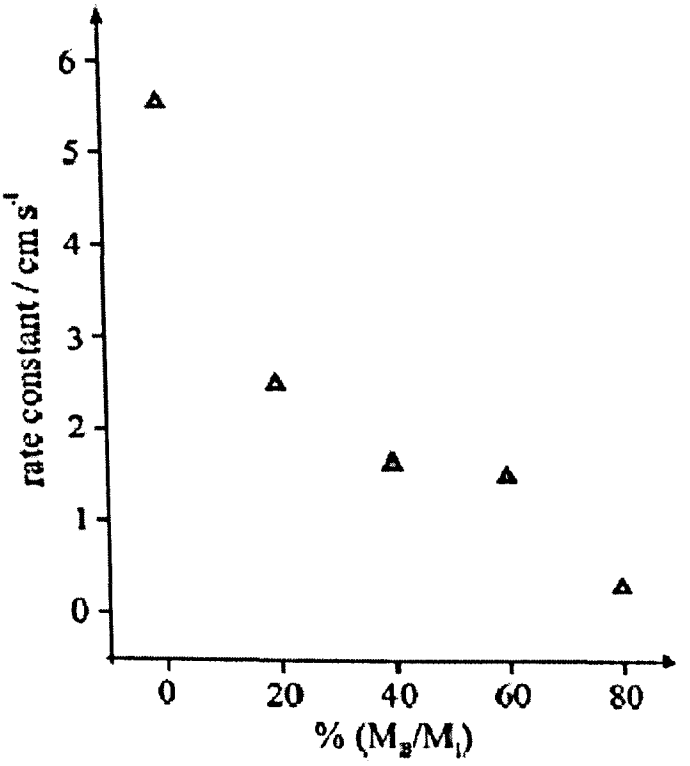

Figure 8.3. Plot of heterogeneous electron transfer rate constant as a function of % (M_B/M_I).

Clearly a reduction in the effective electron transfer rate constant is observed which is likely due to the increment in polymeric domains and the reduction in conductive pathways and changing the percolation nature of the electrode structure. The effect of binder on the electron transfer rates of screen-printed electrodes, to our knowledge, has never been

investigated. The global coverage of edge plane defects (H^{edge}) on the electrochemical platform can be approximated from the following relationship:

$$K^0_{eff} = \theta_{edge} K^0_{edge} \qquad (1)$$

Analysis of the electron transfer rate of edge plane of highly ordered pyrolytic graphite ($k0_{edge}$) with a commercial simulation package has reported a value of 0.4 cm s^{-1}.[6, 20] Using this value, the deduced coverage of edge plane defects was found to be 5.5%, 2.5%, 1.6%, 1.5% and 0.3% for 0%, 20%, 40%, 60% and 80% (M_B/M_I), respectively; thus the electron transfer rate of screen-printed electrode surface can be readily tailored. These % values agree well with that previously reported for highly ordered pyrolytic graphite which can be over the range of 1–10% depending on surface preparation[6, 20] indicating that we have fabricated disposable highly ordered pyrolytic graphite-like electrodes. The cyclic voltammetric (I–E) response observed at a screen-printed electrochemical platform from various contribution components may be described by the following:

$$I - E_{SPE} = \beta [I - E_{basal}] + \Upsilon[I - E_{binder}] + \varepsilon [I - E_{edge}] \qquad (2)$$

It has been shown that due to nonlinear diffusion over an electrode surface, the individual contributions of edge and basal plane graphite do not scale with relative areas[6]. In Eq. (2) b, c and e are complicated functions that take into account the relative areas and sizes of the two electrode materials as well as the contribution from nonlinear diffusion[6]. It has been conveniently demonstrated for electroactive species with diffusion coefficients of ~1x10^{-6} cm^2 s^{-1} and greater, there is no contribution from basal plane terraces.[6]

Additionally in this work, we have demonstrated that the polymeric formulation used in ink formulations is electrochemically inert and does not contribute to the cyclic voltammetric response but allows for a convenient methodology for modifying the electrochemical reactivity of screen-printed electrochemical platforms. Thus Eq. (2) reduces to Eq. (3) and describes cyclic voltammetry observed at screen-printed electrodes:

$$I - E_{SPE} = \varepsilon [I - E_{edge}] \qquad (3)$$

8.5 Conclusions

To conclude, previously the understanding of the electrochemical performance of screen-printed electrodes has not been reported. This work shows that the polymeric formulation used to construct the electrodes has no contribution to the electrochemical response of a screen-printed electrode. It is also demonstrated that the electrochemical reactivity of screen-printed electrodes can be readily tailored such that basal plane like disposable electrodes, that is, electrodes with a low proportion of edge-plane like – sites/defects can be readily produced. Given the cost of HOPG which can be tailored through cleaving the surface against that of disposable electrodes, it is anticipated that these tailored screen-printed electrodes will become widely used as a convenient and economical electrode alternative to basal plane pyrolytic graphite electrodes. For example, having a convenient electrode-to-hand allows one to readily explore and understand the role of basal vs. edge in electrochemical experiments which are of fundamental and applied use; these new type of electrodes will allow researchers to design efficient and intelligent electrodes for a plethora of applications.

8.6 References

1. A.K.M. Kafi, G. Wu, A. Chen, Biosens. Bioelectron. **24**, 566, 2008.
2. C.E. Banks, R.G. Compton, Analyst **131**, 15, 2006.
3. R.G. Compton, J.S. Foord, F. Marken, Electroanalysis **15**, 1349, 2003.
4. D.W.M. Arrigan, Analyst **129**, 1157, 2004.
5. R.L. McCreery, Chem. Rev. **108**, 2646, 2008.
6. T.J. Davies, M.E. Hyde, R.G. Compton, Angew. Chem. **117**, 5251, 2005.
7. C.E. Banks, T.J. Davies, G.G. Wildgoose, R.G. Compton, Chem. Commun. **103**, 829, 2005.
8. R.R. Moore, C.E. Banks, R.G. Compton, Anal. Chem. **76**, 2677, 2004.
9. G.G. Wildgoose, H.C. Leventis, R.G. Compton, Microchim. Acta **152**, 187, 2006.
10. I. Streeter, G.G. Wildgoose, L.D. Shao, R.G. Compton, Sens. Actuators B **133**, 462, 2008.
11. M.A. Edwards, P. Bertoncello, P.R. Unwin, J. Phys. Chem. C **113**, 9218, 2009.
12. O.D. Renedo, M.A. Alonso-Lomillo, M.J.A. Martinez, Talanta **73**, 202, 2007.
13. S.C. Wang, K.S. Chang, C.J. Yuan, Electrochim. Acta **54**, 4937, 2009.
14. J. Cai, K. Cizek, B. Long, K. McAferty, C.G. Campbell, D.R. Allee, B.D. Vogt, J. La Belle, J. Wang, Sens. Actuators B **137**, 379, 2009.
15. C.O. Parker, I.E. Tothill, Biosens. Bioelectron. **24**, 2452, 2009.
16. E. Kazimierska, M. Muchindu, A. Morrin, E. Iwuoha, M.R. Smyth, A.J. Killard, Electroanalysis **21**, 595, 2009.
17. J. Wang, G. Chen, M.P. Chatrathi, M. Wang, R. Rinehart, A. Muck, Electroanalysis **20**, 2416, 2008.

18. R.O. Kadara, N. Jenkinson, C.E. Banks, Sens. Actuators B **138**, 556, 2009.

19. T.J. Davies, R.R. Moore, C.E. Banks, R.G. Compton, J. Electroanal. Chem. **574**, 123, 2004.

Chapter 9

9.0 Screen-Printed Electrodes Provide Micro-Domain Sites for Fabricating Disposable Electro-Catalytic Ensembles

9.1 Abstract

Building on the fundamental screen-printing concept, attention is turned to bespoke screen-printed electrodes which are basal plane-like in nature can be used as a template to produce randomly dispersed electro-catalytic micro-domains for analytical sensing purposes. Proof-of-concept is shown for the case of copper ensembles for nitrate detection and palladium ensembles for hydrazine sensing. The advantageous disposable nature of the ensemble precludes the need of pre-treatment between measurements. The screen-printed ensembles act as excellent substrates for the deposition of a range of metals allowing the screen-printed electrodes to act as a template for micro-domain ensembles of many different electrode materials for a variety of analytical challenges.

*This work was published in Electrochemistry Communication, 2010, **12**, 406 and included contributions from Rashid O' Kadara and Craig E. Banks.*

9.2 Introduction

One of the key questions in electrochemistry is which electrode should one use? When choosing an electrode substrate there are many compelling reasons to select an array of microelectrodes over a single macroelectrode; the increased mass transports results in an improved signal-to-noise ratio and reduced double layer capacitance with large and easily quantifiable signatures allowing lower analytical detection limits and ranges. Additionally the careful choice of the electrode material permits the electro-catalysis of the target analyte.[1, 2, 3] All these unique properties make microelectrode arrays attractive for the trace analysis of target analytes. For example, it has been shown that boron-doped diamond microelectrode arrays can act as a versatile substrate onto which many different types of electro-catalytic materials may be electro-deposited which exhibits beneficial electro-analytical properties.[4] Interestingly, numerical simulations have shown that a random array, of equal macroscopic coverage, can match the voltammetric response of the regular array[5] suggesting that the response of an array, which can be costly and expensive to design and manufacture, can be conveniently replaced with a random dispersion of suitable electro-catalytic material on a electrode surface. Recently, we have demonstrated that the electron-transfer properties of disposable screen-printed electrodes can be readily tailored by manipulating the amount of polymeric formulation in the ink used to fabricate the electrochemical platforms.[6]

This approach has allowed the role of the polymeric binder on the underpinning electrochemical properties to be explored allowing the electrochemical properties of screen-printed electrodes to be readily tailored such that they can act either akin to edge plane or basal plane of highly ordered pyrolytic graphite.[6] These bespoke screen-printed

electrodes can be used as convenient and economical electrode alternatives to basal plane of highly ordered pyrolytic graphite electrodes allowing the understanding of the role of basal vs. edge in electrochemical experiments to be readily determined.

For the first time, it is reported that disposable screen-printed electrodes are basal plane-like in nature[6] act as excellent substrates for producing random micro-domain ensemble modified electrodes. As the amount of polymeric binder is introduced into the ink formulation, electrodes are produced where the edge-plane domains are distributed randomly across the electrode surface and become separated from their nearest neighbour and due to no regular spacing between neighbouring micro-domains as is found in a microelectrode array, the word ensemble is employed[7]. The disposable nature of these electrodes preclude the need for electrode polishing to return the electrode to its former state before further depositing the electro-catalytic material of choice. We demonstrate proof-of-concept for the use of micro-domain ensembles towards a variety of analytical challenges which include the fabrication of copper ensembles for nitrate sensing and palladium ensembles for hydrazine detection.

9.3 Experimental

All chemicals used were of analytical grade and were used as received without any further purification from Sigma–Aldrich. All solutions were prepared with deionised water of resistivity not less than 18.2 MΩ cm. Voltammetric measurements were carried out using a l-Autolab III (Eco Chemie, The Netherlands) potentiostat/ galvanostat. Screen-printed carbon electrodes were fabricated in-house to produce a working electrode with a 3 mm diameter as previously described.[6] All measurements were conducted using a three electrode configureuration with a large surface area platinum wire as a counter and a saturated calomel electrode (SCE, metrohm) as the reference. Connectors for the efficient connection of the screen-printed electrochemical sensors were purchased from Kanichi Research Services Ltd. (UK, http://kanichi-research.com/). All measurements were conducted at 23 °C. Scanning electron microscopy (SEM) images were obtained using a JEOL JSM-5600LV model.

9.4 Results and Discussion

First attention is turned to exploring the electrochemical performance of a standard electrochemical sensing platform as fabricated in previous studies [8,9]with that of a bespoke electrochemical platform. Figure. 9.1 depicts the voltammetric profiles obtained in 1 mM potassium ferrocyanide/1M potassium chloride.

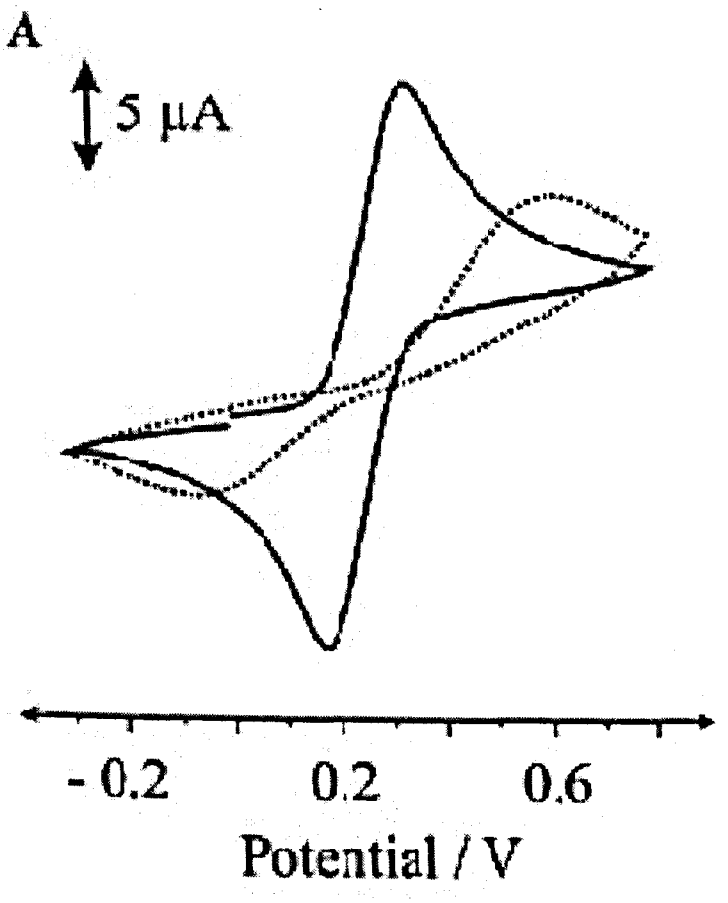

Figure 9.1: (A) Cyclic voltammetric profiles obtained in 1 mM potassium ferrocyanide in 1 M KCl using the standard electrochemical platform (solid line) with that of a bespoke electrochemical platform (dashed line). Scans recorded at 100 mV s^{-1} vs. SCE.

Recently, it has been reported that the electron transfer rates of screen-printed electrodes can be tailored by introducing more binder into the screen-printed ink[6]. The electrochemical response of this bespoke electrochemical platform is shown in Figure. 9.1 which has a larger peak-to-peak separation than that of the standard electrochemical platform indicating slower heterogeneous electron transfer rates. The heterogeneous rate constant, k^0, for the standard and bespoke electrochemical platforms were found to be 1.5×10^{-3} cm s^{-1} and 7.9×10^{-6} cm s^{-1} respectively; the former is in excellent agreement with literature reports[9] while the latter demonstrates the unique heterogeneity of the screen-printed electrode which will be shown below to be highly beneficial in electro-analytical sensing. The bespoke electrochemical platform has electrochemical characteristics consistent with that of a basal-plane pyrolytic graphite electrode and can play an important role in understanding the structure and reactivity of, for example, carbon electrodes and associated materials such as carbon nanotubes.[10, 11]

The batch to batch reproducibility of screen-printing these bespoke electrodes was explored using the ferro/ferri redox probe where random electrode were taken across four batches with the % relative standard deviation of the magnitude of the voltammetric peaks found to fall lower than 2.9%. To highlight the contrasting behaviour between the standard and bespoke electrochemical platforms, the electro-deposition of copper was undertaken. A deposition potential of – 1.2 V (vs. SCE) for 30 s was employed in a solution containing 50 mM Cu^{2+} in 0.1 M sodium sulfate[12] (adjusted to pH 2.5 with HCl). Figure. 9.1 depicts SEM images comparing the copper modified standard (Figure. 9.1B) with that of the bespoke (Figure. 9.1C) electrochemical platform. The standard electrochemical platform is plated with a copper film while the bespoke electrochemical platform has formed random distributed copper domains. Analysis of the electrode surface with SEM reveals that the

copper domains are on average spherical in nature, but some are clearly non-spherical. Analysis of the SEM images reveals an average diameter of 2.5 (standard deviation of 0.5) l_M. This corresponds to an average total surface coverage of appropriately 3.4 x 10^5 micro-particles with a surface coverage, l_H; of 0.23.1 Note that when employing glassy carbon, for example, a random dispersion of metal micro-sized particles can be deposited due to the electrode heterogeneity[13]. However, this approach has its drawbacks, as do other electrodes used in this fashion due to the requirement to clean and return the electrode to its former state before modification. Clearly a disposable version is highly advantageous and we report the first example where a screen-printed electrode is made more heterogeneous to facilitate a large random dispersion of micro-domain sites. It should be noted, that in this thesis we have not explored or are concerned with the mechanism of deposition of the target metal and but rather the use of the deposited metal as catalytic micro-domain sites. However, it is highly likely, in line with other studies on graphitic surfaces that the metal nucleates onto edge plane-like sites/defects[14] of the graphite particles used to fabricate the screen-printed electrodes. The deposition and stripping mechanisms in terms of nucleation processes are important when determining metals at screen-printed electrodes, for example the determination of lead at an unmodified screen-printed electrode and the authoritative work of Honeychurch *et al.*[15] and Brainina *et al.*[16] is recommended.

Next the electrochemical reduction of nitrate was explored at the copper ensemble. Using an *ex situ* prepared copper ensemble, the electrochemical reduction of nitrate was explored in 0.1 M sodium sulfate (adjusted to pH 2.5 with hydrochloric acid). The first voltammetric scan, as shown in Figure. 9.2A has two distinct voltammetric features at ~ - 0.56 V and - 0.78 V (vs. SCE). According to previous studies these peaks are due to stripped copper being complexed with chloride ions present in the electrolyte solution, and as a result the re-

reduction occurs at more negative potentials in two processes.[17] The first peak at ~ - 0.56 V is the reduction of copper (II) to copper (I) followed by copper (I) to copper (0) at - 0.78 V. Additions of nitrate were explored with the copper ensemble where it was observed that the peak at - 0.78 V grows in magnitude with increasing additions. Figure. 9.2B depicts the plot of peak height against concentration of nitrate where a linear response is obtained over the range 10–70 I_M ($I_H/A = 0.15$ [nitrate] $AM^{-1} - 1.3 \times 10^{-6}$ A; $R^2 = 0.998$; N = 13). Note that the peak height was measured by subtracting the peak current obtained in the absence of nitrate.[17] Further additions were made with a second linear range observed over the range 125–1000 I_M ($I_H/A = 0.11$ [nitrate] $AM^{-1} - 3.2 \times 10^{-6}$ A; $R^2 = 0.997$; N=8). Based on the linear range shown in Figure. 2B, a limit of detection was found to correspond to 2.8 I_M.

This copper assemble is superior to copper nanoparticle modified boron-doped diamond electrodes.[18] The micro-domains are randomly distributed across the electrode surface and it is likely that partial overlap of diffusion zones occurring around each micro-domain result rather than Independent behaviour but to a lesser extent than that observed at copper nanoparticle boron-doped diamond electrodes and hence the improvement in the detection towards hydrazine.

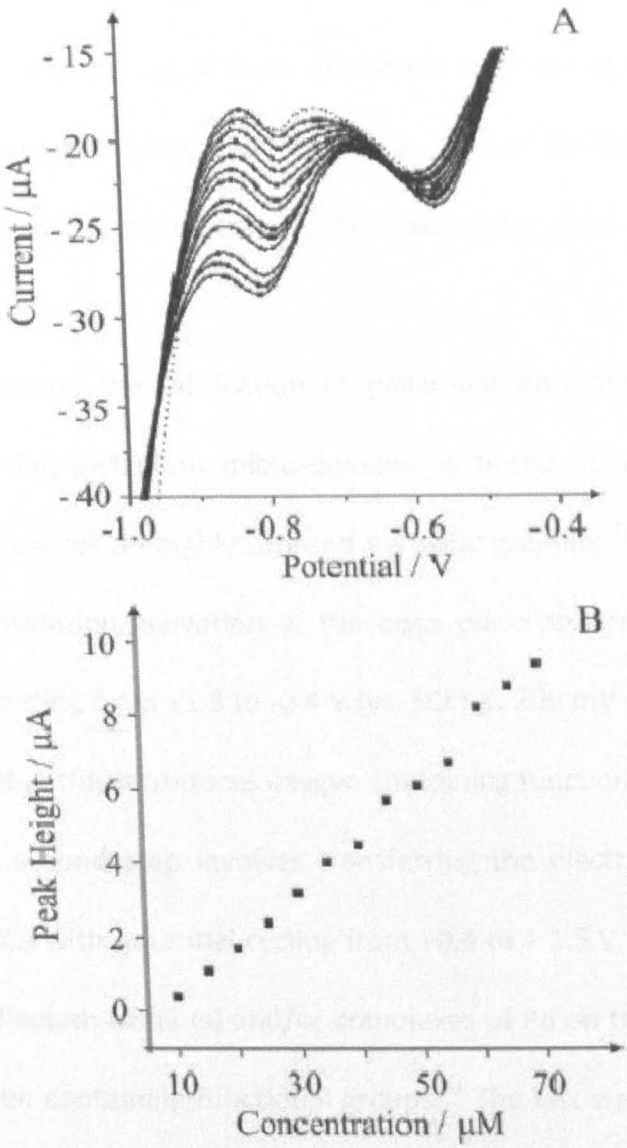

Figure 9.2. Cyclic voltammetric profiles (A) obtained for the electrochemical reduction of nitrate using a copper assemble with the corresponding analysis of the peak height vs. added nitrate concentration shown in (B).

Previous work using copper modified electrodes have been demonstrated to be analytically useful in determining nitrate in treated sewage discharge water. Given the voltammetric position of our observed analytical signal with that reported previously, which is well

resolved from interferents,[14] we expect our methodology to perform similarly but with enhancements in the analytical signal from enhanced mass transport due to the micro-domain nature of the fabricated electrode. However, it must be noted that the electrode will still be susceptible to the adsorption of small molecular sized species which may be present.

We now turn to exploring the fabrication of palladium ensemble micro-domains. The methodology for forming palladium micro-domains is based on a previous method for producing elegant nanowires on highly ordered pyrolytic graphite.[11] The first step involves the electrochemical oxidation/activation of the edge plane sites/defects on the graphite surface via potential cycling from +1.8 to -0.4 V (vs. SCE) at 200 mV s^{-1} for 10 cycles in 0.5 M Na_2SO_4. It is thought that this introduces oxygen containing functional groups on the surface of the graphite. The second step involves transferring the electrode into a 1 mM $PdCl_2$ solution in 0.1 M H_2SO_4 with potential cycling from +0.4 to + 1.5 V for five cycles at 200 mV s^{-1}. This produces palladium oxide (s) and/or complexes of Pd on the edge plane-like defect sites at various oxygen containing functional groups.[11] The last step involves the formation of palladium micro-domains by transferring the modified electrode into 0.1 M H_2SO_4 and potential cycling from +1.1 to -0.5 V at a scan rate of 300 mV s^{-1} for five scans. SEM images of the modified electrode surface reveal palladium metal micro-domains, again with the majority spherical in nature but of course with some micro-domains which are non-spherical. Analysis of the SEM images reveals an average radius of 2.7 (standard deviation 0.4) μm.

A)

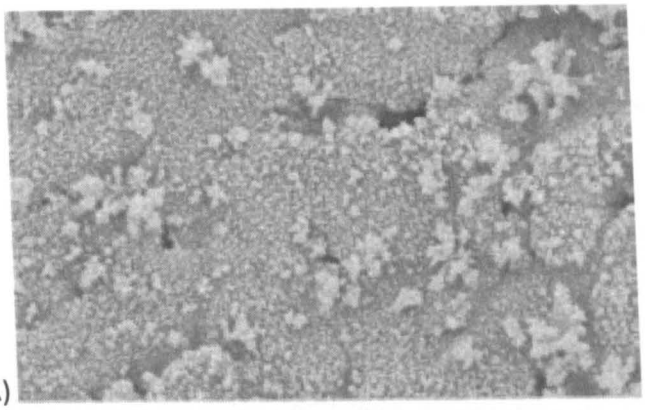

B)

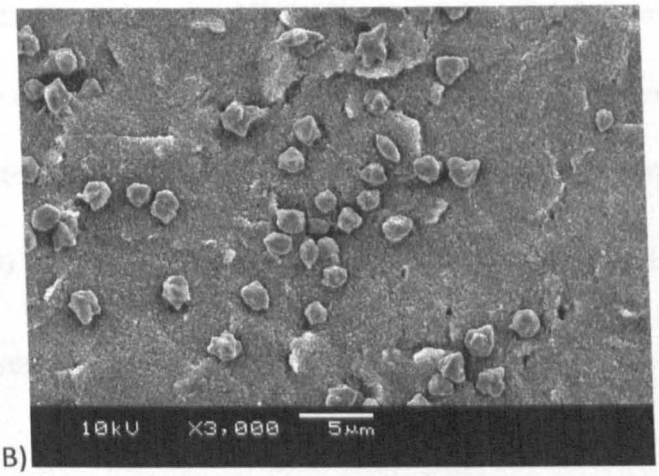

Figure 9.3. SEM images of the copper plated standard (A) and bespoke (B) screen-printed electrochemical platforms.

The surface coverage of palladium micro-domains, H, is estimated to be 0.27. Hydrazine is used in a range of industrial applications and has carcinogenic and mutagenic properties requiring careful control and measurements protocols.[19, 20, 21, 22] The electro-analytical oxidation of hydrazine was explored at the palladium ensemble where a large and easily quantifiable peak is observed to occur with a steady-state response, as shown in Figure. 9.3, which is consistent with the high current density at random arrays. This catalytic oxidation wave is resolved from the solvent window and occurs exclusively on the palladium surface with no voltammetric responses observed in the accessible potential window using the bare

screen-printed micro-domain electrode. The electrochemical oxidation of hydrazine has been studied on palladium previously with the voltammetric wave likely due to the following:[23, 24]

$$N_2H_5^+ - 4e^- \rightarrow N_2 + 5H^+$$

The response of the palladium ensemble was explored by making additions of hydrazine into pH 7 phosphate buffer solutions. Figure 9.4A depicts the voltammetric profiles from additions of hydrazine with the analysis of the limiting current (I_L) taken at + 0.15 V (vs. SCE) vs. added hydrazine, depicted in Figure. 9.3B, which exhibits a linear response from 12.5 to 175 μM($I_L/A = 1.7 \times 10^{-2} AM^{-1} + 6.7 \times 10^{-7} A$; $R^2 = 0.997$; N = 12). Based on this linear range a limit of detection (based on 3σ) was found to correspond to 8.9 μM.

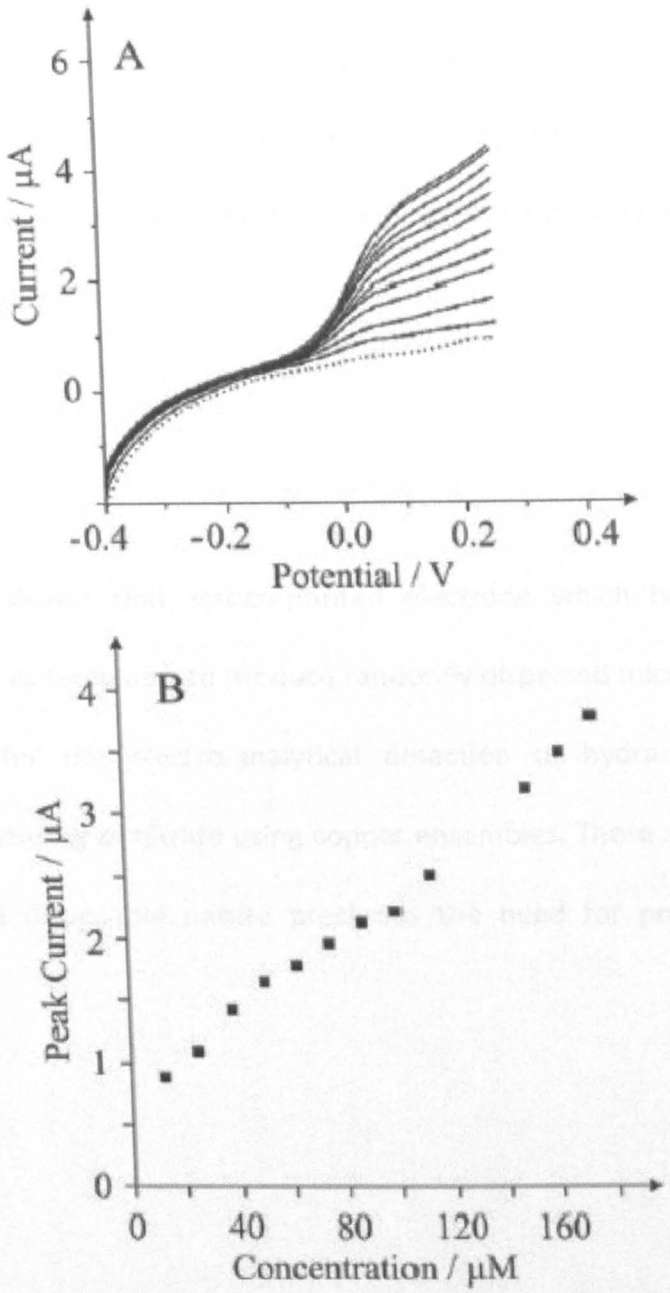

Figure 9.4. Cyclic voltammetric profiles (A) obtained for the electrochemical oxidation of hydrazine using a palladium assemble with the corresponding analysis of the peak height vs. added hydrazine concentration shown in (B).

The application of hydrazine sensing finds use in niche applications which will be further explored to determine specificity in that context. The limit of detection compares well with that reported by Batchelor- McAuley and co-workers using palladium plated boron-doped diamond arrays[24], palladium nanoparticles[25] and gold electrodes modified with iron phthalocyanine complexes.[26]

9.5 Conclusions

It has been shown that screen-printed electrode which have basal plane-like qualities can be used as templates to produce randomly dispersed micro-domains. Proof-of-concept is shown for the electro-analytical detection of hydrazine using palladium ensembles and the sensing of nitrate using copper ensembles. These sensors can be readily mass produced and disposable nature precludes the need for pre-treatment between measurements.

9.6 References

1. Arrigan, D.W.M., *Nanoelectrodes, nanoelectrode arrays and their applications.* Analyst, **129**, 1157, 2004.
2. Welch, C.M, *The detection of nitrate using in-situ copper nanoparticle deposition at a boron doped diamond electrode.* Analytical Sciences, **21**, 1421, 2005..
3. Berduque, A, *Voltammetric characterisation of silicon-based microelectrode arrays and their application to mercury-free stripping voltammetry of copper ions.* Talanta, **71**, 1022, 2007..
4. Simm, A.O, *Boron-doped diamond microdisc arrays: electrochemical characterisation and their use as a substrate for the production of microelectrode arrays of diverse metals (Ag, Au, Cu) via electrodeposition.* Analyst, **130**, 1303, 2005..
5. Davis, J, *Electrochemical detection of nitrate at a copper modified electrode under the influence of ultrasound.* Electroanalysis, **12**, 1363, 2000.
6. Choudhry, N.A., *Screen-printed electrodes provide micro-domain sites for fabricating disposable electro-catalytic ensembles.* Electrochemistry Communications, **12**, 406, 2010.
7. Fletcher, S. and M.D. Horne, *Random assemblies of microelectrodes (RAM (TM) electrodes) for electrochemical studies.* Electrochemistry Communications, **1**, 502, 1999.
8. Kadara, R.O., N. Jenkinson, and C.E. Banks, *Characterisation of commercially available electrochemical sensing platforms.* Sensors and Actuators B-Chemical, **138**, 556, 2009.

9. Kadara, R.O, *Manufacturing electrochemical platforms: Direct-write dispensing versus screen printing.* Electrochemistry Communications, **10**, 1517, 2008.

10. Moore, R.R., C.E. Banks, and R.G. Compton, *Basal plane pyrolytic graphite modified electrodes: Comparison of carbon nanotubes and graphite powder as electrocatalysts.* Analytical Chemistry, **76**, 2677, 2004.

11. Ji, X.B., *Edge plane sites on highly ordered pyrolytic graphite as templates for making palladium nanowires via electrochemical decoration.* Journal of Physical Chemistry B, **110**, 22306, 2006.

12. Ordeig, O, *Electroanalysis of Bromate, iodate and chlorate at tungsten oxide modified platinum microelectrode arrays.* Electroanalysis, **18**, 1672, 2006.

13. Stozhko, N.Y., *Modified carbon-containing electrodes in stripping voltammetry of metals - Part I. Glassy carbon and carbon paste electrodes.* Journal of Solid State Electrochemistry, **12**, 1185, 2008.

14. Banks, C.E, *Electrocatalysis at graphite and carbon nanotube modified electrodes: edge-plane sites and tube ends are the reactive sites.* Chemical Communications, **7**, 829, 2005

15. Honeychurch, K.C., J.P. Hart, and D.C. Cowell, *Voltammetric behavior and trace determination of lead at a mercury-free screen-printed carbon electrode.* Electroanalysis, **12**, 171, 2000.

16. Brainina, K.Z., Discharge-ionization of metals on an indifferent electrode. Journal of Electroanalytical Chemistry, **35**, 165, 1972.

17. Davies, T.J. and R.G. Compton, *The cyclic and linear sweep voltammetry of regular and random arrays of microdisc electrodes: Theory.* Journal of Electroanalytical Chemistry, **585**, 63, 2005.

18. Welch, C.W. and R.G. Compton, *The use of nanoparticles in electroanalysis: a review.* Analytical and Bioanalytical Chemistry, **384**, 601, 2006.

19. Zelnick, S.D., D.R. Mattie, and P.C. Stepaniak, *Occupational exposure to hydrazines: Treatment of acute central nervous system toxicity.* Aviation Space and environmental Medicine, **74**, 1285, 2003.

20. Vernot, E.H, Long-term inhalation toxicity of hydrazine. Fundamental and Applied Toxicology, **5**, 1050, 1985.

21. Yamada, K, *Potential application of anion-exchange membrane for hydrazine fuel cell electrolyte.* Electrochemistry Communications, **5**, 892, 2003.

22. Poso, A., A. Vonwright, and J. Gynther, An empirical and theoretical-study on mechanisms of mutagenic activity of hydrazine compounds. Mutation Research-Fundamental and Molecular Mechanisms of Mutagenesis, **332**, 63, 1995.

23. Bard, A.K. and C.G. Zoski, *Voltammetry retrospective.* Analytical Chemistry, **72**, 346A, 2000.

24. Batchelor-McAuley, C., *The electroanalytical detection of hydrazine: A comparison of the use of palladium nanoparticles supported on boron-doped diamond and palladium plated BDD microdisc array.* Analyst, **131**, 106, 2006.

25. Baron, R, *Development of an electrochemical sensor nanoarray for hydrazine detection using a combinatorial approach.* Electroanalysis, **19**, 1062, 2007.

26. Ozoemena, K.I. and T. Nyokong, *Electrocatalytic oxidation and detection of hydrazine at gold electrode modified with iron phthalocyanine complex linked to mercaptopyridine self-assembled monolayer.* Talanta, **67**, 162, 2005.

Chapter 10

Modification of Screen-Printed Electrodes

10.0 Electrochemical Sensors - Modification of the conductive carbon ink: Electrolytically Fabricated Nickel Microrods on Screen-Printed Electrodes: Electro-Catalytic Oxidation of Alcohols

10.1 Abstract

Nickel-modified graphite screen-printed electrodes are explored towards the sensing of alcohols in alkaline solutions. Electrochemically formed nickel microrods with average dimensions of 12 μM length and 2 μM diameter are shown to be readily formed on the surfaces of graphite screen-printed electrodes. This is the first example of electrolytically formed nickel nanorods which exhibit electro-catalysis towards the sensing of ethanol over the range 2.6 – 23 mM and and glycol over the range 230 – 1840 μM with limits of detection of 1.4 mM and 186 μM respectively. *This work was published in Analytical Methods, **3**, 74, 2011.*

10.2 Introduction

The electrochemical oxidation of alcohols is of wide importance in high performance fuel cells which hold promise as renewable and low cost alternative fuels sources.[1, 2] A plethora of electrocatalytic materials have been explored with platinum based materials which are the current contenders, with research into other possible materials a highly active area in order to reduce the associated cost.[3] One such potential electro-catalyst is nickel oxide which has been explored as a potential catalyst towards alcohols.[1, 4, 5, 6, 7] While research is heavily focused with a view to develop fuel cell technologies, the analytical utilisation of such a system should not be overlooked and novel low cost, simple and disposable

analytical tools are urgently required. For example, this might be utilised as a sensor for the monitoring of operational safety in the form of fuel cell leaks. Towards these goals, recently nickel nano-particle modified boron-doped diamond electrodes have been explored towards the sensing of ethanol and glycerol[8] as well as a nickel microparticle modified boron-doped diamond electrode for methanol sensing.[9] There is considerable merit in this approach over that of a solid electrode consisting completely of nickel which includes reduced cost, ease of fabrication and a renewable surface and an improvement in the accessible linear ranges towards the target analyte due to improvements in diffusion to effectively a nickel micro/nano array. An alternative to commercially available solid electrodes such as boron-doped diamond and glassy carbon are disposable and cost effective screen-printed electrodes.[10, 11, 12, 13] In this chapter we explore the fabrication of electrolytically fabricated nickel microstructures using graphite screen-printed graphite electrodes. It is found that nickel microrods can be readily formed at the surface of a screen-printed electrode with average lengths and diameters of 12 mM and 2 mM respectively. While screen-printed electrodes have been routinely used as templates for the electro-deposition of different nanoparticles compositions for a range of analytical targets, [14, 15, 16] we find no literature reports of producing microrod structures in this way.

Additionally we note that nickel hydroxide microrods have seldom been reported with fabrication methods involving solvothermal approaches[17] and vertically aligned nickel oxide microrods on silicon substrates have also been reported via thermal heating.[18] The electrolytically fabricated nickel microrods are explored as a potential electro-catalyst, in particular, towards the electro-catalytic oxidation of alcohols.

10.3 Experimental Section

All chemicals used were of analytical grade and were used as received without any further purification from Sigma-Aldrich. All solutions were prepared with deionised water of resistively not less than 18.2MΩ cm. All solutions were vigorously degassed with nitrogen to remove oxygen. Voltammetric measurements were carried out using a μ-Autolab III (Eco Chemie, The Netherlands) potentiostat/galvanostat and controlled by Autolab GPES software version 4.9 for Windows XP. Screen-printed graphite macroelectrodes which have a 3 mm diameter working electrode were fabricated as reported previously.19 These electrodes have been characterised electrochemically as previously reported in this thesis and have heterogeneous electron transfer rate constants ~ 1.7×10^{-3} cm s^{-1}. [12] In addition to the screen-printed graphite electrodes being used as the working electrode, a large surface area platinum wire as a counter electrode and a Saturated Calomel Electrode (SCE) as the reference electrode were utilised. Connectors for the efficient connection of the screen-printed electrochemical sensors were purchased from Kanichi Research Services Ltd.[20] Scanning electron microscopy (SEM) images were obtained using a JEOL JSM-5600LV model.

10.4 Results and Discussion

Screen-printed graphite macroelectrodes were electrolytically modified with nickel using a previously reported methodology[8] from a solution containing 1 mM nickel (II) in a 0.1 M sodium acetate solution (pH 5) employing a deposition potential of -1.2 V for 300 s. Figure. 10.1 depicts SEM images of the modified electrode which indicates that the electrode surface has been modified with unique structures which have average lengths of 12 mm with diameters of 2 mm.

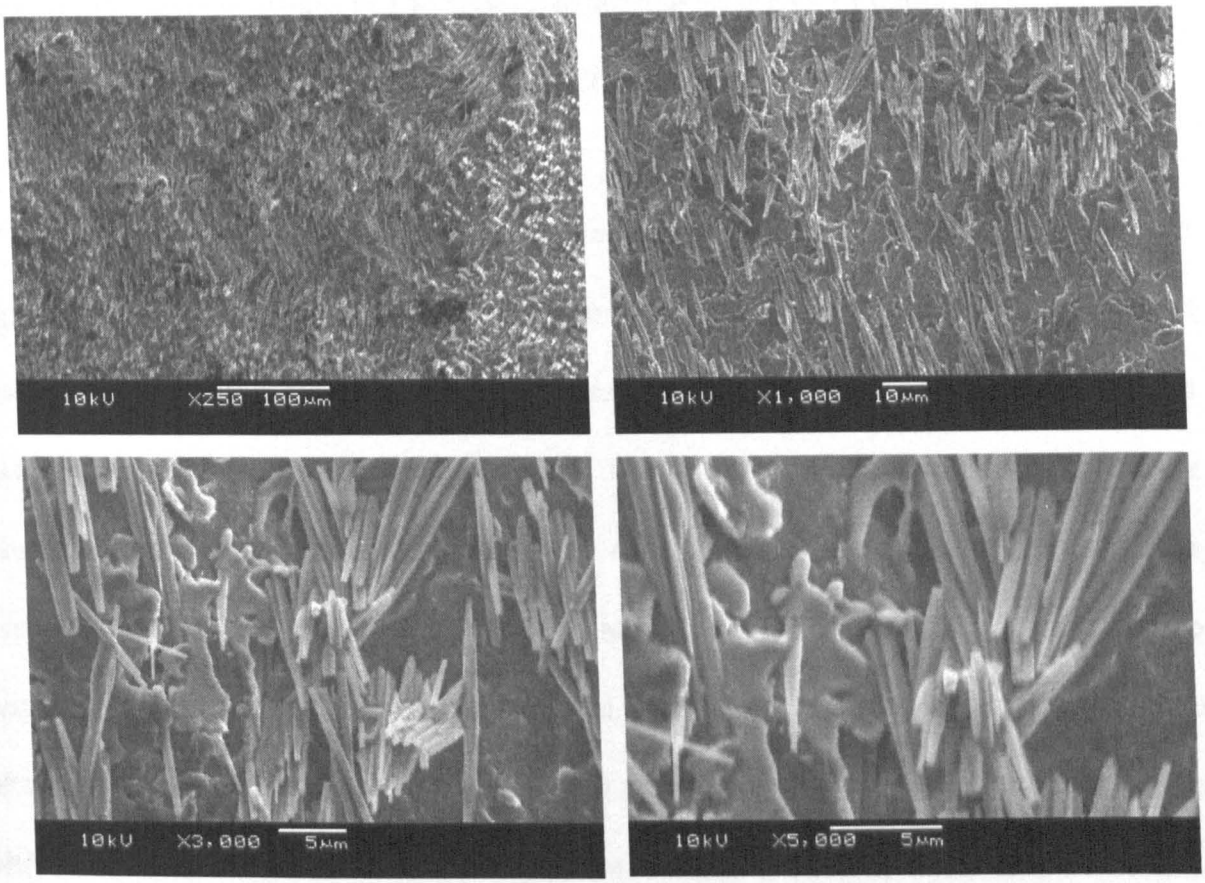

Figure 10.1. SEM images of nickel modified screen-printed platforms.

It is interesting to note that using identical electrochemical parameters and solutions as reported in the literature[8] that utilising boron-doped diamond electrodes results in the formation of nanoparticles which indicates that the nucleation dynamics are quite different to that observed at boron-doped diamond electrode surfaces. Given the wide range in the size of the microrods, as observed in Figure. 10.1, a progressive growth processes arising from continued nucleation of metallic nickel to the active sites of the screen-printed surface is highly likely.[21] A survey of the literature reveals that nickel microrods have been fabricated but never electrochemically as presented here.[17, 18] We next turn to exploring the nickel microrod modified screen-printed graphite macroelectrodes towards the electrochemical sensing of alcohols. Figure. 10.2A depicts voltammetric profile of the nickel

microrod modified electrodes in 1 M sodium hydroxide where an oxidation wave at +0.44 V (vs. SCE) and a reduction wave at +0.35 V (vs. SCE) are observed.

EDAX analysis of the nickel microrods exhibited three peak corresponding to nickel, an oxygen peak and of course a carbon peak from the underlying electrode surface. It is well established in the literature that deposited nickel metal spontaneously forms $Ni(OH)_2$ in alkaline solutions,[8] likely surface oxide rather than complete bulk transformation and we observe an electrochemical oxidation wave at ~ +0.4 V which is due to the Ni^{2+}/Ni^{3+} signal as described by equation (1). Previous research has shown that the nickel can exist in two crystallographic forms, hydrated a-$Ni(OH)_2$ and anhydrous b-$Ni(OH)_2$ which produces two voltammetric oxidation peaks.[8] However in our case the observation of a single voltammetric wave indicates that the nickel microrods are highly likely to be in the b-$Ni(OH)_2$ form.[8] Figure. 10.2A also depicts the voltammetric profiles resulting from the additions of 1.3 mM ethanol using a nickel microrod modified electrode where analysis of the anodic wave, as depicted in Figure. 10.2B increases with additions of ethanol coupled with the position of the voltammetric peak moving to more anodic potentials with each addition. It is clear at this concentration level a linear response over the range 4 to 10 mM (Figure. 10.2B) is observed. The observed voltammetric profiles are due to the Ni^{2+}/Ni^{3+} redox couple which is electro-catalytic origin undergoing the following process:

$$Ni(OH)_2 \rightleftharpoons NiOOH + H^+ + e^- \qquad (1)$$

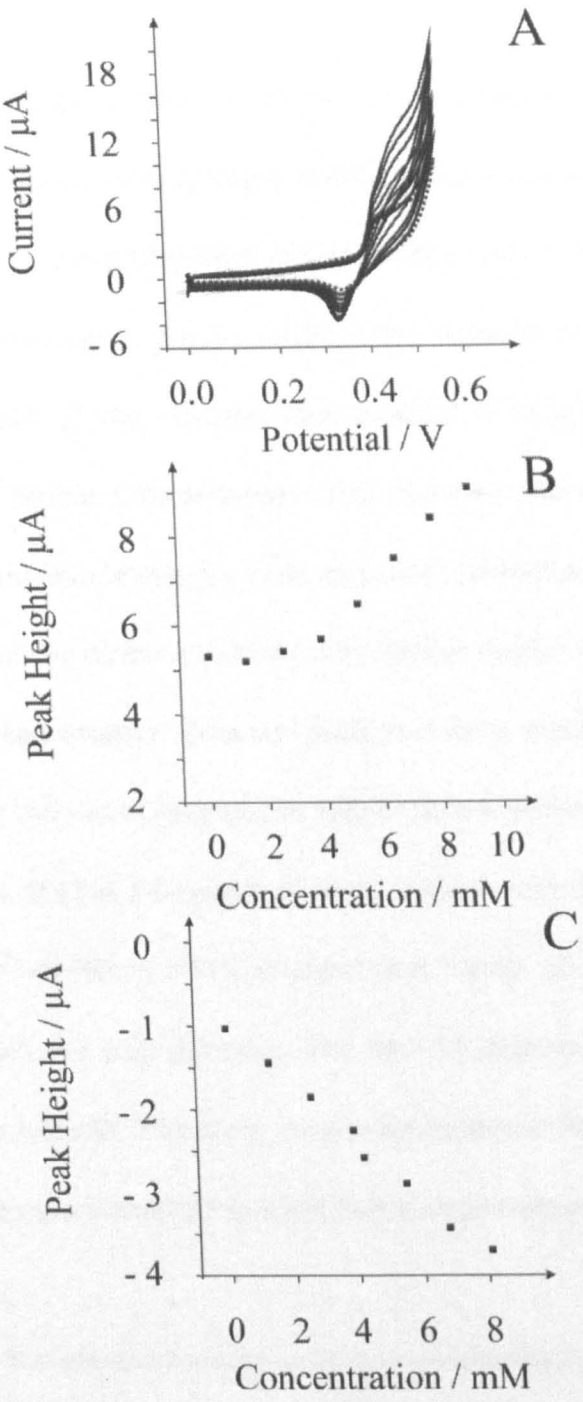

Figure 10.2.Cyclic voltammetric profiles showing 1.3 mM ethanol additions into a 0.1 M sodium hydroxide obtained with a nickel microrod modified screen-printed electrochemical platform. All scans recorded at 50 mVs^{-1} vs. SCE. Below are plotted graphs for the oxidation peak height (B) and reduction peak height (C) as a function of added ethanol concentrations.

With the adsorption of the target alcohol on the electrode surface occurring with the NiOOH and the adsorbed target alcohol undergoing a hydrogen-abstraction reaction producing an intermediate and starting material ($Ni(OH)_2$) with the subsequent oxidation of the adsorbed intermediate.[4, 7, 22] Also observed in Figure. 10.2A is the increase of the cathodic wave in a linear fashion, the analysis of the voltammetric peak as a function of concentration is depicted in Figure. 10.2C where a linear response is observed and while the exact origin of this is unclear, it is evident that it may be used as a possible indirect sensing methodology. The analytical response of the nickel microrods was further explored towards the sensing of ethanol using chronoamperometry. Ethanol additions were made into a 0.1 M sodium hydroxide solution using the nickel microrod modified screen-printed sensor with analysis of the current at +0.4 V (vs. SCE) as a function of concentration reveals a linear response ($I/A = 0.08AM^{-1} + 2.9x10^{-6}A$; $R^2 = 0.983$; $N = 17$), as depicted in Figure. 10.3, over the range 2.6 mM to 23 mM beyond which the plot plateaus. The limit of detection, based on 3-sigma[23] is found to correspond to 1.4 mM. This linear range and detection limit is identical to state-of-the art nickel hydroxide nanoparticles modified boron-doped diamond electrodes.[8]

To understand further the electrochemical oxidation mechanism using the nickel microrods, the Langmuir adsorption isotherm is employed.[3, 24] Assuming that the catalytic peak current (Icat) is proportional to the surface concentration of the alcohol under investigation, the electrochemical adsorption equilibrium constant, b, can be determined according to the Langmuir equation

$$\frac{[alcohol]}{I_{cat}} = \frac{[alcohol]}{I_{cat,max}} + \frac{1}{\beta I_{cat,max}}$$

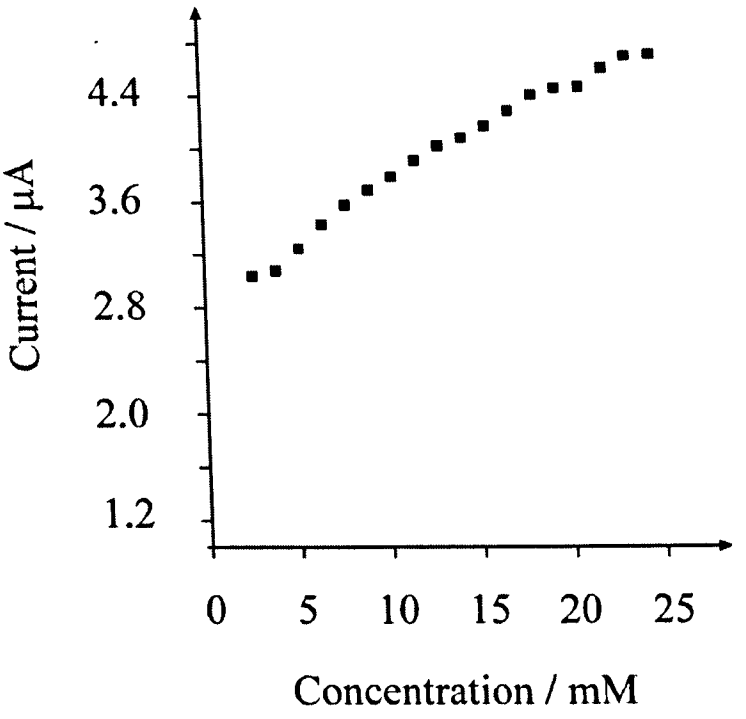

Figure 10.3. Analysis of chronoamperometric response of the nickel microrod modified screen-printed graphite electrode resulting from ethanol additions over the range of 0 to 26 mM. The electrode was held at a potential of +0.4 V (vs. SCE).

A plot of $\frac{[alcohol]}{I_{cat}}$ against $[alcohol]$ allows the adsorption equilibrium constant, β, to be estimated as 356 (± 3) M^{-1}. Thus the Gibbs energy changes due to adsorption may be deduced from:

$$\Delta G^0 = -RTIn\beta$$

which was found to correspond to –14.7 kJ mol^{-1} suggesting that the overall electrochemical oxidation reaction is governed by adsorption-controlled kinetics rather than diffusion processes.

Next, attention is turned to exploring the nickel microrod modified screen-printed platforms for the sensing of glycerol. Figure. 10.4 depicts typical voltammetric profiles obtained from additions of glycerol into a 0.1 M NaOH solution where a linear type response is observed (Figure. 10.4B).

To access the analytical response of the nickel microrods towards the sensing of glycerol, chronoamperometry was employed. As shown in Figure. 10.4C, analysis of the limiting current as a function of added glycerol concentration exhibits a linear response (I/A ¼ 0.004 AM^{-1} + 1.3 x 10^{-6}A; R^2 = 0.991; N = 8) over the range of 230 mM to 1840 mM with a limit of detection (3-sigma) found to correspond to 186 mM. Unfortunately this limit of detection is not as competitive as nickel nanoparticle modified boron-doped diamond electrodes or a nickel macroelectrode.[8] Given that a very good analytical output is observed for the case of ethanol (see above) this suggests that the nickel microrods likely have a different amount of oxide on the nickel metal which might reduce the rate of reaction in the rate determining hydrogen-abstraction step in the electrochemical oxidation mechanism. While this is speculation, the unexpectedly poor analytical performance might still have analytical utility in niche applications.

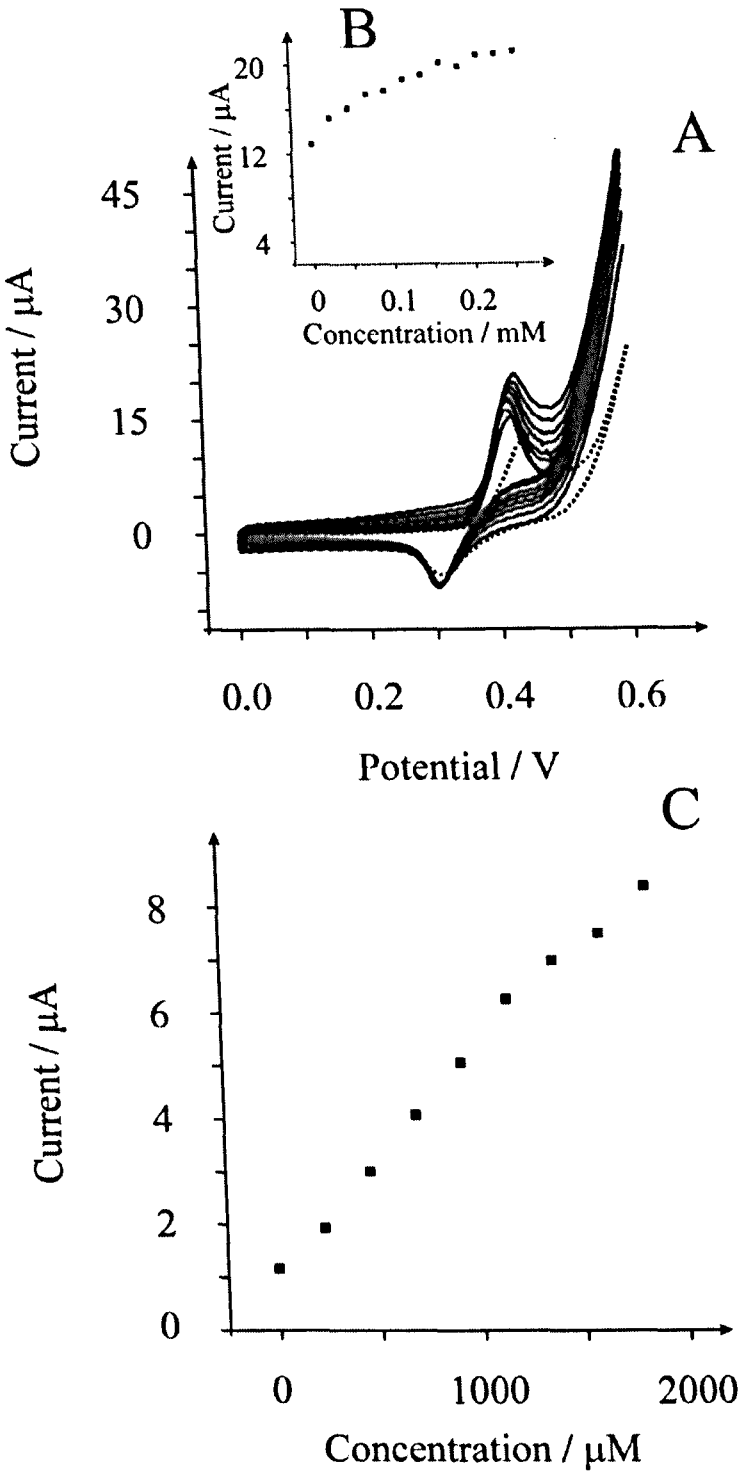

Figure 10.4. Cyclic voltammetric profiles (A) recorded showing 230 µM glycerol additions into a 1M sodium hydroxide solution using the nickel microrod modified screen-printed graphite electrode. All scans recorded at 50 mVs^{-1} vs. SCE. Part B depicts the analysis of the oxidation peak height as a function of glycerol concentrations. Part C is the analysis of chronoamperometric responses using the nickel microrod modified screen-printed graphite electrode. The electrode was held at a potential of + 0.4 V (vs. SCE).

10.5 Conclusions

The first electrochemical fabrication of nickel microrods is reported which have been shown to be electroanalytical useful for the sensing of ethanol which perform analytically similar to current state-of-the-art using nickel nanoparticle modified electrodes and to a lesser extent the microrods can be utilised for glycerol sensing. The simple and low cost fabrication process of the nickel microrods suggest their use in the electroanalytical quantification of ethanol and glycol, for example in the monitoring for potential fuel cell leaks. The potential use of the nickel microrods in alcohol fuel cells as a electro-catalyst should also not be overlooked and are also being explored in other sensing applications.

10.6 References

1 AE. Antolini, J. Power Sources, **1**, 170, 200.

2 E. Antolini and E.R. Gonzalez, J. Power Sources, **195**, 3431, 2010,.

3 N.W. Maxakato, C.J. Arendse and K.I. Ozoemena, Electrochem. Commun., **11**, 534, 2009.

4 M. Fleischmann, K. Korinek and D. Pletcher, J. Electroanal. Chem., **31**, 39, 1971.

5 A. Amajad, D. Pletcher and C. Smith, J. Electrochem. Soc., **124**, 203, 1977.

6 C-C. Pang, M-H. Chen, T-Y. Lin and T-C. Chou, Electroanalysis, **13**, 499, 2000.

7 Y. G. Lee and T-C. Chou, Electroanalysis, **15**, 1589, 2003.

8 N.R. Stradiotto, K. E. Toghill, L. Xiao, A. Moshar and R.G. Compton, Electroanalysis, **21**, 2627, 2009.

9 K. E. Toghill, L. Xiao, N.R. Stradiotto and R.G. Compton, Electroanalysis, **22**, 491, 2010.

10 N. A. Choudry, D.K. Kampouris, R.O. Kadara and C. E. Banks, Electrochem. Commun., **12**, 6 2010.

11 J.P. Hart and S.A. Wring, Electroanalysis, **6**, 617, 1994.

12 R.O. Kadara, N. Jenkinson and C. E. Banks, Sens. Act. B, **138**, 556, 2009.

13 K.C. Honeychurch, J.P. Hart and D.C. Cowell, Electroanalysis, **12**, 171, 2000.

14 S. Sanllorent-Mendez, O. Dominguez-Renedo and M. J. Arcos-Martinez, Electroanalysis, **21**, 635, 2008.

15 G.D. Liu, Y.Y. Lin, H. Wu and Y. Lin, Environmental Science & Technology, **41**, 8129, 2007.

16 M.E.B. Calvo, O.D. Renedo and A.J.A. Martinez, Talanta, **74**, 59, 2007.

17 F.F. Tao, J.P. Lu, L.M. Lang and Z. Xu, Chinese J. Inorg. Chem., **25**, 296, 2009.

18 K. Kobayashi, F.A. Harraz, S. Izuo, T. Sakka and Y.H. Ogata, J. Electrochem. Soc., **153**, 218, 2006.

19 Z.J. Zhang, Y. Zhao and M.M. Zhu, Appl. Phys. Lett., **88**, 033101, 2006,

20 R. O. Kadara, N. Jenkinson, B. Li, K. H. Church and C. E. Banks, Electrochemistry Communications, **10**, 1517, 2008.

21 Kanichi.com [internet]. London: Bismuth oxide electrodes/ [Updated 2011 June 21; cited 2011 July 10]. Available at http://kanichi-research.com

22 A. Kowal, S.N. Port and R.J. Nichols, Cat. Today, **38**, 483, 1997.

23 C.M.A. Brett and A.M.O. Brett, *Electroanalysis*, Oxford Science Publications, 2011

24 Z-N. Gao, J. Zhang and W-Y. Lin, J. Electroanal. Chem. , **580**, 9, 2005.

25 C. E. Banks, A.S. Yashina, G.J. Tustin, V.G.H. Lafitte, T.G.J. Jones and N.S. Lawrence, Electroanalysis, **19**, 2518, 2007.

26 H. Ju and D. Leech, J. Electroanal. Chem., **484**, 150, 2000.

Chapter 11

11.0 Gold Nanoparticle Ensembles Allow Mechanistic Insight into Electrochemical Processes

11.1 Abstract

Gold-nanoparticle-modified electrodes find wide and diverse applications in the area of electrochemistry. We demonstrate for the first time that gold-nanoparticle-modified electrodes can provide mechanistic information and we exemplify this with the electrochemical deposition of arsenic(III). Our approach of using nanoparticle ensembles is a facile and economical methodology that provides an alternative to using expensive gold single-crystal electrodes that require careful surface preparation before each measurement. This work was published in *ChemPhysChem*, **11,** 875, 2010, which included contributions from Mohammed Khairy, Mohammed Ouasti, Dimitrios Kampouris, Rashid O' Kadara and Craig E. Banks.

11.2 Introduction

Nanoparticles find wide and diverse applications in a plethora of technologically important disciplines ranging from catalysis[1], nano-engineering of surfaces[2], energy generation using fuel cells[3] and solar cells[4], and sensor applications.[2] Nanoparticle covered surfaces provide unique benefits which have been exploited in amplifying electrochemical DNA sensors,[5, 6] nanowiring redox enzymes,[7] and allow the development of advanced glucose[8] and peroxide sensors.[9] The advantages of employing nanoparticles over micron-sized particles is the enhancement of mass transport of the target analyte, high effective surface area, control over nano-environment and electro-catalysis[10]. Nanoparticle modified surfaces, where the surfaces are usually an electrode substrate providing electronic communication to randomly

distributed nanoparticles, are readily employed due to their facile fabrication and due to diffusional interaction between neighboring nanoparticles, an electrode surface modified with a few percentage of nanoparticles acts akin to that of a macroelectrode constructed from the same electrode material but is a fraction of the cost[11, 12]. Note in the case of randomly distribute nanoparticles on an electrode surface the distance between neighboring nanoparticles is variable across the surface of the electrode and are termed nanoparticle *ensembles*.[13]

While reports of using gold nanoparticle ensembles as sensors are abundant, no attempt to use nanoparticle ensembles to gain electrochemical mechanistic information has been reported to date. We demonstrate for the first time the ability to use gold nanoparticle ensembles to extract mechanistic information which is demonstrated with the example of the electro-deposition of arsenic. Note that the determination of arsenic (III) is a widely sought analytical task due to its toxicity and natural occurrence worldwide in drinking water and its electrochemical reduction mechanism is of vital theoretical and practical significance.

Our approach of using nanoparticle ensembles reported herein precludes the need for gold single crystal electrodes which are expensive and require carefully surface preparation in the form of heat annealing before each measurement. In contrast, disposable nanoparticle ensembles can be readily and inexpensively fabricated and can be disposed after measurement and thus do not suffer any 'memory affects' from prior analysis which would otherwise give inaccurate mechanistic information.

Screen-printed electrodes were fabricated as described in the experimental section and explored towards the electrochemical oxidation of 1mM potassium ferrocyanide / 0.1

M potassium chloride. The response of the bare screen-printed electrode exhibits a large peak-to-peak separation which is indicative of slow heterogeneous electron transfer which is consistent with these screen-printed electrodes. The response from dispersing gold nanoparticles onto the bare screen-printed electrochemical platform was explored. The deposited mass of gold, M_{gold} on the electrode can be deduced from the knowledge of the gold nanoparticle suspension (g/L) and the volume of the applied suspension, *V* (in L) from equation (1):

$$M_{gold} = cV \tag{1}$$

If we assume that the gold nanoparticles are spherical in shape with a constant radius, *r*, we may estimate the total number of gold nanoparticles on the electrode surface, *N*, using equation (2):

$$N = \frac{3M_{gold}}{4\rho\pi r^3} \tag{2}$$

where ρ is the density of gold. From this the microscopic coverage of gold nanoparticles on the electrode surface, Θ, can be deduced from equation (3):

$$\Theta = \frac{Nr^2}{A} \tag{3}$$

where *A* is the area of the underlying electrode surface.

11.2 Experimental

All chemicals used were of analytical grade and were used as received without any further purification from Sigma-Aldrich. All solutions were prepared with deionised water of resistively not less than 18.2 MΩ cm. All solutions were vigorously degassed with nitrogen to remove oxygen.

Voltammetric measurements were carried out using a μ-Autolab III (Eco Chemie, The Netherlands) potentiostat/galvanostat and controlled by Autolab GPES software version 4.9 for Windows XP.

Screen-printed carbon electrodes were fabricated in-house with appropriate stencil designs using a microDEK 1760RS screen-printing machine (DEK, Weymouth, UK). A carbon-graphite ink formulation previously utilised[5]was first screen-printed onto a polyester flexible film (Autostat, 250 μm thickness). This layer was cured in a fan oven at 60 degrees for 30 minutes. Next a silver/silver chloride reference electrode was included by screen printing Ag/AgCl paste (Gwent Electronic Materials Ltd, UK) on to the plastic substrate. Last a dielectric paste ink (Gwent Electronic Materials Ltd, UK) was printed to cover the connections and define the 3mm diameter graphite working electrode. After curing at 60 degrees for 30 minutes the screen-printed electrode is ready to use. All measurements were conducted using a three electrode configureuration with a saturated calomel electrode as the reference rather than the onboard silver-silver chloride reference electrode to allow comparison with the literature. Connectors for the efficient connection of the screen-printed electrochemical sensors were purchased from Kanichi Research Services Ltd.[6]

Scanning electron microscopy (SEM) images were obtained using a JEOL JSM-5600LV model. Polaron (Quorum Technologies) SC76640 Auto/Manual High Resolution Sputter coater was used to produce the palladium sputtered electrodes.

11.3 Results and Discussion

The effect on the electron transfer rate, as evaluated with the potassium ferro/ferricyanide redox probe, is clearly observed in figure 11.1 which depicts the analysis of the inverse of the peak-to-peak separation as a function of coverage. As the microscopic coverage of gold nanoparticles is increased on the surface of the screen-printed electrochemical platform the heterogeneous electron transfer rate increases. This is due to the introduction of the gold nanoparticles which results in a gold ensemble where heterogeneous electron transfer is faster on the gold nanoparticle than the underlying graphite surface of the screen-printed electrode.

At higher coverage's a decrease in the heterogeneous electron transfer is observed likely due to the high microscopic coverage of gold nanoparticles becoming unstable which likely become displaced from the electrode surface during measurements. The gold nanoparticles produced have been shown to be single crystals and thus the overall response of the gold nanoparticle is averaged over the total number of nanoparticles on the electrode surface due to diffusional interaction and consequently should behavior voltammetrically similar to a gold single crystal electrode.

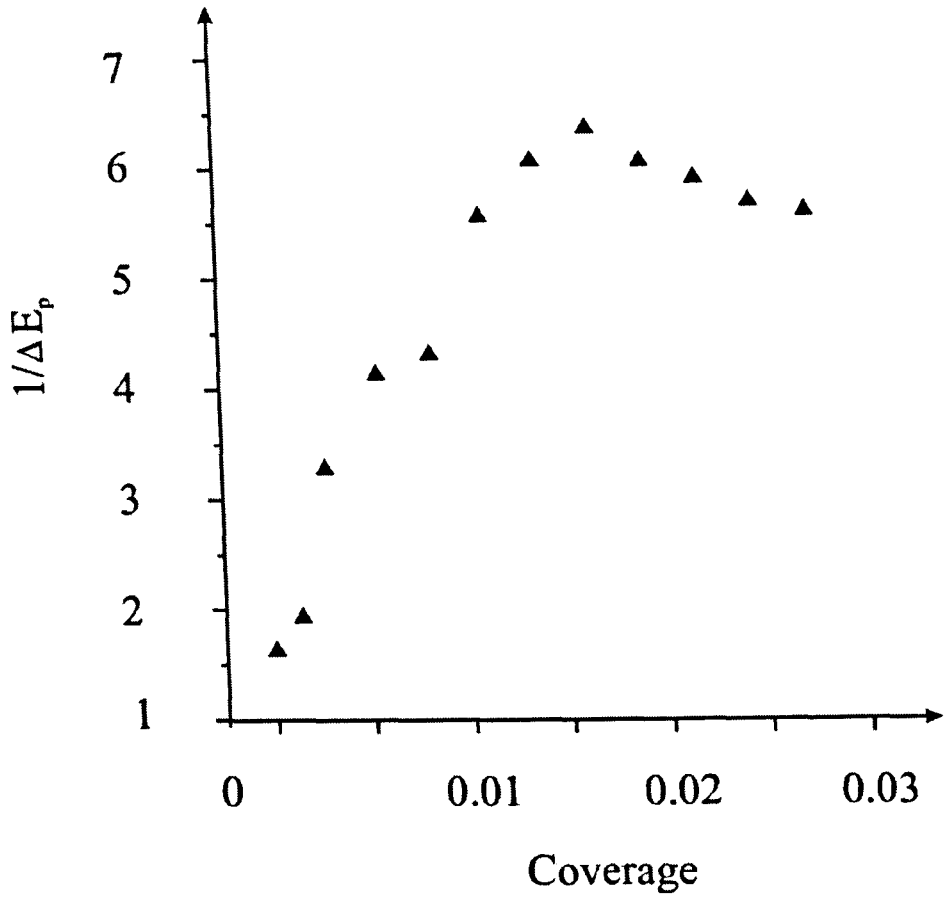

Figure 11.1. Typical plot of the inverse of the peak-to-peak separation as a function of coverage. Data recorded using 1mM potassium ferrocyanide / 0.1 M potassium chloride.

The cyclic voltammetric response of the gold nanoparticle ensemble was recorded in 0.1mM sodium arsenite in phosphate buffer (pH 1). Figure 11.2 depicts a typical cyclic voltammogram where an electrochemical reduction wave corresponding to the electrochemical deposition of arsenic metal is observed on the cathodic sweep while on the anodic scan, the electrochemical stripping of arsenic back to arsenic (III) is clearly evident; this electrochemical process forms the basis of arsenic (III) electro-analytical sensors.

It was found that employing an *in-situ* pre-treatment before arsenic (III) was added is critical. A range of deposition times and potentials were explored with its impact on the profile of the cyclic voltammograms with the aim of reducing the background non-faradaic

processes. We infer that the gold ensemble due to their chemical synthesis and fabrication of the gold nanoparticle ensemble, results in the formation of a thin layer of gold oxide on the gold nanoparticles which is removed by applying the in-situ pre-treatment. It was found that by holding the potential at -1.0 V for 5 second prior to the addition of arsenic (III), the background currents observed on the cyclic voltammetric profiles are greatly reduced allowing mechanistic information to be deduced. Without this pre-treatment meaningless data was extracted and we believe that this has been an issue as to why gold nanoparticle modified electrodes have never been reported before allowing mechanistic information to be extracted.

Returning to the cyclic voltammetry of arsenic (III) at the gold ensemble, intergration of the anodic peak allows the charge resulting from the application of different deposition potentials for different deposition times to readily be calculated, where the deduced charged is directly proportional to the amount of arsenic deposited on the gold nanoparticle ensembles.

It can be assumed that one arsenic atom deposited on the electrode is associated with one gold surface atom where the deposition/stripping mechanism involves 3 electrons, the number of arsenic monolayers deposited on the gold nanoparticle ensembles as a function of the applied deposition time and deposition potential from knowing that the specific charge data at gold (111) surface atom number of 1.5×10^{15} atom cm^{-2}.[15]

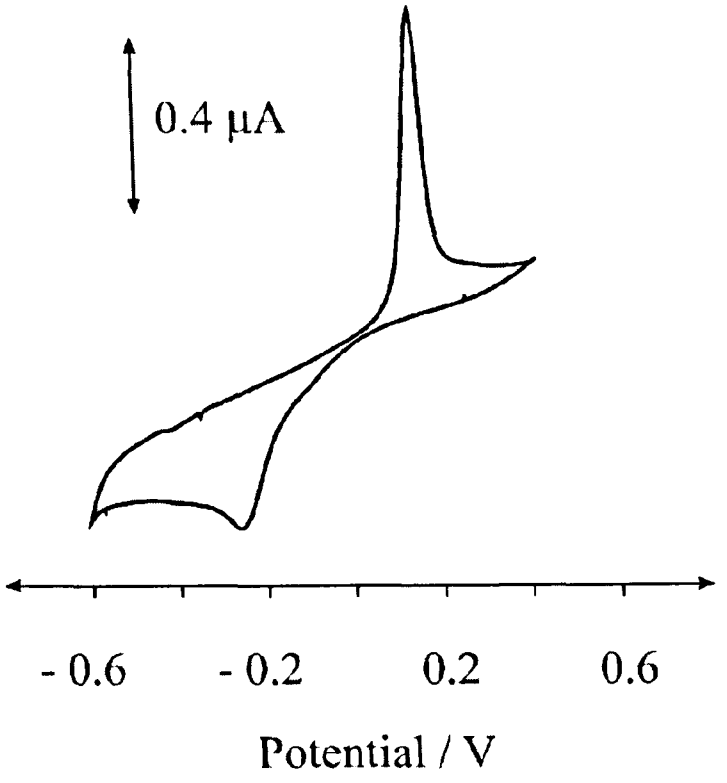

Figure 11.2. Typical cyclic voltammogram using the gold ensemble in 1mM Arsenic (III) in pH 1 phosphate buffer at a scan rate 0f 5 mv/s. The potential was held at -1.0 V for 5 seconds before the addition of arsenic (III).

Plots of arsenic monolayers versus deposition time are shown in figure 11.3A where it is observed that the amount of arsenic limits as the deposition time is increased. Figure 11.3B depicts a plot of arsenic monolayers versus natural logarithm of the deposition time and it is clear that the amount of arsenic deposited on the gold (111) surface is less than one monolayer which limits as the deposition time is increased. As the amount of the arsenic deposit on the gold nanoparticle ensembles increases, the rate of deposition decreases.

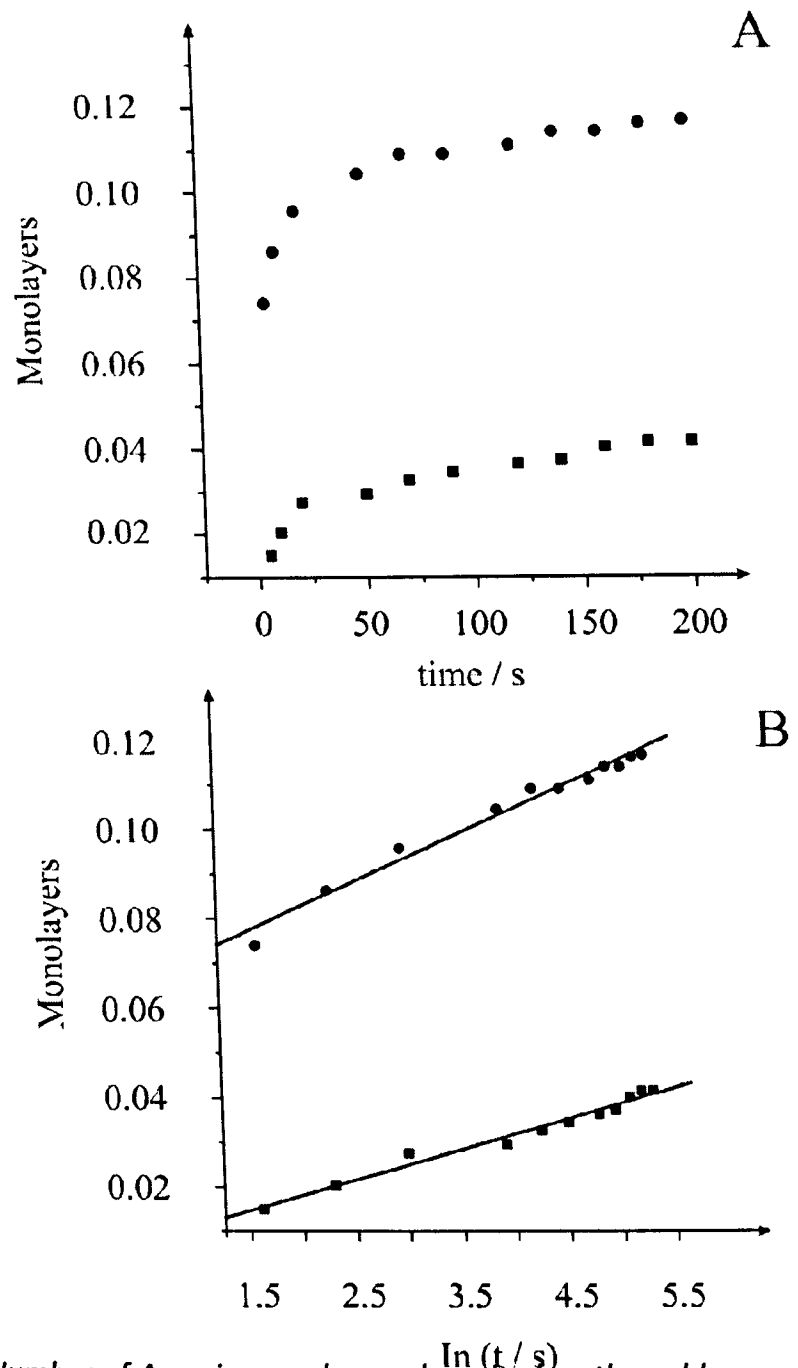

Figure 11.3. Number of Arsenic monolayers deposited on the gold nanoparticle ensemble at the deposition potential of – 0. 25 V (squares) and – 0.6 V (circles) in phosphate buffer (pH 1) and 0.1 mM arsenic (III) solution as function of the deposition time (A) and of the natural logarithm of the applied deposition time (B). Shown in (B) is the linear regression fits of the data.

Previous theory has been developed to extract mechanistic information from the electrochemical deposition of Arsenic (III) on a gold (111) single crystal electrodes.[15] The theory considers that for the electrochemical reduction of as described by equation (4),

$$O + ne^- \rightarrow R \qquad (4)$$

that n occurs in continuous steps, as described below:

$$O + e^- \leftrightarrow A_1,\ A_1 + e^- \leftrightarrow A_2,$$

and so forth

where m steps are in equilibrium, as described in the general form:

$$A_{m-1} + e^- \leftrightarrow A_m \qquad (5)$$

In the electrochemical reaction, the rate-determining step is described by:

$$A_m + e^- \longrightarrow B_{m+1} \qquad (6)$$

and (n-m-1) steps are in equilibrium:

$$A_{m+1} + e^- \longleftrightarrow A_{m+2}$$

$$A_{n-1} + e^- \longleftrightarrow R$$

The overall current can be described as:

$$-i = i^0\left[\exp\left(\frac{\vec{\alpha}F\eta}{RT}\right) - \exp\left(-\frac{\vec{\alpha}F\eta}{RT}\right)\right] \qquad (7)$$

where $\eta = E_{eq} - E$ is the cathodic overpotential and E_{eq} is the equilibrium potential and the constants $\vec{\alpha} = m + \alpha$ and $\overleftarrow{\alpha} = n - m - \alpha$ are the apparent transfer coefficients. Note that $\vec{\alpha} + \overleftarrow{\alpha} = n$ and at the same time $\vec{\alpha} / \overleftarrow{\alpha} = (m + \alpha) / (n - m - \alpha)$.

In the case that the total number of electrons in the electrochemical process is 3, we may write $\vec{\alpha}/\overleftarrow{\alpha} = (m+\alpha)/(3-m-\alpha)$.

If the transfer of the first electron is the rate-determining step, $m=0$ and $\vec{\alpha}/\overleftarrow{\alpha} = \alpha/(3-\alpha)$ since $0 \le \alpha \le 1$, $0 \le \vec{\alpha}/\overleftarrow{\alpha} \le 0.5$

If the transfer of the second electron is the rate-determining step, $m=1$ and $\vec{\alpha}/\overleftarrow{\alpha} = (1+\alpha)/(2-\alpha)$. In this case, $0.5 \le \vec{\alpha}/\overleftarrow{\alpha} \le 2$.

If the transfer of the third electron is the rate-determining step, $m=2$ and $\vec{\alpha}/\overleftarrow{\alpha} = (2+\alpha)/(1-\alpha)$. In this case, $2 \le \vec{\alpha}/\overleftarrow{\alpha} \le \infty$.

When the cathodic overpotential is large enough and its satisfies $\eta >> 0$ and equation (7) is simplified to

$$\eta = E_{eq} - E = -\frac{RT}{\tilde{\alpha}F} In\, i^0 + -\frac{RT}{\tilde{\alpha}F} In\, i \qquad (8)$$

and when the anodic overpotential is large, $\eta << 0$, equation (7) becomes:

$$\eta = E_{eq} - E = -\frac{RT}{\tilde{\alpha}F} In\, i^0 + -\frac{RT}{\tilde{\alpha}F} In\, i \qquad (9)$$

Tafel plots based on equations (8) and (9) were constructed from the cyclic voltammetric profiles of arsenic (III) electrochemically reduced on the gold nanoparticle ensemble. Figure 11.4 depicts typical Tafel plots from the cyclic voltammetric profiles.

Linear regression fit of the cathodic and anodic Tafel plots were determined with the cathodic Tafel slope found to be -0.296 V Dec^{-1} where $\vec{\alpha}=0.25$ and the anodic Tafel plot found to correspond to 0.02 V Dec^{-1} where $\overleftarrow{\alpha}=2.62$. As $\vec{\alpha}+\overleftarrow{\alpha}=n$, we deduced that $\vec{\alpha}+\overleftarrow{\alpha}$ =2.87 This value is in excellent agreement to the expected number of transferred electrons of 3. Note that literature reports of using a gold (111) single crystal yielded a *n* value of 3.19.[15] From the conditions identified above the rate determining step can be deduced, thus $\vec{\alpha}/\overleftarrow{\alpha}=0.09$ and given that $0\leq\vec{\alpha}/\overleftarrow{\alpha}\leq 0.5$ indicates that the transfer of the first electron is the rate determining step. This is in excellent agreement with that reported using single crystal gold electrodes[15] again confirming the accuracy of our method. The overall reaction mechanism may now be written as:

$$As(III)(aq)+e \longrightarrow As(II)(aq) \qquad \text{rds} \qquad (10)$$

$$As(II)(aq)+e \Leftrightarrow As(I)(aq) \qquad \text{equilibrium} \qquad (11)$$

$$As(I)(aq)+e \Leftrightarrow As(0)(ads) \qquad \text{equilibrium} \qquad (12)$$

From the analysis above, $\vec{\alpha}=m+\alpha$ and $\overleftarrow{\alpha}=n-m-\alpha$ which can now be written as: $\vec{\alpha}=m+\alpha=0.25$ where $\alpha=0.25$ and $\overleftarrow{\alpha}=3-\alpha=2.62$ where $\alpha=0.38$. The average value of α is thus 0.32. This lower value results from a dissymmetry of the potential energy curves of the reactant and products in the context of Butler–Volmer kinetics which is due to the irreversibility of the first electron transfer (rate determining step) in the electrochemical deposition of arsenic.

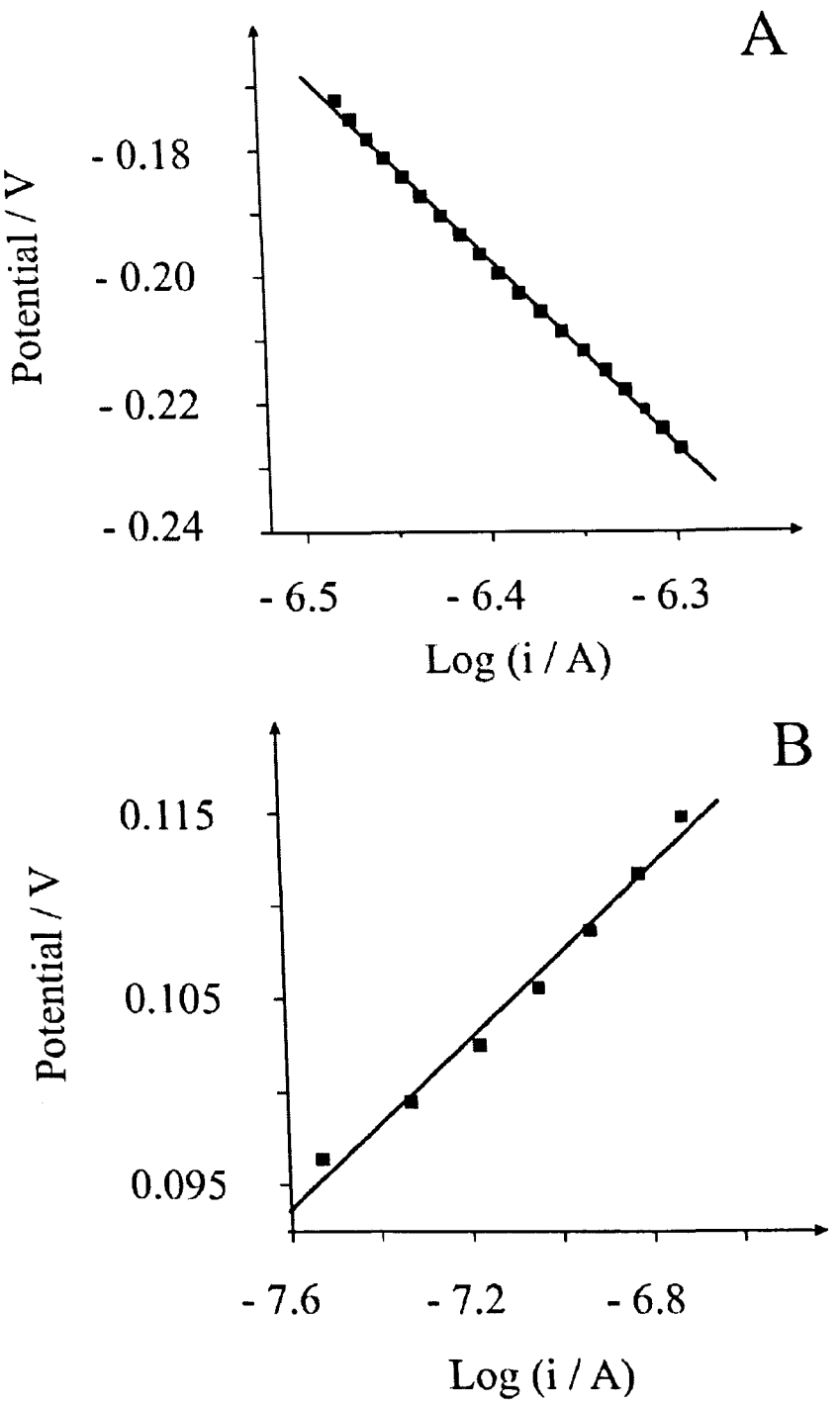

Figure 11.4. Cathodic and anodic Tafel plots of arsenic (III) deposited on a gold ensemble in phosphate buffer (pH 1) and 0.1 mM arsenic (III) solution at a scan rate of 5 mVs^{-1}. An in-situ pre-treatment was applied by holding the potential at – 1.0 V for 5 second in phosphate buffer (pH 1) only. The lines between points are linear regression fits of the data.

Next the deposition of arsenic on the gold nanoparticle ensembles was explored over a range of voltammetric scan rates. A plot of cathodic peak current versus the square root of scan rate is depicted in figure 11.5A displaying a highly linear response. A plot of cathodic peak potential versus the logarithm of scan rate is also highly linear, as shown in figure 11.5B, indicating that the deposition of arsenic is an irreversible reaction.

The relationship between the peak potential, E_p as a function of the logarithm of the scan rate, since the transfer of the first electron is the rate determining step, is the same as that of a one-step, one-electron reaction:[15]

$$E_p = E^\circ - (RT/\alpha n_a F)[0.78 - \ln(k^o/(D)^{1/2} + \ln(\alpha n F v/RT)^{1/2}] \qquad (13)$$

where E is the cathodic peak potential, $E^{0'}$ is the formal potential, D is the diffusion coefficient of As(III), k^o is the standard electrode reaction rate constant, v is the voltammetric scan rate and α is the cathodic transfer coefficient of the rate-determining step. From equation (13) α can be readily deduced from the plot of E versus log v. Consequently α was deduced to be 0.30 which is in excellent agreement with that deduced above.

The electron transfer of the first electron is rate-determining, the peak current for a totally irreversible one step, one electrode reaction is given by equation (14):

$$I_p = (2.98 \times 10^5)\, n(\alpha^2 n)^{1/2}\, A D^{1/2}\, C V^{1/2} \qquad (14)$$

where i is the cathodic peak current, n is the number of electrodes transferred, D is the diffusion coefficient of arsenic (III), C is the concentration of Arsenic (III) and v is the scan rate.

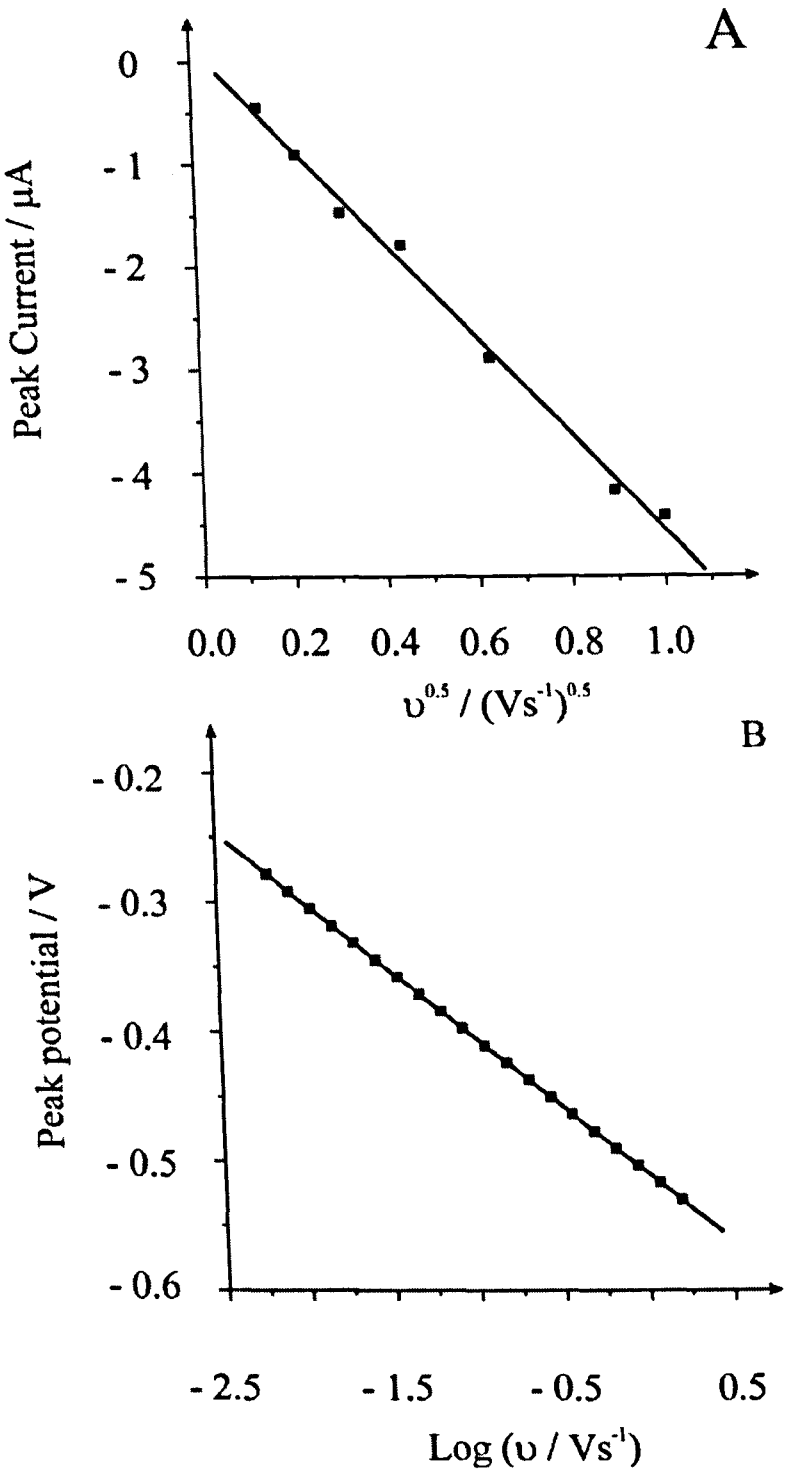

Figure 11.5. A: Plot of cathodic peak current obtained from cyclic voltammetric profiles of arsenic deposited using a gold ensemble in 0.1 mM arsenic (III) in pH 1 phosphate buffer as a function of the square root of scan rate. B: Cathodic peak potential of the cyclic voltammetric profiles as a function of the logarithm of scan rate. The lines between points are linear regression fits of the data.

The electrode area was deduced by assuming that the gold nanoparticles form hemispheres on the electrode surface since the underlying graphite screen-printed electrode is relatively porous which was found to correspond to 0.019 cm^2. From invoking equation (14) and using a α value of 0.30 and an n of 3, the diffusion coefficient of arsenic (III), using was determined to be 2.5 x 10^{-5} cm^2s^{-1} (in pH 1 phosphate buffer). This value agrees extremely well with literature reports[16] of 0.99 (±0.02) x 10^{-5} cm^2s^{-1} in 0.2 M KBr + 1M H_2SO_4 and 1.5 x 10^{-5} cm^2s^{-1} (pH 1 phosphate buffer)[15] indicating the applicability of the gold ensembles for extracting mechanistic electrochemical information.

11.5 Conclusion

To conclude, it has been demonstrated that gold nanoparticle ensembles can be conveniently used to extract mechanistic information from electrochemical processes. Given the inherent facile fabrication and low cost compared to gold single crystal electrodes we envisage that nanoparticle ensembles will become widespread in the pursuit of fundamental electrochemical information.

11.6 References

1. Heller, A. and B. Feldman, *Electrochemical glucose sensors and their applications in diabetes management.* Chemical Reviews, **108,** 2482, 2008.
2. Lin, J.H., C. Zhao, Y. Zhang,S., Sens.Actuators B, **137**, 768, 2009.
3. Tominaga, M., Y. Taema, and I. Taniguchi, Electroanalytical Chemistry, **624**, 5, 2008.
4. Oshea, T.J., S.M. Lunte, and W.R. Lacourse, Analytical Chemistry, **65**, 948, 1993.
5. Zook, C.M., Agricultural and Food Chemistry, **44**, 1773, 1996.
6. Luo, P.F., F.Z. Zhang, and R.P. Baldwin, Analytical Chemistry, **63**, 1702, 1991.
7. Nagy, L., G. Nagy, and P. Hajos, Sensors and Actuators B-Chemical, **76**, 494, 2001.
8. LaCourse, W.R., E. Grushka and N. Grinberg, Crc Press-Taylor & Francis Group: Boca Raton. 47, 247, 2009.
9. Male, K.B., Analytica Chimica Acta, **516**, 35, 2004. **516**.
10. Umar, A., Electrochemistry Communications, **11**, 278, 2009.
11. Reitz, E., Electroanalysis, **20**, 2482, 2008.
12. Luque, G.L., M.C. Rodriguez, and G.A. Rivas, Talanta, **66**, 467, 2005.
13. Zen, J.M., H.H. Chung, and A.S. Kumar, Analyst,. **125,** 1633, 2000.
14. Zen, J.M., Analytical Chemistry, **74,** 6126, 2002
15. Tsai, D.M., Journal of the Chinese Chemical Society,. **52,** 773, 2005.
16. Kumar, A.S. and J.M. Zen, Electroanalysis, **14,** 671, 2002.
17. Kadara, R.O., N. Jenkinson, and C.E. Banks, Sensors and Actuators B-Chemical, **138,** 556, 2009.
18. Kadara, R.O., Electrochemistry Communications, **10,** 1517, 2008.
19. Kano, K., Electroanalytical Chemistry,. **372,** 137, 1994.

20. Torto, N., T. Ruzgas, and L. Gorton, Electroanalytical Chemistry,. **464,** 252, 1999.

21. Ju, H.X. and D. Leech, Analytica Chimica Acta, **345**, 51, 1997.

22. Zang, J.F., Electroanalysis, **19** 1008, 2007.

23. Gao, R.F. and J.B. Zheng,. Electrochemistry Communications, **11,** 608, 2009.

24. Xie, Y.Q. and C.O. Huber, Analytical Chemistry, 1991. **63**, 1714, 1991.

25. Xu, J.Z, Analytical Letters, **36,** 2723, 2003.

26. Safavi, A., N. Maleki, and E. Farjami,. Biosensors & Bioelectronics, **24,** 1655, 2009.

27. Patake, V.D., Materials Chemistry and Physics, **114,** 6, 2009.

28. Hasanzadeh, M,. Catalysis Communications, **10,** 295, 2008.

29. Gao, S.G, Physical Chemistry C; **112,** 19324, 2008.

30. Sljukic, B, Electroanalysis, **19,** 79, 2007.

31. Xu, Q., Sensors and Actuators B-Chemical, **114,** 379, 2006.

Chapter 12

12.0 Cosmetic Electrochemistry: The Facile Production of Graphite Microelectrode Ensembles

12.1 Abstract

The facile and rapid production of microelectrode ensembles is shown to be possible using off-the-shelf cosmetic products and is exemplified with the electrochemical sensing of a toxic metal offering a novel fabrication methodology. *This work was Published in PhysChemChemPhys, **12**, 2285, 2010.*

12.2 Introduction

As previously discussed in chapter 1, microelectrode arrays are a unique tool in the electrochemist's arsenal due to their well identified advantages such as large current densities, high spatial resolution, reduced capacitive charging currents and find beneficial use in a range of applications such as clinical chemistry, electroanalysis, biosensing, environmental sensing and electrophysiology.[1, 2, 3, 4, 5, 6, 7, 8] In microelectrode arrays, microelectrodes are at a fixed distance from their nearest neighbour and an alternative is to have a random array of microelectrodes which are termed as ensembles due to no regular spacing between neighbouring microelectrodes.[3, 9] It has been shown by simulations that a random array can produce the same (but never greater) current–potential response as that of a regular array of equal macroscopic coverage[10] and, due to their nature, random arrays are generally easier to fabricate.[11, 12, 13, 14]

Inspired by the technological importance of microelectrode arrays/ensembles in a plethora of areas, we explore the novel and rapid methodology for producing graphite microelectrode ensembles.

12.3 Experimental

All chemicals used were of analytical grade and were used as received without any further purification from Sigma-Aldrich. All solutions were prepared with deionised water of resistively not less than 18.2 MΩ cm. All solutions were vigorously degassed with nitrogen to remove oxygen.

Voltammetric measurements were carried out using a μ-Autolab III (Eco Chemie, The Netherlands) potentiostat/galvanostat and controlled by Autolab GPES software version 4.9 for Windows XP.

Screen-printed carbon electrodes were fabricated in-house with appropriate stencil designs using a microDEK 1760RS screen-printing machine (DEK, Weymouth, UK). A carbon-graphite ink formulation previously utilised[5]was first screen-printed onto a polyester flexible film (Autostat, 250 μm thickness). This layer was cured in a fan oven at 60 degrees for 30 minutes. Next a silver/silver chloride reference electrode was included by screen printing Ag/AgCl paste (Gwent Electronic Materials Ltd, UK) on to the plastic substrate. Last a dielectric paste ink (Gwent Electronic Materials Ltd, UK) was printed to cover the connections and define the 3mm diameter graphite working electrode. After curing at 60 degrees for 30 minutes the screen-printed electrode is ready to use. All measurements were conducted using a three electrode configureuration with a saturated calomel electrode as the reference rather than the onboard silver-silver chloride reference electrode

to allow comparison with the literature. Connectors for the efficient connection of the screen-printed electrochemical sensors were purchased from Kanichi Research Services Ltd.[6] The polymeric formulation used to create the ensembles is the commercial product 'Nivea for Men silver protect 24h', Beiersdorf AG, Germany. Spray distances refer to the distance from the dispensing nozzle to the electrode surface.

Scanning electron microscopy (SEM) images were obtained using a JEOL JSM-5600LV model. Polaron (Quorum Technologies) SC76640 Auto/Manual High Resolution Sputter coater was used to produce the palladium sputtered electrodes.

12.4 Results and Discussion

Screen-printed macroelectrodes (3 mm diameter) were fabricated as reported previously[15, 16] and their electrochemical performance examined in 1 mM potassium ferrocyanide^{-1} M potassium chloride[17] as depicted in Figure. 12.1.

The heterogeneous rate constant, k^o, was evaluated from fitting of the voltammetric peaks over a range of scan rates with a simulation package which was found to correspond to 0.7 x 10^{-3} cm s^{-1} indicating a quasi-reversible electron-transfer process in agreement with previous studies.[15, 16] The screen-printed electrode was then 'sprayed' with a commercial deodorant, "Nivea For Men Antiperspirant". The modified macroelectrode was then examined using potassium ferrocyanide, and, as depicted in figure 12.1, a change in the voltammetric profile is clearly evident. Increasing the spray time has a dramatic effect compared to the bare macroelectrode where the peak-to-peak separation increases and the magnitude of voltammetric peaks decreases, the response of which is consistent with that of a partially blocked electrode.[18]

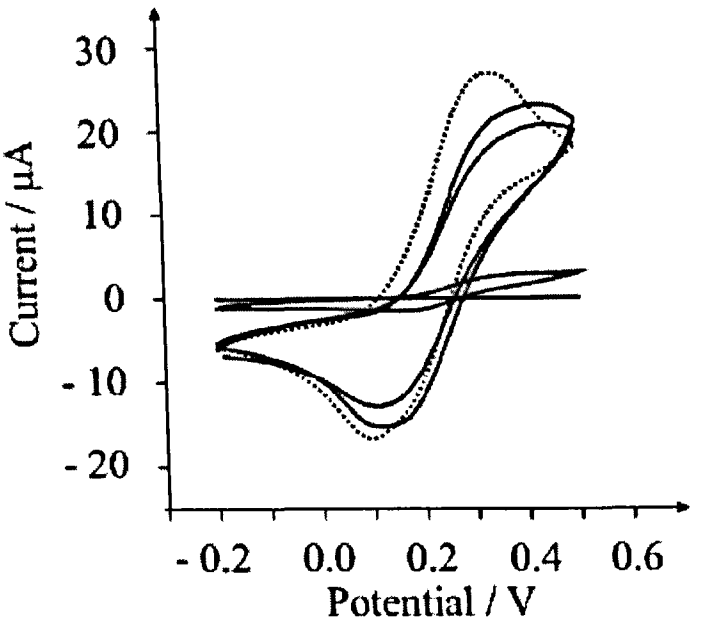

Figure 12.1. Cyclic voltammetric profiles obtained at a bare screen-printed electrochemical platform (dotted line) and then following modification with the cosmetic product at a distance of 200 mm for 2, 5, 8 and 12 seconds. All scans recorded at 0.1 V s^{-1} vs. SCE.

The heterogeneous rate constant observed at the partially blocked electrode surface, k^o_{obs}, is related to the fractional coverage (y) and the heterogeneous rate constant observed at the unmodified (bare) electrode k^o_{bare} via:[18]

$$K^o_{obs} = K^o_{bare}(1 - \theta) \qquad (1)$$

Note that for an overlapping random distribution, the real coverage is given by:[19]

$$\theta_R = 1 - e^{-\theta} \qquad (2)$$

Consequently the real fractional coverage, θ_R, of the partially blocked electrode from increasing spray times was deduced to be 0.3 (±0.1) and 0.5 (±0.12). In the case where quasi-reversible voltammetric profiles are obtained in the accessible range of scan rates, as found here, information for the diffusion domain sites and their sizes is unable to be gathered. However an approximate value of the active site radius (R_a) may be estimated (the exposed working electrode area). The maximal value for R_0 (which is the radius of the diffusion domain, blocking part) can be determined by:[18]

$$Ro \leq \frac{\left(\frac{DRT}{Fv}\right)1}{14.8\,B\,(1-\theta R} \qquad (3)$$

Where for disc-type active sites:

$$B\,(1-\theta_R) = 0.3\,(1-\theta_R)^{-½} \qquad (4)$$

In the above expressions, F is the Faraday constant, D is the diffusion coefficient of the electro-active species (6.5×10^{-6} cm^2 s^{-1}), T is the temperature, R is the gas constant and n is the scan rate. The average radius of the active sites, R_a, which is the underlying substrate, can then be estimated from:

$$R_a = R_0\,(1-\theta_R)^{½} \qquad (5)$$

It follows that $R_a \leq 2.0$ (±0.2) mm and thus the surface now consists of randomly distributed graphite domains which have a radius smaller than 2 microns. SEM images are

shown in Figure. 12.2 where comparison of a standard electrochemical platform and a spray modified electrochemical platform is observed to cover the electrode surface and a decrease in the 'webbed' aspect is clearly evident indicating that the polymer in the cosmetic spray has filled in these gaps and thus reduces the amount of accessible graphite which is attributable for the reduction in the voltammetric profiles.

Noticeable is the presence of smaller clumps of polymer and spherical objects with EDAX indicating that these are aluminium which is a common component in cosmetic 'antiperspirant' sprays. It was found that the aluminium, which is commonly used in deodorant products, is not electrochemically active and consequently does not interfere with our electrochemical measurements.

A recent paper by Zen et al.[20] reported on an electroanalytical method to determine the aluminium content of deodorant products and also reported that electrochemical signals are only possible on silver screen-printed electrodes and not graphite screen-printed electrodes, confirming our observations.

From modification with a cosmetic product, a macroelectrode has been turned into a partially blocked electrode with numerous graphite microdomains. We can estimate the number of graphite domains from the following:

$$N = \frac{A\,\theta_R}{\pi R^2_0}$$

where A is the electrode area of the macroelectrode. From this we can estimate the number of graphite domains to be of the order ~4×10^5.

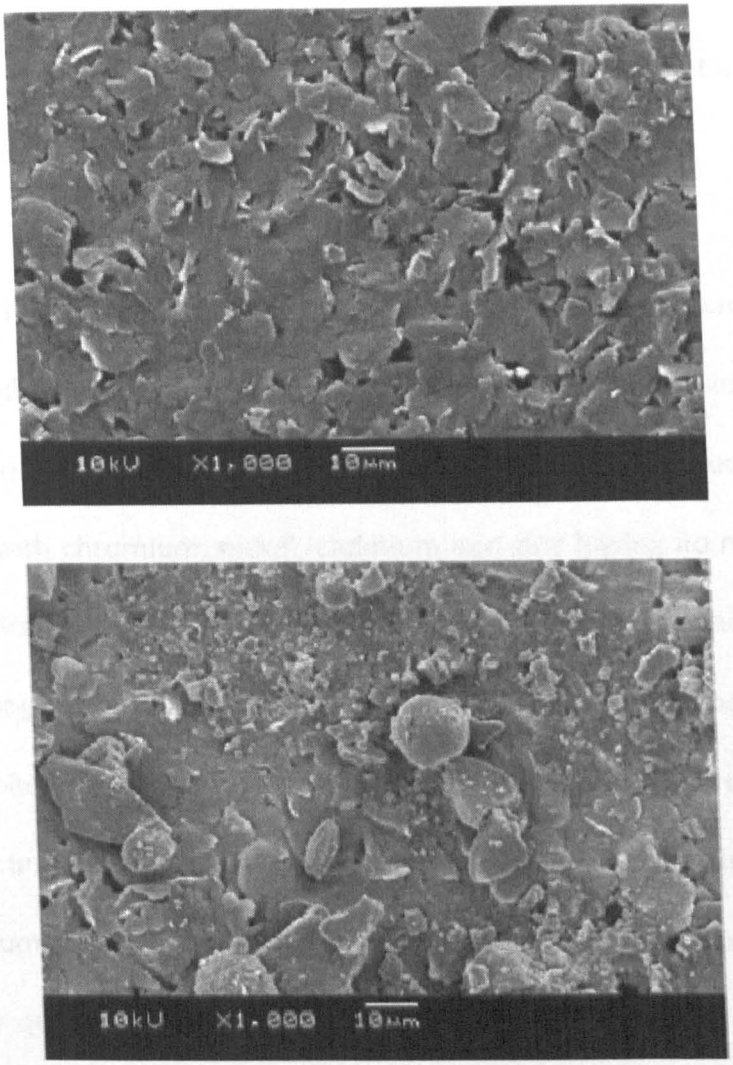

Figure 12.2. SEM images of the unmodified (top) and spray modified (bottom) screen-printed electrodes.

The voltammetric profiles indicate diffusional overlap between neighbouring microdomains such that there is no regular spacing and thus an ensemble[3] of graphite microdomains has been fabricated. Other ways of fabricating ensembles include covering the electrode surface with inert materials,[19] sealing microelectrodes into epoxy resin,[3] covering the electrode surface with a polymer,[21] and sonochemical fabrication.[22] Clearly this approach allows the fabrication of microdomains within seconds and given the low cost of the underlying electrode substrate and the cosmetic modifier these electrodes are very economical. We

believe that through the controlled modification with the cosmetic product this is a potential manufacturing route for these devices.

Last to explore, the electroanalytical utility of our fabricated microdomain electrode, attention is turned to showing proof-of-concept for the electrochemical detection of lead using cathodic stripping voltammetry.[23] The cathodic stripping is, due to its very nature, highly selective, with chromium, nickel, cadmium and zinc having no measurable effect on the electroanalytical measurement. In the case of copper and iron, these may be detected by this methodology but their stripping peaks occur at well resolved potentials from that of lead.[23] Using a solution of 0.1 M nitric acid and a deposition potential of +1.65 V (vs. SCE) in accordance with previous studies, additions of lead were made over the range 0 to 300 mM using a 30 s accumulation time. Figure 12.3 depicts a typical voltammetric profile where a large and easily quantifiable peak is observed at +1.38 V (*vs.* SCE) which is in excellent agreement with literature reports.[23]

Analysis of the peak height (I_H) plotted against added lead concentration (as shown in the inset of Figure. 12.3) reveals two distinct linear ranges, the first over the range 20 to 50 mM (I_H/A = 3.0 X$10^{-1}$$AM^{-1}$ - 6.2 X 10^{-6} A; R^2 = 0.987) and 75 mM to 200 mM (I_H/A=8.6 X 10^{-2} AM^{-1} + 8.8 X10^{-6} A; R^2 = 0.988). Based on the first linear part, the limit of detection (3s) was found to correspond to (N = 3) 9.5 mM. This linear range and the un-optimised detection limit are comparable to ultrasound-assisted deposition using a boron-doped diamond electrode[23] employing a 60 s accumulation time. This comparability is due to the enhanced mass transport at the graphite microdomains.

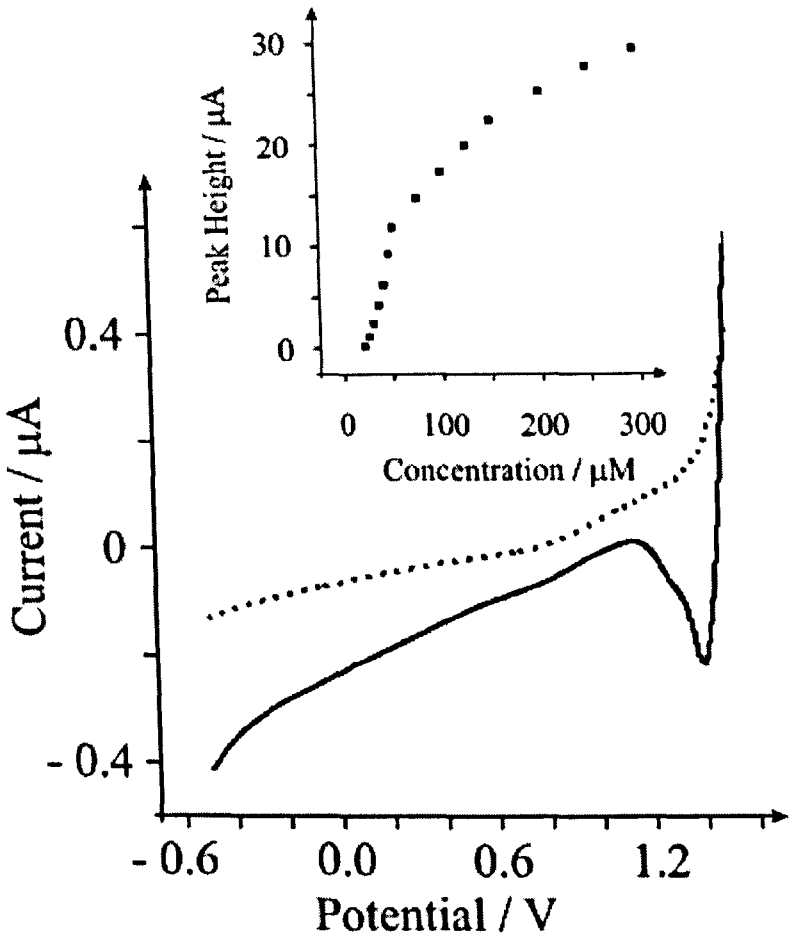

Figure 12.3. Square-wave voltammogram in the absence (dashed line) and presence (solid line) of 20 mM lead (in 0.1 M nitric acid) using the graphite microdomain ensemble. Parameters: square-wave voltammetry using a conditioning potential at -0.5 V (vs. SCE) for 20 s followed by+1.65 V for 30 s. Spraying conditions were 200 mm for 12 s. The inset shows the analysis of peak height from additions of lead.

12.4 Conclusions

To conclude, it has been demonstrated that microelectrode behaviour can be conferred on a macroelectrode through the use of readily available commercial cosmetics. That is, by taking a cosmetic product which is then used to spray a macroelectrode surface, a partially blocked electrode is rapidly and easily fabricated which exhibits steady-state type voltammetric behaviour. The polymer contained within the cosmetic product rapidly binds to the electrode surface and sets within seconds coating the electrode surface but leaving the underlying graphite electrode exposed in the form of graphite micron-sized sites; this new application of commercial products with electrochemistry is aptly termed "cosmetic electrochemistry".

12.5 References

1. J. Gou and E. Lindner, Anal. Chem., **81**, 130, 2009.
2. X.-J. Huang, A. M. O'Mahony and R. G. Compton, Small, **5**, 776, 2009.
3. S. Fletcher and M. D. Horne, Electrochem. Commun., **1**, 502, 1999.
4. Y. H. Lanyon, G. De Marzi, Y. E. Watson, A. J. Quinn, J. P. Gleeson, G. Redmond and D. W. M. Arrigan, Anal. Chem., **79**, 3048, 2007.
5. M. Wei, C. Terashima, M. Lv, A. Fujishima and Z.-Z. Gu, Chem. Commun., **16**, 3624, 2009.
6. M. Varshney and Y. Li, Biosens. Bioelectron., **24**, 2951, 2009.
7. S. Myllymaa, K. Myllymaa, H. Korhonen, J. Toyras, J. E. Jaaskelainen, K. Djupsund, H. Tanila and R. Lappalainen, Biosens. Bioelectron., **24**, 3067, 2009.
8. J. Orozco, C. Jimenez-Jorguera and C. Fernandez-Sanchez, Bioelectrochemistry, **75**, 176, 2009.
9. S. J. Hood, D. K. Kampouris, R. O. Kadara, N. Jenkinson, F. Javier del Campo, F. Xavier Mun˜ oz and C. E. Banks, Analyst, **134**, 2301, 2009.
10. T. J. Davies and R. G. Compton, J. Electroanal. Chem., **63**, 585, 2005.
11. B. Kralj and R. A. W. Dryfe, Phys. Chem. Chem. Phys., **3**, 3156, 2001.
12. A. Berduque, Y. H. Lanyon, V. Beni, G. Herzog, Y. E. Watson, K. Rodgers, F. Stam, J. Alderman and D. W. M. Arrigan, Talanta, 2007, **71**, 1022, 2007.
13. O. Ordeig, J. Del Campo, F. X. Munoz, C. E. Banks and R. G. Compton, Electroanalysis, **19**, 1973, 2007.
14. R. O. Kadara, N. Jenkinson and C. E. Banks, Sens. Actuators, B, **11**, 1377, 2009.
15. R. O. Kadara, N. Jenkinson and C. E. Banks, Sens. Actuators, B, **138**, 556, 2009.

16. R. O. Kadara, N. Jenkinson, B. Li, K. H. Church and C. E. Banks, Electrochem. Commun., **10**, 1517, 2008.

17. The reference electrode was an SCE with a platinum wire as the counter electrode.

18. C. Amatore, J. M. Saveant and D. Tessier, J. Electroanal. Chem., **147**, 39, 1983.

19. T. J. Davies, E. R. Lowe, S. J. Wilkins and R. G. Compton, ChemPhysChem, , **6**, 1340, 2005.

20. J.-H. Zen, T.-H. Yang, A. S. Kumar, Y.-J. Chen, J.-C. Hsu and Y. Shih, Electroanalysis, **21**, 2272, 2009.

21. L. Xiao, I. Streeter, G. G. Wildgoose and R. G. Compton, Sens. Actuators, B, **133**, 118, 2008.

22. A. C. Barton, S. D. Collyer, F. Davis, D. D. Gornall, K. A. Law, E. C. D. Lawrence, D. W. Mills, S.Myler, J. A. Pritchard, M. Thompson and S. P. J. Higson, Biosens. Bioelectron., **20**, 328, 2004.

23. A. J. Saterlay, C. Agra-Gutierrez, M. P. Taylor, F. Marken and R. G. Compton, Electroanalysis, **11**, 1083, 1990.

Chapter 13

13.0 Cosmetic Electrochemistry II: Rapid and Facile Production of Metallic Electrocatalytic Ensembles

13.1 Abstract

A facile methodology for the production of metallic electro-catalytic micro-domain ensembles for a range analytical sensing challenges is reported. A commercially available off-the-shelf cosmetic product can change the voltammetric characteristics of a metallic macro-electrode created via electro-deposition into that of a random ensemble of metallic microelectrode domains. Proof-of-concept is show for three examples; a palladium ensemble for hydrazine sensing, a gold ensemble for the electroanalytical arsenic (III) via anodic stripping voltammetry and platinum ensembles for the direct oxidation of arsenic (III). Last, that the fabrication of metallic micro-domains is demonstrated which can be simplified by sputter-coating (as discussed in chapter 2) screen-printed electrochemical sensing platforms which are beneficially constructed using this cosmetic methodology. Given the facile fabrication and low cost of the underlying electrode substrate and the cosmetic modifier, the widespread implementation of this novel fabrication methodology is expected. *This work was published in Electroanalysis, **22**, 1831, 2010.*

13.2 Introduction

In the pursuit of enhancing electroanalytical performance towards target analytes, one can employ a microelectrode array where the increased mass transport compared to that achievable at a macroelectrode results in an improved signal-to-noise ratio, reduced double layer capacitance and large and easily quantifiable signatures allowing access to lower analytical detection limits and ranges.[1, 2, 3, 4, 5, 6, 7] Microelectrode arrays consist of microelectrodes in a suitable arrangement separated at a fixed distance from their nearest neighbour but despite their inherent advantages in sensing, their application can be limited by their cost of fabrication.[1] A lesser known approach is to employ a microelectrode ensemble where in this arrangement there is no regular spacing between neighbouring microelectrodes and are termed ensembles.[2, 3] It has been shown by simulations that a random array can produce the same, but never greater, current-potential response as that of a regular array of equal macroscopic coverage.[2] Microelectrode ensembles are generally easier to fabricate with notable approaches including, sealing thousands of microelectrodes in epoxy resin,[2] electro-deposition of polymers onto screen-printed electrode followed by sonochemical ablation revealing the underlying carbon surface,[4] fabrication of boron-doped diamond nano-disc electrodes by a three step methodology involving polymeric coatings.[5]

In chapter 12, the concept of Cosmetic Electrochemistry has been introduced[6] where a commercially available cosmetic product, a deodorant, can be used to confer microelectrode behaviour on a macroelectrode. Proof-of-concept was demonstrated, that a graphite screen-printed electrode can be sprayed with an off-the-shelf cosmetic product and within seconds is ready to use. The polymer contained within the cosmetic product partially blocks the graphite screen-printed electrode surface leaving the underlying

graphite electrode exposed in the form of graphite micron-sized sites which are randomly distributed across the electrode surface. The creation of microdomain sites enhances mass transport of the target analyte and it was demonstrated that the electroanalytical performance of the cosmetically modified electrode, via the cathodic stripping of lead could achieve a similar performance to current state-of-the-art sensing employing power ultrasound.

In this chapter, proof-of-concept is further demonstrated for fabricating graphite micro-ensemble and demonstrate that this facile methodology can be utilised for the manufacture of electro-catalytic micro-ensembles for a range of electroanalytical challenges.

13.3 Experimental Section

All chemicals used were of analytical grade and were used as received without any further purification from Sigma-Aldrich. All solutions were prepared with deionised water of resistively not less than 18.2 MΩ cm. All solutions were vigorously degassed with nitrogen to remove oxygen.

Voltammetric measurements were carried out using a μ-Autolab III (Eco Chemie, The Netherlands) potentiostat/galvanostat and controlled by Autolab GPES software version 4.9 for Windows XP.

Screen-printed carbon electrodes were fabricated in-house with appropriate stencil designs using a microDEK 1760RS screen-printing machine (DEK, Weymouth, UK). A carbon-graphite ink formulation previously utilised[5]was first screen-printed onto a polyester flexible film (Autostat, 250 μm thickness). This layer was cured in a fan oven at 60 degrees for 30

minutes. Next a silver/silver chloride reference electrode was included by screen printing Ag/AgCl paste (Gwent Electronic Materials Ltd, UK) on to the plastic substrate. Last a dielectric paste ink (Gwent Electronic Materials Ltd, UK) was printed to cover the connections and define the 3mm diameter graphite working electrode. After curing at 60 degrees for 30 minutes the screen-printed electrode is ready to use. All measurements were conducted using a three electrode configureuration with a saturated calomel electrode as the reference rather than the onboard silver-silver chloride reference electrode to allow comparison with the literature. Connectors for the efficient connection of the screen-printed electrochemical sensors were purchased from Kanichi Research Services Ltd.[6] The polymeric formulation used to create the ensembles is the commercial product 'Nivea for Men silver protect 24h', Beiersdorf AG, Germany. Spray distances refer to the distance from the dispensing nozzle to the electrode surface.

Scanning electron microscopy (SEM) images were obtained using a JEOL JSM-5600LV model. Polaron (Quorum Technologies) SC76640 Auto/Manual High Resolution Sputter coater was used to produce the palladium sputtered electrodes.

13.4 Results and Discussion

First, the response of a gold plated screen-printed electrode is considered. Using a gold solution consisting of 1 mM $HAuCl_4$ in 0.1M H_2SO_4 a screen-printed electrode, reported previously,[7] was electrochemically modified with gold via chronoamperometry by holding the potential at - 0.4 V (vs. SCE) for 300 seconds. The gold modified electrode was explored in 1 mM potassium ferrocyanide / 0.1 M potassium chloride with figure 13.1 depicting typical cyclic voltammetric profiles.

The heterogeneous rate constant, k^0, was evaluated from fitting of the voltammetric peaks over a range of scan rates with a simulation package which was found to correspond to 3.2×10^{-3} cm s^{-1} indicating a quasi-reversible electron transfer process. This gold modified screen-printed electrode was modified with the polymeric formulation using a constant spraying distance of 200 milli-metres with the effect of different spray times explored. As depicted in figure 13.1, a change in the voltammetric profile is clearly evident. Increasing the spray time has a dramatic effect compared to the bare macro-electrode where the peak-to-peak separation increases and the magnitude of voltammetric peaks decrease, the response of which is consistent with that of a partially blocked electrode.[10] SEM was used to explore the gold modified screen-printed electrode before and after modification with the cosmetic product which is shown in figure 13.2.

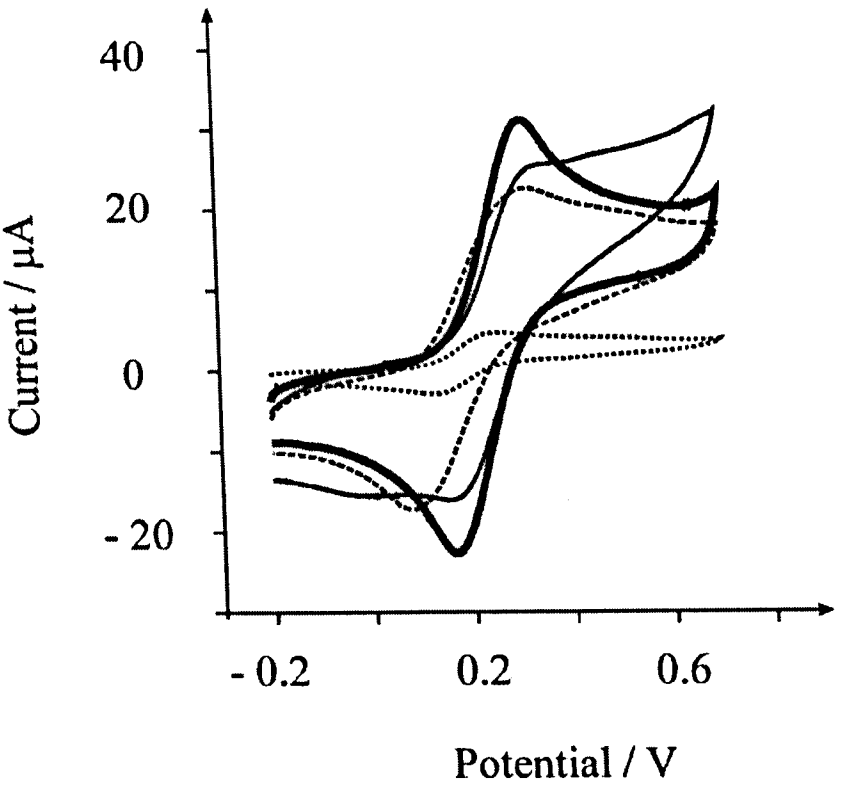

Figure 13.1. Cyclic voltammetric profiles recorded in 1mM potassium ferrocyanide / 0.1 M potassium chloride obtained with a gold modified screen-printed electrochemical platform (thick line) and from applying spray times of 2 (thin line), 4 (dashed line) and 6 (dotted line) seconds at a distance of 200 mm. All scans recorded at 50 mVs^{-1} vs. SCE.

It is evident that the electrode surface is covered with a polymeric formulation and has reduced the amount of accessible graphite which is attributable for the reduction in the voltammetric profiles. Noticeable is the presence of smaller clumps of polymer and components of the cosmetic 'antiperspirant' spray which was identified via EDAX as aluminium and magnesium. The magnitude of modification is greater in this example compared to that observed at cosmetically modified graphite screen-printed electrodes[6] indicating a possible greater adherence of the polymeric formulation to the gold surface.

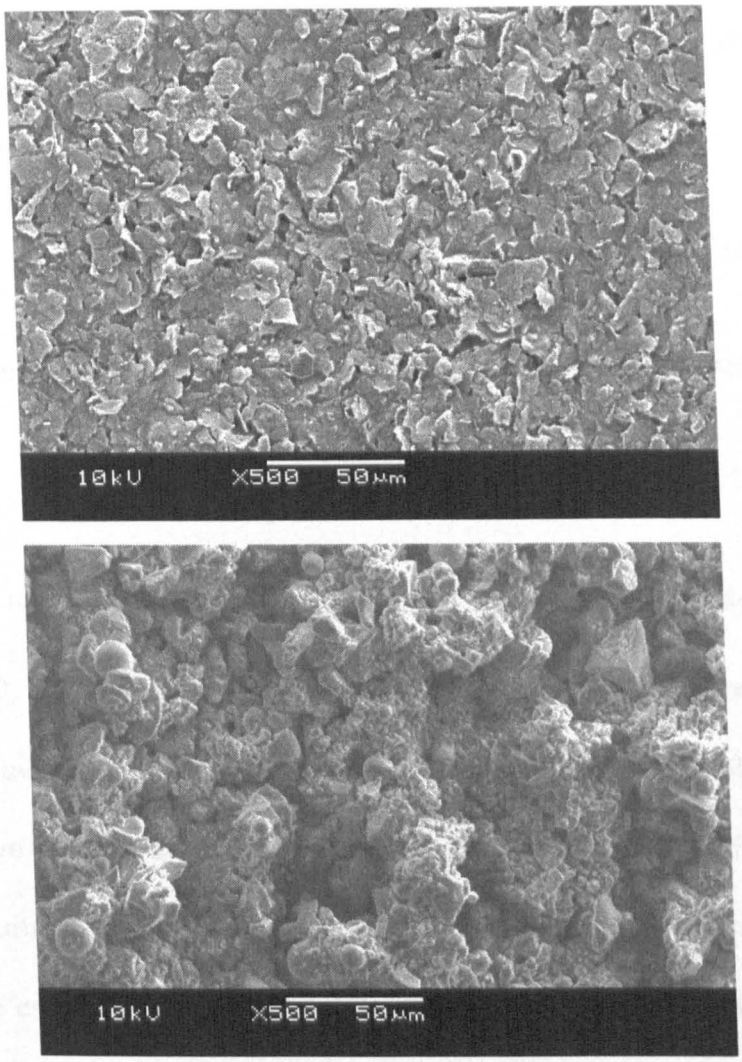

Figure 13.2. SEM images of a gold plated screen-printed electrode (top image) and after polymeric modification (bottom image).

The voltammetric profiles (see figure 13.1) clearly indicate that polymeric formulation has not completely covered the electrode surface and discrete domain of the underlying gold surface must be accessible to give rise to the voltammetry observed in figure 13.1 but unfortunately is not easily identified with SEM.

Returning to the voltammetric profiles observed in figure 13.1, the heterogeneous rate constant observed at the partially blocked electrode surface, k^{o}_{obs} is related to the

fractional coverage (θ) and the heterogeneous rate constant observed at the unmodified (bare) electrode k^o_{bare} via :

$$k^o_{obs} = k^o_{bare}(1-\theta) \qquad (1)$$

Note that for an overlapping random distribution, the real coverage is given by:

$$\theta_R = 1-e^{-\theta} \qquad (2)$$

Consequently the real fractional coverage, θ_R of the partially blocked electrode was deduced to be 0.30, 0.51 and 0.56 for spray times of 2, 4 and 6 second respectively. In the case where quasi-reversible (as discussed in chapter 5) voltammetric profiles are obtained in the accessible range of scan rates, as found here, information for the diffusion domain sites and their sizes is unable to be gathered. However an approximate value of the active site radius (R_a) may be estimated. The maximal value for R_o (which is the radius of the diffusion domain, in this case the blocking polymer) can be determined by:

$$R_0 \leq \frac{\left(\frac{DRT}{F\upsilon}\right)^{\frac{1}{2}}}{14.8B(1-\theta_R)} \qquad (3)$$

where $B(1-\theta_R) = 0.3(1-\theta_R)^{\frac{1}{2}}$ for disc-type active sites. In the above expressions, F is the Faraday constant, D is the diffusion coefficient of the electro-active species (6.5 x 10^{-6} cm^2 s^{-1}),[11] T is the temperature, R is the gas constant and υ is the scan rate. The average radius of the active sites, R_a which is the underlying substrate, can then be estimated from: $R_a = R_0(1-\theta_R)^{\frac{1}{2}}$ It follows that $R_a \leq$ 1.3 (± 0.4) μm and thus the surface consists of randomly distributed gold domains which have an average radius smaller than 1.3 microns;

this is in excellent agreement with that reported previously for producing graphite microdomains via this methodology.[6] It is clear from the voltammetric characterisation that the modification of the gold macroelectrode has resulted in the creation of random array of gold microelectrodes and the terminology, gold ensembles, is quite appropriate. We now turn to demonstrating that a range of electro-catalytic ensembles are possible for a range of analytical challenges.

Attention was turned to exploring the analytical utility of the gold ensembles with the example of the electroanalytical sensing of Arsenic (III). Arsenic (III) is an important analyte due to its reported toxicity and presence in drinking water samples/wells.[8, 9, 10, 11] Gold ensembles were produced by spray coating the gold modified screen-printed electrode with the polymeric formulation using a spray distance and time of 200 mm and 6 seconds respectively. Linear sweep voltammetry was employed using a deposition time and potential of 120 seconds and - 1.2 V (vs. SCE) respectively with micro-molar additions of Arsenic (III) made into 1M nitric acid solution(double distilled sulphuric) Figure 13.3 depicts typical voltammograms. Analysis of the peak height (I_H) from Arsenic (III) additions were found to be linear over the range 1 μM to 15 μM ($I_H / A = 266 \times 10^{-3} AM^{-1} + 1.02 \times 10^{-6} A$; $R^2 = 0.998$; $N = 5$) with a detection limit found to correspond to 4.8×10^{-7} M. This detection limit is comparable to gold nanoparticle arrays [12] and with further optimisation by applying linger deposition times and more sensitive electrochemical techniques, improvements to the limit of detection are possible.

Next attention is turned to exploring the fabrication of platinum ensembles. A graphite screen-printed electrode was modified via chronoamperometry by holding the potential at -

1.2 V (vs. SCE) for 300 seconds in a solution containing 1mM $PtCl_6^{2-}$ / 0.1M KCl. The platinum ensemble was fabricated by applying the polymeric formulation with a distance and time of 200 milli-metres and 8 seconds respectively. Work by Dai and Compton[13] have shown that platinum nanoparticle decorated glassy carbon electrodes can be used for the electro-analytical sensing of Arsenic (III) without any interference from copper. Copper is always present in water samples and the voltammetric signal from copper can, in some cases, detrimentally affect the voltammetric signal of Arsenic (III). The methodology of Dai and Compton is based on the direct electrochemical oxidation of Arsenic (III) to Arsenic (V) which occurs at relatively high potentials, well resolved from the voltammetric signals from copper.[13]

The platinum ensembles towards the electrochemical oxidation of Arsenic (III) were explored. Using 0.1 M H_2SO_4 (double distilled) additions of Arsenic (III) were made over the range 100 to 1000 μM. Figure 13.4A depicts the electrochemical response of the platinum ensembles where the electrochemical oxidation of Arsenic (III) to Arsenic (V) is evident at + 0.85 V (vs. SCE) which is in excellent agreement with previous studies.[13]

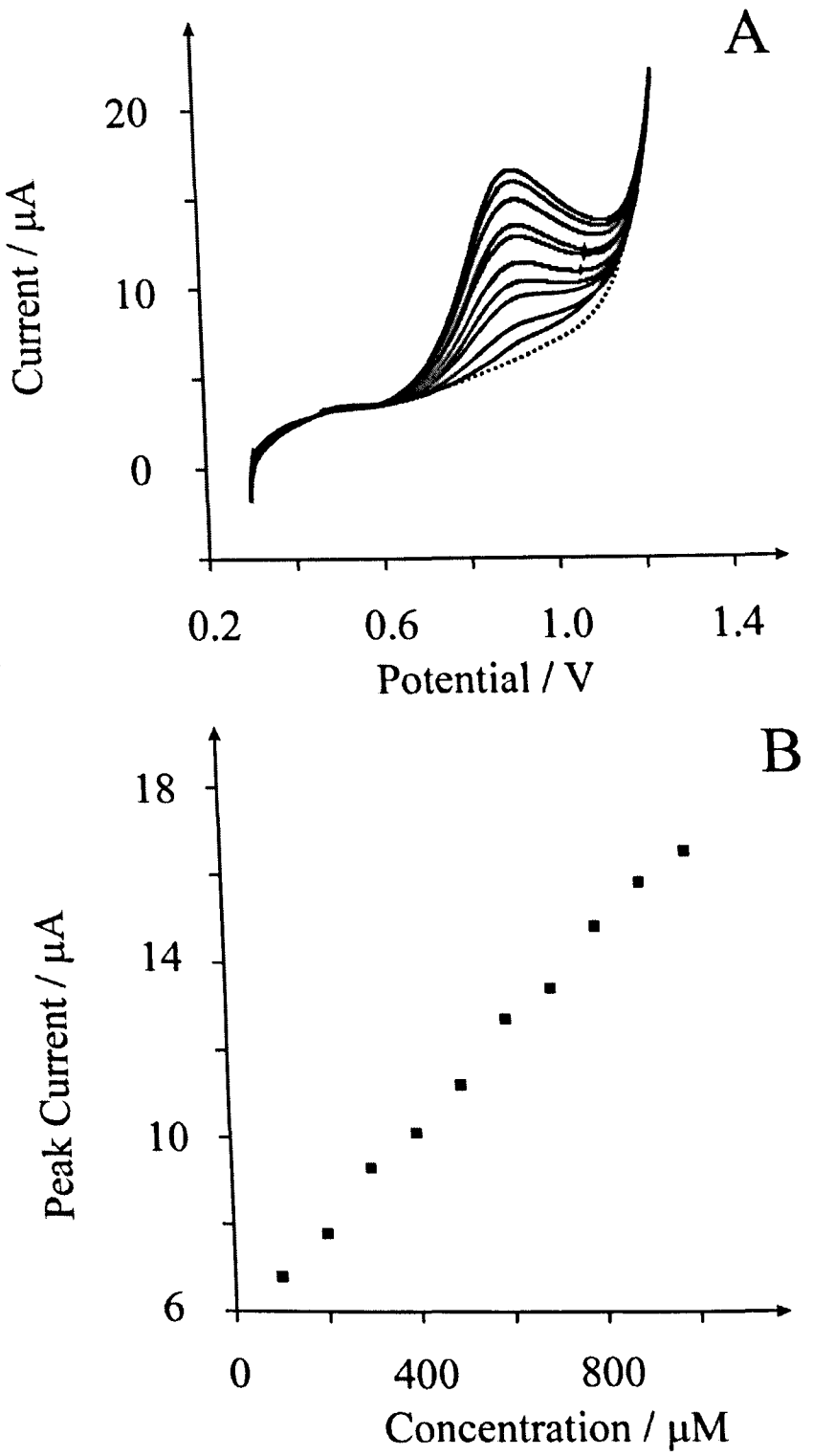

Figure 13.3. Linear sweep voltammetry resulting from additions of arsenic(III) into 1 M sulfuric acid using a gold ensemble. Parameters: deposition potential and time of -1.2 V (vs. SCE) and 120 seconds. Part B is the analysis of the peak current as a function of added arsenic(III) concentrations.

A large background current is evident which may likely be related to the thickness of the platinum film used to create the platinum ensembles. The analysis of the peak height against Arsenic (III) concentration is shown in figure 13.4B where a linear response (I_H / A = 11 x 10^{-3} AM^{-1} + 5.76 x 10^{-6} A; R^2 = 0.998; N = 10) is observed over the concentration range studied. A limit of detection, (based on three sigma), was found to correspond to 1.3 μM. This analytical response in terms of linear range, detection limit and sensitivity is comparable to that previously reported using platinum nanoparticle modified glassy carbon electrodes.[13] It was found that the detection of lower concentrations of Arsenic (III) is not possible even through tailoring the size and distribution of the polymeric formulation by adapting the spraying times and applied distances. While the analytical protocol may have some analytical merit given that the concentration of arsenic in Bangladesh water wells has been reported to be as low as 0.06 μM up to 10 μM, this methodology appears to not be suitable for Arsenic (III) determination via the direct electrochemical oxidation.[13, 14]

Next, exploring the response of palladium ensembles was studied. The method of Ji *et al.*[9] was utilised which involves four steps. The first step involves the electrochemical oxidation activation of the edge plane like - sites/defects on the screen-printed electrode surface by cycling the potential from +1.8 V to -0.4 V (vs. SCE) using a scan rate of 200mV s^{-1} for 10 cycles in 0.5M Na_2SO_4. This step likely introduces oxygen containing functional groups on the edge plane like – sites/defects on the surface of the screen-printed electrode. The second step involves transferring the screen-printed electrode into a 1mM $PdCl_2$ solution in 0.1M H_2SO_4 with potential cycling from +0.4 V to +1.5 V for 5 cycles at 200 mV s^{-1}.

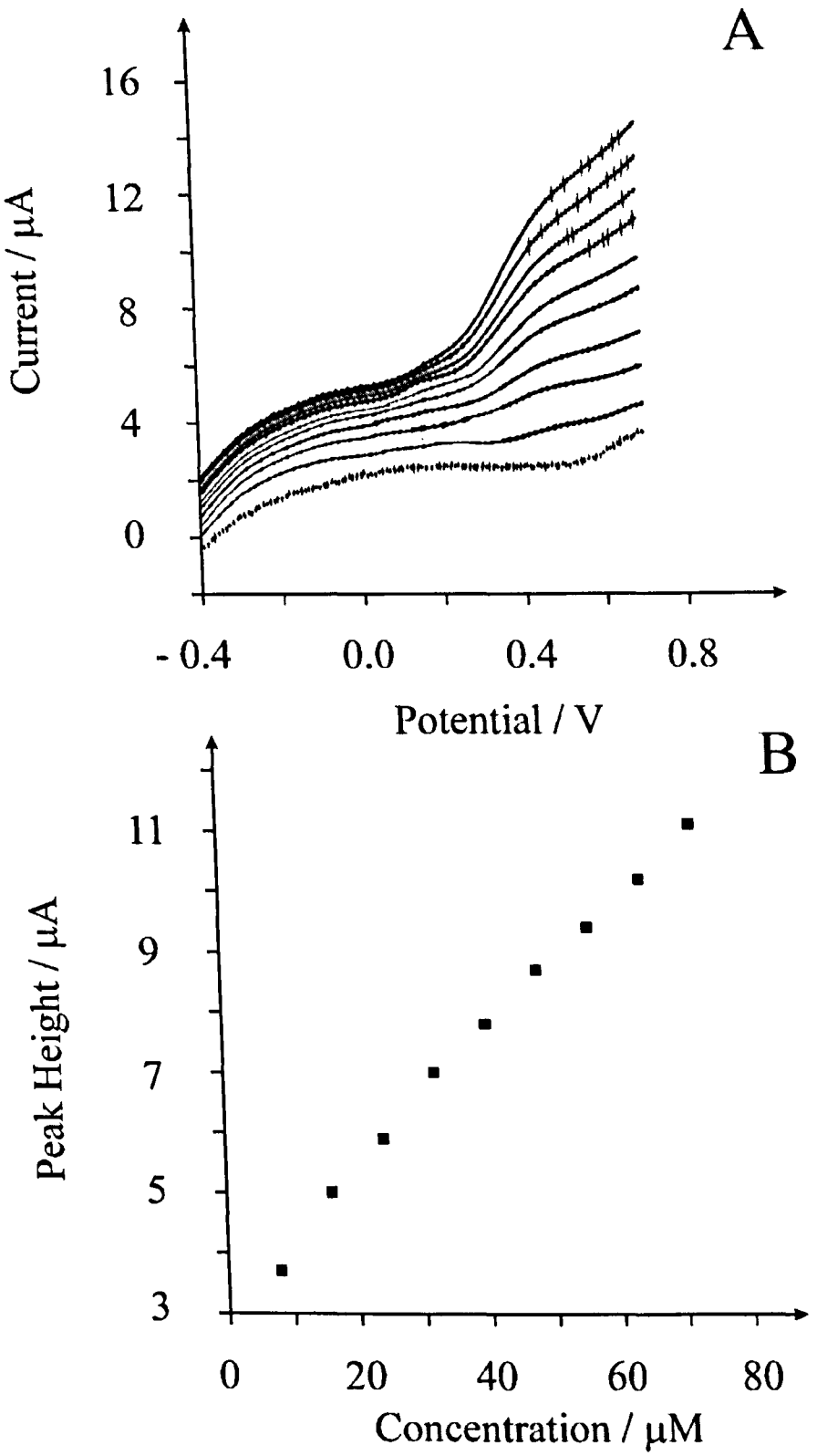

Figure 13.4 (A) Linear sweep voltammetry resulting from the direct oxidation of arsenic(III) using a platinum ensemble. (B) is the analysis of the peak current as a function of added arsenic(III) concentrations.

Palladium oxide (s) and/or complexes of palladium on the screen-printed electrode surface at various oxygen containing functional groups is expected to be produced at this stage. The third step involves the formation of palladium metal by transferring the modified electrode into 0.1M H_2SO_4 and potential cycling from +1.1 V to -0.5 V at 300 mV s^{-1} for 5 scans. The final step involves spray coating with the polymeric formulation to produce palladium ensembles.

Next the electrochemical oxidation of hydrazine using the palladium ensembles was explored. Figure 13.5A depicts the voltammetric profiles observed from additions of hydrazine in to a pH 7 solution where a well defined limiting current is observed. Figure 5B depicts the analysis of the peak height (I_H) recorded at + 0.45 V vs. SCE which is observed to produce a linear response over the concentration range 8 to 72 μM (I_H / A = 1.1 x 10^{-7} A/μM + 3.1 x 10^{-6} A; R^2= 0.998; N = 9). The limit of detection (based on three sigma) was found to correspond to 3.7 μM.

This is competitively comparable to palladium plated boron-doped diamond arrays,[15] caffeic acid modified glassy carbon electrode,[16] catechol modified carbon nanotubes,[17] Ni(II)-baicalein complex modified multi-wall carbon nanotube paste electrode,[18] and is enhanced over electrospun palladium nanoparticle/carbon nanofibers[19] and nickel hexacyanoferrate nanoparticles.[20]

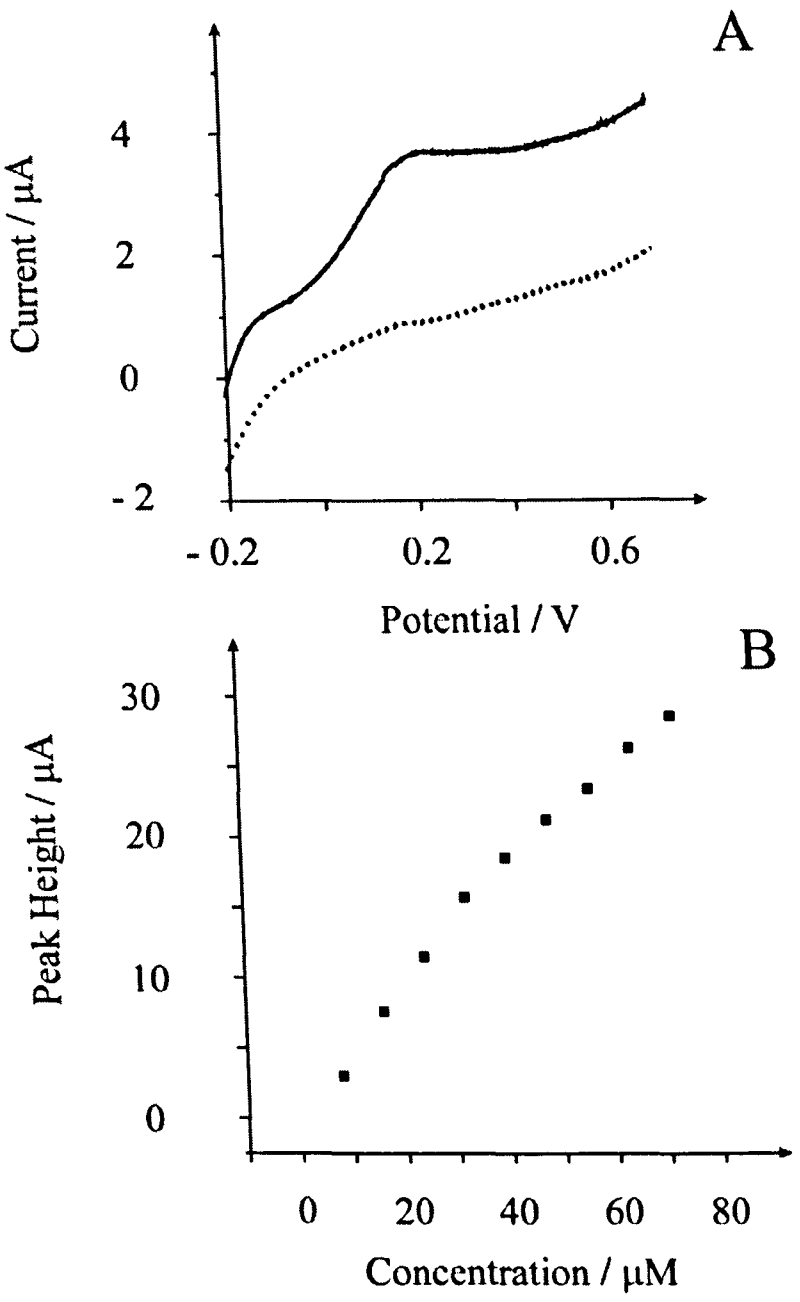

Figure 13.5 Linear sweep voltammograms (A) of the electrochemical oxidation of hydrazine into a pH 7 buffer solution using a palladium ensemble. (B) depicts the analysis of the peak current versus hydrazine additions.

Last, consideration into the possible scaling up of the methodology was explored. Rather than use electrochemical deposition to modify the screen-printed electrodes, the bare electrode was placed into a sputtering device to produce a palladium film. This electrode was explored towards the sensing of hydrazine using the same parameters used in figure 13.5.

Typical voltammetric profiles and analysis of the analytical signal as a function of hydrazine concentration is depicted in Figure 13.6.

An analytically useful response is observed with a linear response over the range 8 to 48 mM (I_H (A) = 0.46 A/M + $1.0x10^{-6}$ A; R^2=0.998; N = 6) is evident with a limit of detection (based on three sigma) found to correspond to 1.9 mM. This analytical performance is quantitatively similar to that observed above with the exception that the linear range is not as extended as observed in Figure 13.5 but yet the sensitivity is improved likely due to the porous nature of the sputtered film. The analytical response indicates that the underlying catalytic electrode can be fabricated via other methods which might be easier to scale up for mass production.

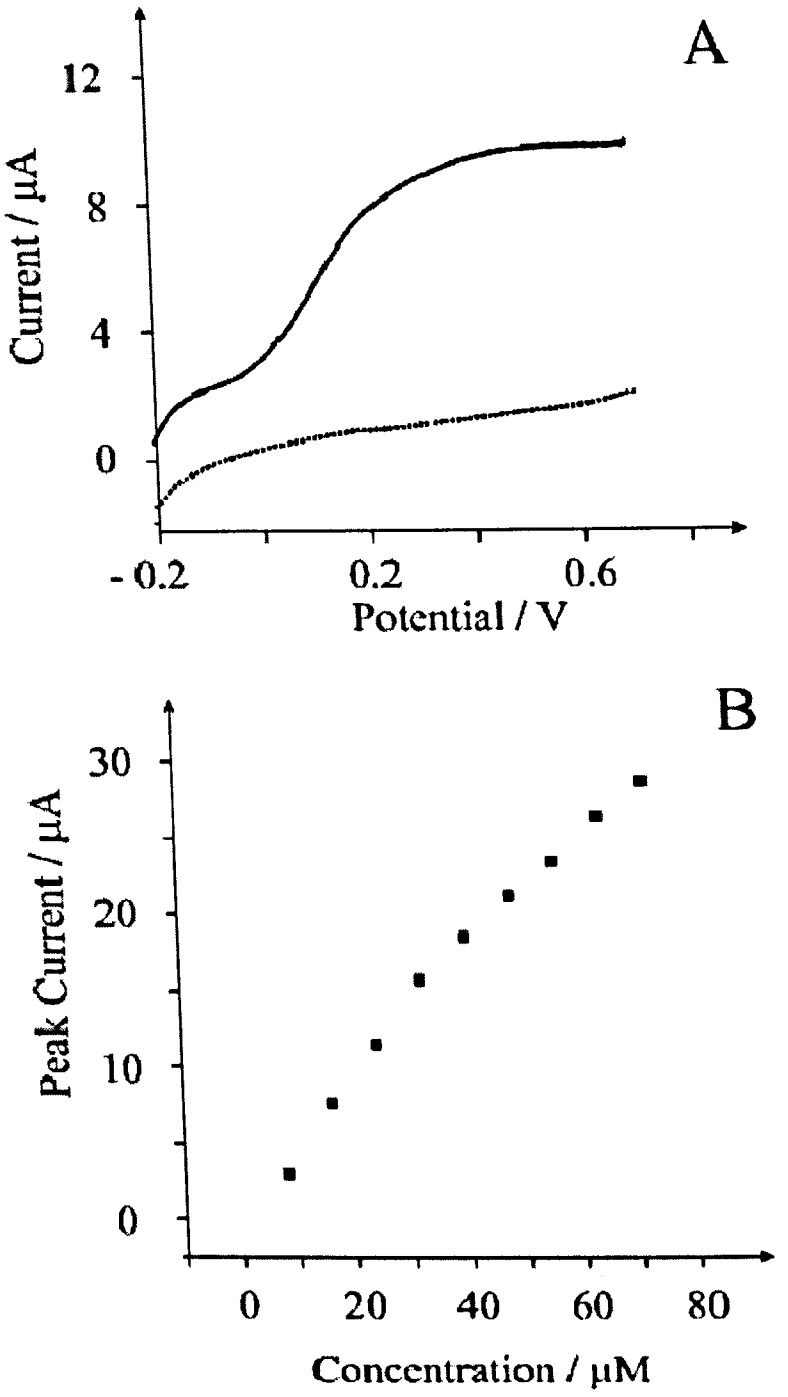

Figure 13.6. Typical voltammetric response (A) resulting from the electrochemical oxidation of hydrazine in a pH 7 buffer solution using a palladium ensemble produced via sputtering. (B) depicts the analysis of the peak current versus hydrazine additions.

13.5 Conclusions

In this chapter, proof-of-concept has been demonstrated that recently developed cosmetic electrochemistry can be adapted to produce ensembles of electrocatalytic materials for a selection of analytical challenges. Given the facile route of fabrication and low cost of the sensors coupled with the benefits in the electrochemical response from using an ensemble, this methodology is expected to be widely adopted.

13.6 References

1. I. Streeter, R. G. Compton, Sens. Actuators B **130**, 620, 2008
2. S. Fletcher, M. D. Horne, Electrochem. Commun. **1**, 502, 1999.
3. X. J. Huang, A. M. O'Mahony, R. G. Compton, Small. **5**, 776, 2009.
4. A. C. Barton, S. D. Collyer, F. Davis, D. D. Gornall, K. A. Law, E. C. D. Lawrence, D. W. Mills, S. Myler, J. A. Pritchard, M. Thompson, S. P. J. Higson, Biosens. Bioelectron. **20**, 328, 2004.
5. L. Xiao, I. Streeter, G. G. Wildgoose, R. G. Compton, Sens. Actuators B **133**, 118, 2008.
6. N. A. Choudry, R. O. Kardara, N. Jenkinson, C. E. Banks, PhysChemChemPhys **12**, 2285, 2010.
7. R. O. Kadara, N. Jenkinson, B. Li, K. H. Church, C. E. Banks, Electrochem. Commun. 2008, 10, 1517.
8. Kanichi.com [internet]. London: Bismuth oxide electrodes/ [Updated 2011 June 21; cited 2011 July 10]. Available at http://kanichi-research.com
9. X. Ji, C. E. Banks, W. Xi, S. J. Wilkins, R. G. Compton, J. Phys. Chem. B **110**, 22306, 2006.
10. R. G. Compton, C. E. Banks, Understanding Voltammetry, World Scientific, Singapore 2007.
11. R. N. Adams, Electrochemistry at Solid Electrodes, Marcel Dekker, New York 1969.
12. R. Baron, B. Sljukic, C. Salter, A. Crossley, R. G. Compton, Russ. J. Phys. Chem. A **81**, 1443, 2007.
13. X. Dai, R. G. Compton, Analyst, **131**, 516, 2006

14. H. M. Anawar, J. Akai, K. M. G. Mostofa, S. Safiullah, S. M. Tareq, Environ. Int. **27**, 597. 2002

15. C. Batchelor-McAuley, C. E. Banks, A. O. Simm, T. G. J. Jones, R. G. Compton, Analyst **131**, 106, 2006.

16. S. M. Golabi, H. R. Zare, Electroanalysis, **11**, 1293, 1999

17. A. Salimi, L. Miranzadeh, R. Hallaji, Talanta, **75**, 147, 2008

18. L. Zheng, J. F. Song, Talanta, **79**, 319, 2009

19. H. J. Zhang, J. S. Huang, H. Q. Hou, T. Y. You, Electroanalysis., **21**, 1869, 2009

20. A. Abbaspour, A. Khajehzadeh, A. Ghaffarinejad, J. Electroanal. Chem., **631**, 52, 2009.

Chapter 14

14.0 Cosmetic Electrochemistry III: Electroanalytical Sensing of Nitrite

14.1Abstract

The use of Cosmetic Electrochemistry, is reported, towards the electro-analytical sensing of nitrite based on the direct oxidation of the target analyte at graphitic micro ensembles. The sensing of nitrite is shown to be possible over the linear range 1 μM to 17 μM with a limit of detection of 0.7 μM feasible in model aqueous solutions. This approach is shown to be possible to the sensing for nitrite in canal water samples.

14.2 Introduction

Nitrite is a found in a plethora of samples and ingestion has detrimental health problems following ingestion due to the transformation into *N*-nitrosamines which are known to be mutagenic, tetratogenic[1] or carcinogenic.[1, 2, 3] The fatal dose of nitrite ingestion is reported to lie between 8.7 μM and 28.3 μM[4, 5, 6] and the World Health Organisation state that nitrite should have a guidance level of 65 μM for short-term exposure and 4.3 μM for long-term exposure.[7] It is clear that the sensing of nitrite is of importance with sensitive and selective methodologies are required.

Due to the significance of nitrite, there are a range of analytical techniques that have been developed such as short-column Ion-Pair chromatographic separation with chemiluminescence detection,[8] High Performance Liquid Chromatography with fluorescence detection[9] and electrochemical strategies; Moorcroft and co-workers have provided an elegant overview of this area.[1] Electrochemical techniques are favourably looked upon due

to their portability, relative low cost and rapid throughput. It was thought however that the direct oxidation of nitrite at bare electrode is reported to be inadequate due to the oxidation products adsorbing onto the electrode limiting the analytical utility of the approach.[10, 11] As a consequence electrodes have been modified with platinum,[12] tin,[13] cobalt,[14] silver nanoparticles,[15] boron dope diamond,[16] glassy carbon,[17] manganese dioxide,[18] and copper oxide[19] in order to try and provide electro-catalytic responses. However, recently Kozub and co-workers recently revisited the electrochemical oxidation of nitrite at a bare unmodified glass carbon electrode demonstrating that the detection of the target analyte was indeed feasible.[20] While the main aim of their work was to demonstrate that modifying the electrode surface with mediators may not be beneficial in terms of electroanalytical sensing, some passivation of the electrode surface was evident which required the application of power ultrasound to remove adsorbates.

Previous studies by Khairy *et al.* have reported the use of screen-printed shallow recessed graphite microelectrode arrays to sense nitrite in river water samples.[4] These unique screen-printed arrays comprise 6 microdiscs with radii of 116 microns separated by their nearest neighbour by 2500 microns in an hexagonal array and are recessed by 4 microns. The screen-printed arrays allow the low micromolar sensing of nitrite in aqueous solutions via cyclic voltammetry with the assessable linear range and detection limit further reduced through the application of amperometry. The protocol was shown to be feasible for the sensing of nitrite in river water samples at levels indicated by the World Health Organisation.[3] Additionally no passivation issues were observed.

Previously the concept of Cosmetic Electrochemistry was introduced in chapters 12 and 13 where a commercially available cosmetic product, a deodorant, can be used to

confer microelectrode behaviour on a macroelectrode.[22, 23] We have demonstrated proof-of-concept that a graphite screen-printed electrode can be sprayed with an off-the-shelf cosmetic product and within seconds is ready to use. The polymer contained within the cosmetic product partially blocks the graphite screen-printed electrode surface leaving the underlying graphite electrode exposed in the form of graphite micron-sized sites which are randomly distributed across the electrode surface. The creation of microdomain sites enhances mass transport of the target analyte and it has been demonstrated that the electroanalytical performance of the cosmetically modified electrode, via the cathodic stripping of lead could achieve a similar performance to current state-of-the-art sensing employing power ultrasound.[21]

The concept of Cosmetic Electrochemistry was recently extended[22] for fabricating graphite micron ensembles demonstrating that this facile methodology can be utilised for the manufacture of electro-catalytic graphitic micro-ensembles for a range of electro-analytical challenges where the underlying metallic substrate can be tailored.

14.3. Experimental Section

All chemicals used were of analytical grade and were used as received without any further purification from Sigma Aldrich. These were: sodium nitrite, double-distilled sulphuric acide (99.8%), potassium chloride, sodium phosphate dibasic dehydrate and sodium phosphate monobasic dehydrate, disodium tetraborate, sodium acetate and sodium hydroxide (> 99%). All solutions were prepared with deionised water of resistivity not less than 18.2 MΩ cm. A fresh solution of sodium nitrite (in pH 3) was prepared daily. Canal water was sampled from the Manchester canal on Oxford road, Manchester, UK and collected and utilised in a polyethylene sample container. The sample was stored in the fridge until use, typically one day following collecting the sample. This was acidified to the desired pH (3) with a small addition of concentrated hydrochloric acid.

Voltammetric measurements were carried out using a μ-Autolab III (Eco Chemie, The Netherlands) potentiostat/galvanostat and controlled by Autolab GPES software version 4.9 for Windows XP. All measurements were conducted using a three electrode configureuration with a large surface area platinum wire as a counter and a saturated calomel electrode as the reference. Connectors for the efficient coupling of the screen-printed electrochemical sensors were purchased from Kanichi Research Services Ltd UK. In amperometric experiments, convection was applied via the use of a stirrer plate and a magnetic stirring bar rotating at 6000 rpm.

Screen-printed carbon electrodes were fabricated in-house with appropriate stencil designs using a microDEK 1760RS screen-printing machine (DEK, Weymouth, UK). A carbon-graphite ink formulation was first screen-printed onto a polyester flexible film (Autostat, 250 mm thickness). This layer was cured in a fan oven at 60 degrees for 30 minutes. Next a

silver/silver chloride reference electrode was included by screen printing Ag/AgCl paste (Gwent Electronic Materials Ltd, UK) on to the plastic substrate. Last a dielectric paste ink (Gwent Electronic Materials Ltd, UK) was printed to cover the connections and define the 3 mm diameter graphite working electrode. After curing at 60 degrees for 30 minutes the screen-printed electrode is ready to use. All measurements were conducted using a three electrode configureuration with a silver-silver chloride reference electrode included by screen printing Ag/AgCl paste (Gwent Electronic Materials Ltd, UK) on to the plastic substrate. The polymeric formulation used to create the random micro-electrode is a commercial product "Nivea for Men silver protect 24 h", Beiersdorf AG, Germany. The screen-printed electrode was sprayed using this cosmetic product with the spray distance and time explored following modification the electrode instantly dries and is ready to use. The polymer in the cosmetic product coats the electrode surface leaving micron sized holes, which are the underlying graphite screen-printed electrode accessible to the solution and hence we have quickly and readily produced a graphite ensemble, since these micron sized holes are randomly distributed across the electrode surfaces. Spray distances refer to the distance from the dispensing nozzle to the electrode surface.

14.4 Results and Discussion

The voltammetric response of nitrite sensing using the cosmetically modified screen-printed graphitic electrode was initially considered, which results in a graphite microdomain ensemble, in a 1 mM nitrite solution in pH 3 buffer. Figure 14.1 depicts a typical voltammetric profile corresponding to the electrochemical oxidation of nitrite. Note that rather than a peak shaped response being observed, typical of that observed on graphitic

surfaces,[20] a steady-state type response is observed due to the random nature of the graphitic microdomains.[21]

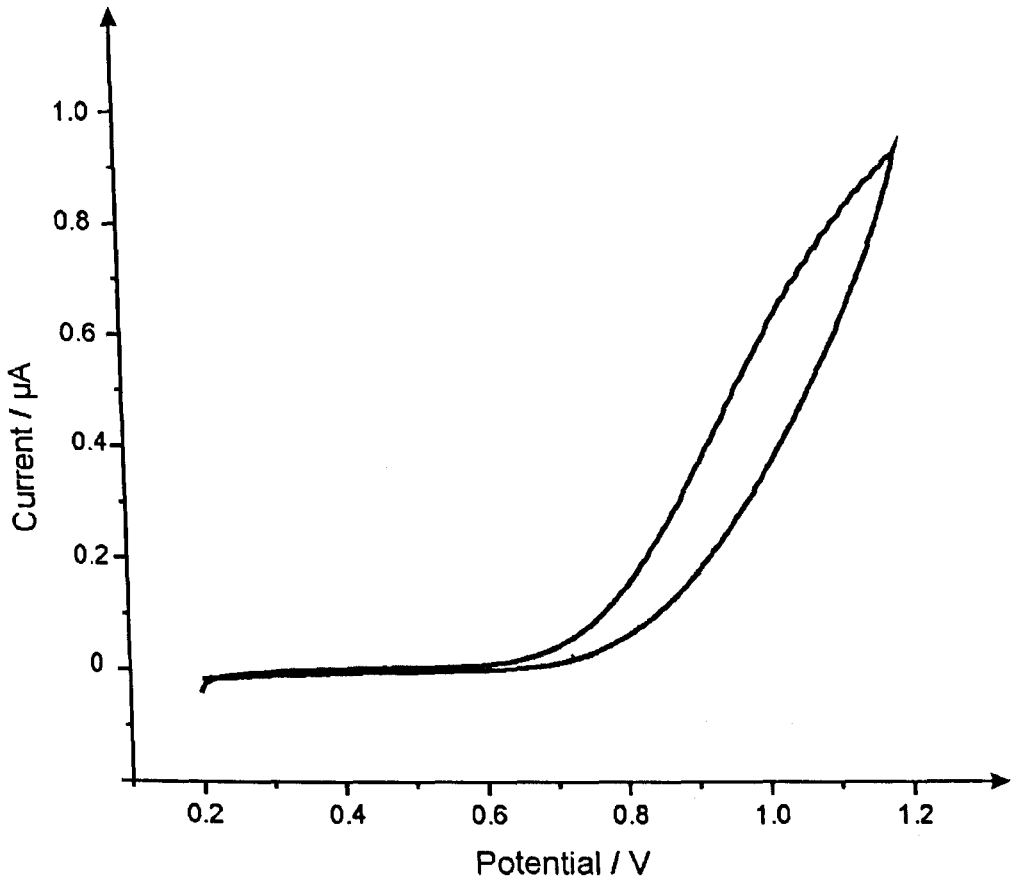

Figure 14.1 Typical cyclic voltammetric profile recorded in a solution of 1 mM nitrite in a pH 3 solution obtained from cosmetically modifying a screen-printed graphitic electrode. Scan Rate: 50 mVs^{-1}.

Based on previous work[20, 21] the electrochemical mechanism on graphitic surfaces is thought to be:

$$NO_2^- + H^+ \rightleftharpoons HNO_2 \quad (1)$$

$$NO_2^- \rightleftharpoons NO_2 + e^- \quad (2)$$

$$2NO_2 + H_2O \rightarrow NO_3^- + NO_2^- + 2H^+ \quad (3)$$

Given that the graphite surface is the same as that used in the fabrication of Screen-printed recessed arrays,[4] it is safe to assume this is the same mechanism here. Furthermore, the effect of nitrate is negligible as reported previously.[4]

Attention was turned to exploring the analytical utility of the cosmetically modified screen-printed graphitic microdomain ensemble towards the sensing of nitrite. Using a pH 3 solution, additions of nitrite were made over the range of 20 μM to 400 μM. Figure 14.2 depicts typical voltammetric responses obtained resulting from the additions of nitrite with analysis of the peak height versus concentration of nitrite also shown in figure 14.2. A linear response is observed over the range 20 μM to 360 μM ($Ip(A) = 1.941X10^{-9}$ A/M + $1.962X10^{-7}$ (A) ; $R^2 = 0.989$; $N = 18$) with a limit of detection (based on 3 SD_{blank}) determined to be 7.25 μM.

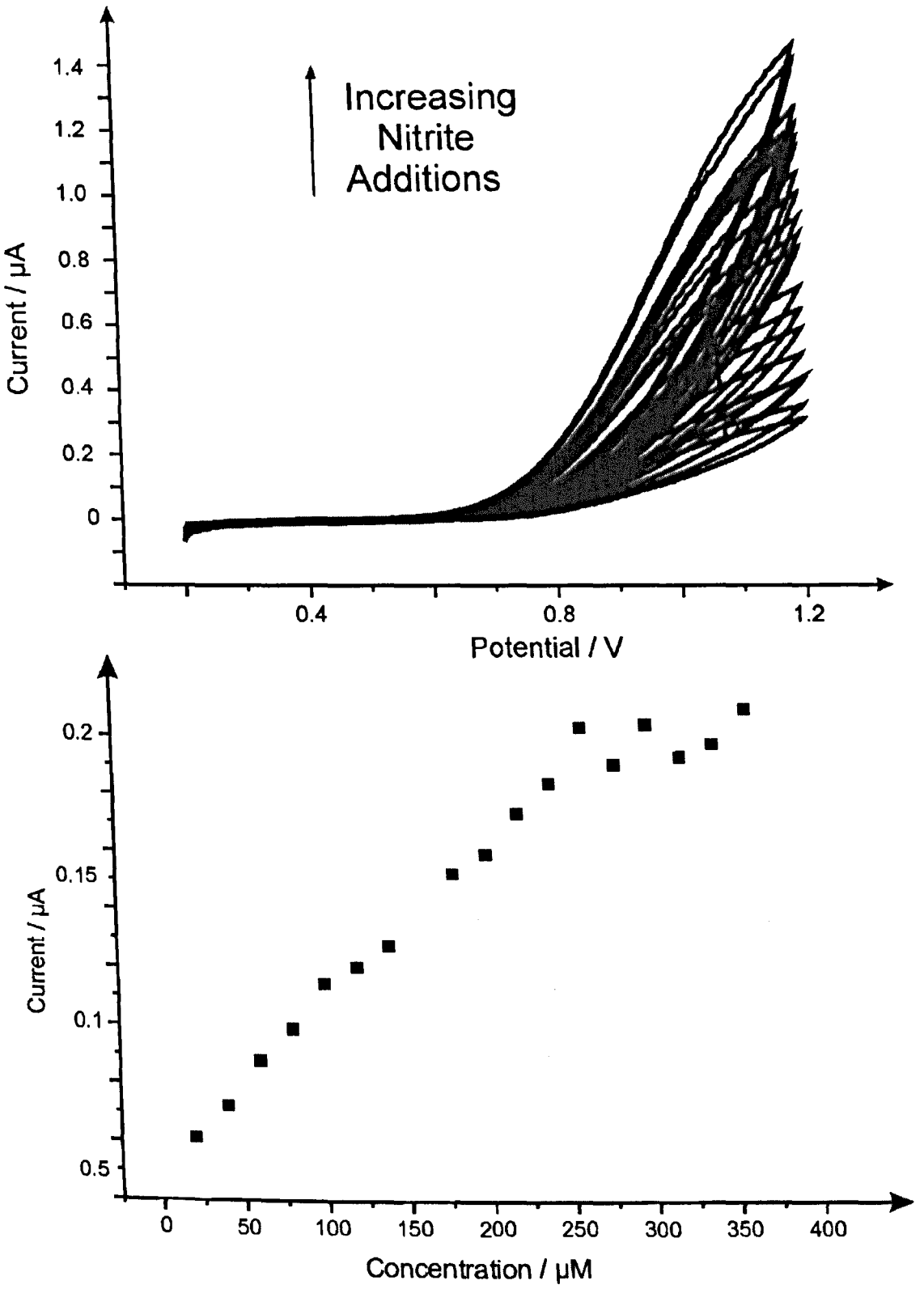

Figure 14.2: Typical cyclic voltammogams resulting from nitrite additions into a pH 3 solution using the graphite micro- ensemble (Top). Also shown are the analysis of the current as a function of nitrite concentration (Bottom).

A constant spray distance and time, which was applied throughout all analyses, was determined to be 15 mm and 1 second respectively. This was determined to by a series of trial and error analyses, where the spray times were varied from 1 second to 8 seconds. We found the time limit to be 1 second, after which the electrode surface becomes blocked and no significant electrochemical response is obtainable. Similarly, the distance was varied from 10 mm to 20 mm, in which case 15 mm was proven to be the optimum conditions to use. The distance from 15 mm was selected as it formed an even spread thin-layer as opposed to 10 and 20 mm where the surface was either too thick or too thin. . This analytical response in terms of linear range, detection limit and sensitivity compare well to previous studies reported where they used a screen-printed shallow recessed graphite microelectrode array using voltammetry for the micro-molar detection of nitrite in river water sample and aqueous solutions. As such our approach can be used as an alternative to arrays.

Next, the amperometric response was studied, of the cosmetically modified screen-printed graphitic microdomain ensemble in exploring nitrite at micro molar range where a linear response range from 1 μM to 17 μM ($Ip(A) = 6.16 \times 10^{-8}$ A/M + 6.24 X 10^{-8} (A) ; R^2 = 0.993; N = 10) was analysed. Figure 14.3 shows the amperometric measurement obtained from such analysis where a limit of detection ($3SD_{blank}$) was found to correspond to 0.7 μM. This limit of detection is within the required range with accordance to the World Health Organisation.[3] Furthermore, this LOD is comparable to shallow recessed screen-printed microelectrode arrays,[4] edge plane pyrolytic graphite – cobalt phthalocyanine modified electrodes,[24] lead (IV) oxide modified carbon powder epoxy electrodes[25] and screen-printed edge band ultramicroelectrodes.[20]

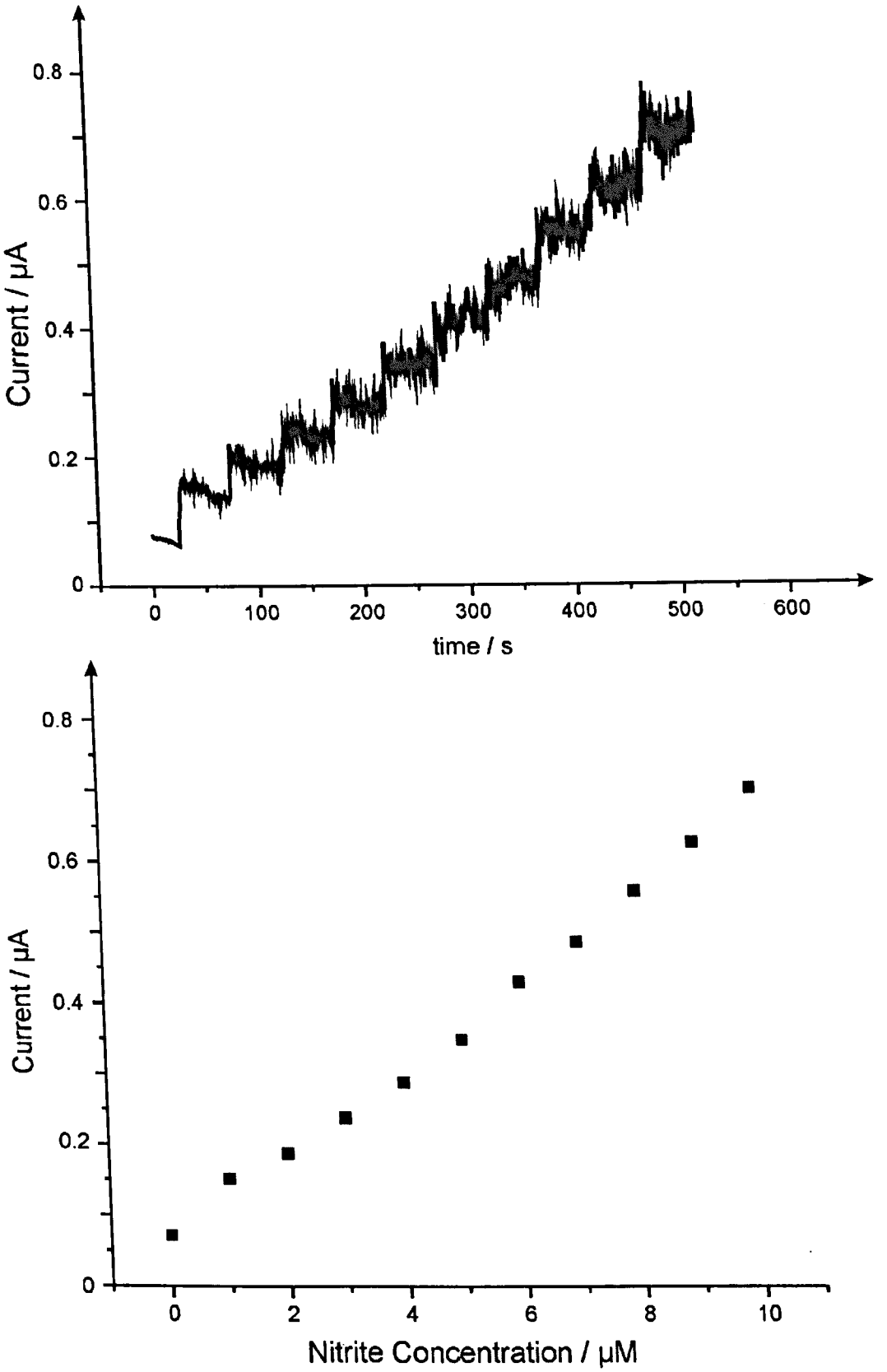

Figure 14.3: Amperometric response using a graphite micro-ensemble for the electroanalytical sensing platform resulting from additions of nitrite into a pH 3 buffer solution. The potential was held at + 0.75 V.

Next, the electroanalytical sensing using the cosmetically modified screen-printed graphitic microdomain ensemble was explored, towards nitrite in canal water samples. Note that the canal water sample was pre-treated to reach the pH 3 by adding small amounts of hydrochloric acid. It was found that the spray time/distance determined above was not at all useful for the measurement in the canal water sample and the voltammetric response degraded back to that observed at a macroelectrode due to dedegradation of the polymeric layer. Thus an adjustment was made to the spray time and distance. In such cases, a spray time of 1 second and a fixed distance of 15 mm were proven to be sufficient to achieve such behaviour. As reported previously in chapters 12 and 13, increasing the spray time will eventually block the electrode surface with no electrochemical response will be observed. Figure 14.4 depicts the voltammetric response of the modified screen-printed microdomain ensemble towards the sensing of nitrite in canal water sample and explored however no significant detection of nitrite was measured implying nitrite only occurs at low levels, thus a recovery experiment was carried out on the canal water sample. This sample was spiked with 20 μM additions of nitrite and a recovery of 94.6 (±1%) was obtained.

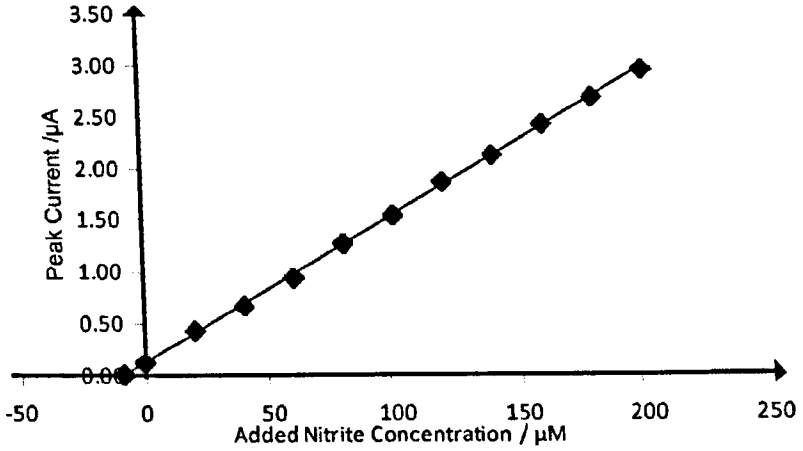

Figure 14.4. Typical standard addition plot resulting from cyclic voltammetry where additions of 20 µM of nitrite were made into a canal water sample using the graphite microensemble. The desired pH 3 was reached by simply adding small amounts of concentrated hydrochloric acid to the canal water sample. A recovery of 96.4% is possible.

14.5 Conclusion

This chapter has reported the use of cosmetically modified screen-printed microdomain ensemble for the low micromolar sensing of nitrite in canal water samples and aqueous solutions. The detection limits and linear range compares well to existing literature, given the facile and rapid production of these unique microelectrode ensembles this methodology will likely to be adopted by electrochemists.

14.6 References

1. M.J. Moorcroft, J. Davis and R.G. Compton, *Talanta* **54,** 785, 2001.
2. A.A. Ensafi and A. Kazemzadeh, *Anal. Chim. Acta* **382,** 15, 1999
3. Nitrate and nitrite in drinking-water; Background document for *development* of WHO *Guidelines for Drinking-water Quality. Document produced by the WHO:* WHO/SDE/WSH/ **7,** 16, 2007.
4. M. Khairy, R. O. Kadara and C.E. Banks, *Anal. Methods,* , **2,** 851, 2010
5. Drinking Water Standards, US Department of Health, Education and Welfare, Public Health Service, Washington, DC, **4,** 47, 1962
6. S. M. Silva and L. Henrique Mazo, Electroanalysis, , **10,** 1200, 1998
7. Who.int [internet]. Online resource: Guidelines for drinking – water quality. [update 2011 June 22; cite 2011 July 25]. Available at http://www.who.int/water_sanitation_health/dwq/gdwq3_8.pdf
8. H. Kodamatani, S. Yamazaki, K. Saito, Y. Komatsu and T. Tomiyasu, *Analytical Science,* **27,** 187, 2011.
9. H. Li, C.J. Meininger and G.Y. Wu, *Journal of Chromatography B-Analytical Technologies in the Biomedical and Life Sciences,* **2,** 199.
10. Y.N. Jiang, H.Q. Luo, N.B. Li, *International Journal of Environmental Analytical Chemistry* **87,** 295, 2007.
11. B.O. Agboola, K.I. Ozoemena, T. Nyokong, *Electrochimica Acta.* **51,** 6470, 2006.
12. M. Berfotti and D. Pletcher, *Journal of the Brazillian Chemical Society* **8,** 391, 1997.
13. K. Nakata, Y. Doi, S. Kubota, K. Shimazu, *Journal of Electroanalytical Chemistry,* **647,** 187, 2010.
14. A.S. Abolanie, J. Pillay, K.I. Ozoemena, *Electrochemica Acta,* **14,** 4319, 2010.
15. M. Pal, V. Ganesan, *Electrochemica Acta,* **13,** 4071, 2010.
16. J.T. Matsushima, W.M. Silva, A.F. Azevedo, M.R. Baldan, N.G. Ferreira, *Applied Surface Science,* **3,** 757, 2009,

17. *A.Y. Chamsi and A.G. Fogg, Analyst*, **113**, 1723, 1988.

18. C.E. Langley, B. Sljukic, C.E. Banks, R.G. Compton, *Analytical Science,* **23**, 165, 2007.

19. B. Sljukic, C.E. Banks, A. Crossley, R.G. Compton, *Electroanalysis,* **19**, 79, 2007.

20. Int.com [internet]. Association of water health; [Updated 2011 July 22; cited 2011 August 15]. Available at http://www.int/water_sanitation_health/dwq/gdwq3_8.pdf. 2011,04

21. N. A. Choudhry, R. O. Kadara and C. E. Banks, *Phys. Chem. Chem. Phys.*, **12**, 2285, 2010.

22. N. A. Choudhry, M. Khairy, R. O. Kadara, N. Jenkinson and C. E. Banks, *Electroanalysis,* , **22**, 1831, 2010.

23. B.R. Kozub, N.V. Rees and R.G. Compton. *Sens. Actuators,* B, **143**, 539, , 2010

24. B. Kozub, R.G. Compton, *Sens. Actuators,* B, **1**, 350, 2010.

25. B. Sljukic, C.E. Banks, A. Crossley, R.G. Compton, *Anal. Chim. Acta,* **2,** 240, 2007

Chapter 15

15.0 Plaster-Trodes for Electro-Analytical Sensing via Electro Deposition with Electro-Catalytic Metals

The conclusion of this thesis was with the development of plaster-trodes, a novel concept where a commercial plaster can be easily modified (electrocatalytically with metals) to detect various analytes.

15.1 Abstract

It is demonstrated that commercially available plasters (band aid) usually used for wound healing, can be electrolytically modified with a range of electro-catalytic metals for a range of analytical sensing purposes. These 'Plaster-trodes' consist of a mesh type surface which have star-shaped microelectrodes of ~150 microns radius in a hexagonal pattern which are separated from its nearest neighbours by ~1250 microns with interlinking connections between each microelectrode which are generally electrochemically active resulting in micro-band-type connections. Proof-of-concept is shown for a range of electro-analytical targets where the Plaster-trode is electrolytically modified with palladium for the sensing of hydrazine and nickel for the direct oxidation of ethanol. Given the low cost of the Plaster-trode which can be readily modified with electro-catalytic metals, this new electrode is expected to be widely utilised in electro-analysis. *This work was published in the Analyst,* **136**, 1153, 2011.

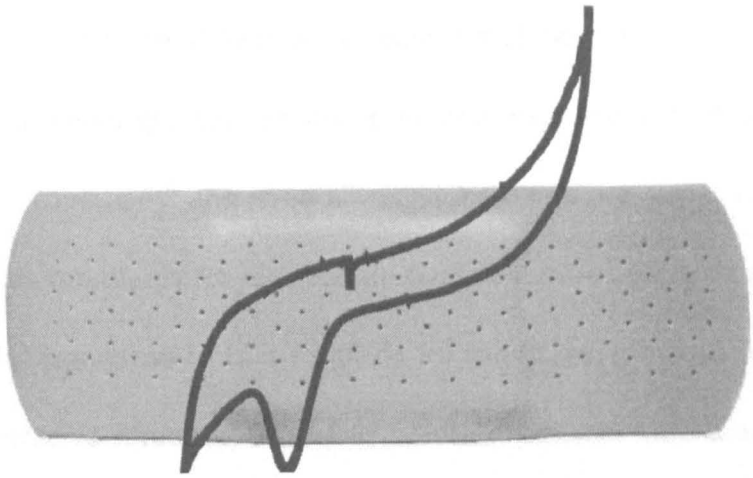

Figure 15.1. Represent a commercially available plasters (band aid) usually used for wound healing, can be electrolytically modified with electro-catalytic metals for a range of analytical sensing purposes

15.2 Introduction

Electro-analysis is a highly active area of research due to its potential portability, low cost, ease of miniaturisation and incorporation into embodiments with other sensors and consequently forms the basis of many commercial sensors. The judicious choice of working electrode can impart the desired sensitivities and selectivities of the electrochemical sensor and consequently electro-analysts are always on the search for new electrodes which can either be used 'as is' or following modification with various electro-catalysts or electro-catalytic metals. Another approach gaining momentum is the use of microelectrode arrays which have well documented benefits in electroanalytical sensing.[1, 2] A variation on this is to use thousands of microelectrode wires embedded into epoxy producing an electrode of 'random assemblies of microelectrodes' (RAM).[3] Note that these vary from microelectrode arrays in the fact that the distance between neighbouring microelectrodes is not uniform

but rather random. It has been shown via elegant simulations that a random array can produce the same, but never greater, current–potential response as that of a regular array of equal macroscopic coverages[4] and generally random arrays are easier to fabricate. Note that arrays can act as templates for electrolytic modification of electro-catalytic materials and use less material compared to that required for modifying a macroelectrode and thus the approach is more cost effective, especially where expensive metals are utilised, and if designed corrected can have substantial analytical benefits from the enhancement in mass transport.

As discussed in chapter 12 we introduced Cosmetic Electrochemistry,[5] where a commercially available cosmetic product, a deodorant, is used to confer microelectrode behaviour on a graphite macroelectrode. Proof-of-concept was demonstrated where the polymer contained within the cosmetic product partially blocks the graphite screen-printed electrode surface leaving underlying randomised graphite microdomains. The change in geometric structure from that of a graphite macroelectrode to graphite microdomain sites results in a change in mass transport of the target analyte and it was demonstrated with the example of the cathodic stripping of lead achieving low ppb levels. More recently in chapter 13, we have demonstrated that this methodology can be extended for the production of metallic electro-catalytic microdomain ensembles.[6]

In this chapter, the introduction of Cosmetic Electrochemistry is extended and demonstrates that an off-the-shelf plaster (band aid) can be used as a template for electrolytically fabricated electro-catalytic metals for sensing a range of target analytes. This electrode is termed 'Plaster-trode' and has a mesh-like surface which consists of star-shaped microelectrode-like geometries of ~150 micron radius in a hexagonal pattern which are separated from its nearest neighbours by ~1250 microns with interlinking connections

between each microelectrode which generally are electrochemically active producing micro-band type connections. The Plaster-trode is explored towards the sensing of hydrazine and ethanol via the electrolytic modification of palladium and nickel oxide respectively and has the advantage of being cost-effective and disposable.

15.3 Experimental

All chemicals used were of analytical grade and were used as received without any further purification from Sigma-Aldrich. All solutions were prepared with deionised water of resistivity not less than 18.2 MΩ cm. Voltammetric measurements were carried out using a m- Autolab III (Eco Chemie, The Netherlands) potentiostat/galvanostat and controlled by Autolab GPES software version 4.9 for Windows XP. All measurements were conducted using a three electrode configureuration with a large surface area platinum wire as a counter and a Saturated Calomel Electrode (SCE) as the reference. A commercial off the shelf plaster product 'Elastoplast Aqua Protect Silver Healing' was used as the working electrode.

Figure 15.2 depicts an image of such a plaster. In preparation of the Plaster-trode, the plastic film of the plaster is peeled off and discarded. Usually one would put the non-woven wound pad, which has a polyethylene net onto a wound; the net is shown schematically in Figure. 15.2A and an SEM image is shown in Figure. 15.2B. Here we use the non-woven wound pad as the electrode surface and use epoxy (Epoxy Technology, Inc, Billerica, MA 01821, USA) to create a defined geometric area of 1 cm^2. To this an electric connection is made to the pad. All experiments were performed in deaerated solutions. Scanning electron microscopy (SEM) images were obtained using a JEOL JSM-5600LV model. For the

modification of the Plaster-trode with palladium, the method of Ji et al.[8] was utilised which involves three key steps.

Step one involves the electrochemical oxidation activation by cycling the potential from +1.8 V to -0.4 V (vs. SCE) using a scan rate of 200 mV s^{-1} for 10 cycles in 0.5 M Na_2SO_4. Step 2 involves transferring the Plaster-trode into a 1 mM $PdCl_2$ solution in 0.1MH_2SO_4 with potential cycling from +0.4 V to +1.5 V for 5 cycles at 200 mV s^{-1}. Palladium oxide(s) and/or complexes of palladium on the Plaster-trode surface at various oxygen containing functional groups are likely produced at this stage. Step three involves the formation of palladium metal by transferring the modified Plaster-trode electrode into 0.1 M H_2SO_4 and potential cycling from +1.1 V to -0.5 V at 300 mV s^{-1} for 5 scans.

15.4 Results and Discussion

Figure 15.2 depicts the plaster which has a non-woven wound pad with a polyethylene net which is impregnated with metallic silver and the initial aim was to try and utilise the metallic silver contained with the plaster as a silver type-electrode. EDAX was performed on the Plaster-trode which shows 66.76% carbon, 27.39% oxygen, 1.30% chloride, and 4.54% silver ions. However, in aqueous solutions we found no electrochemical signals corresponding to the impregnated metallic silver.

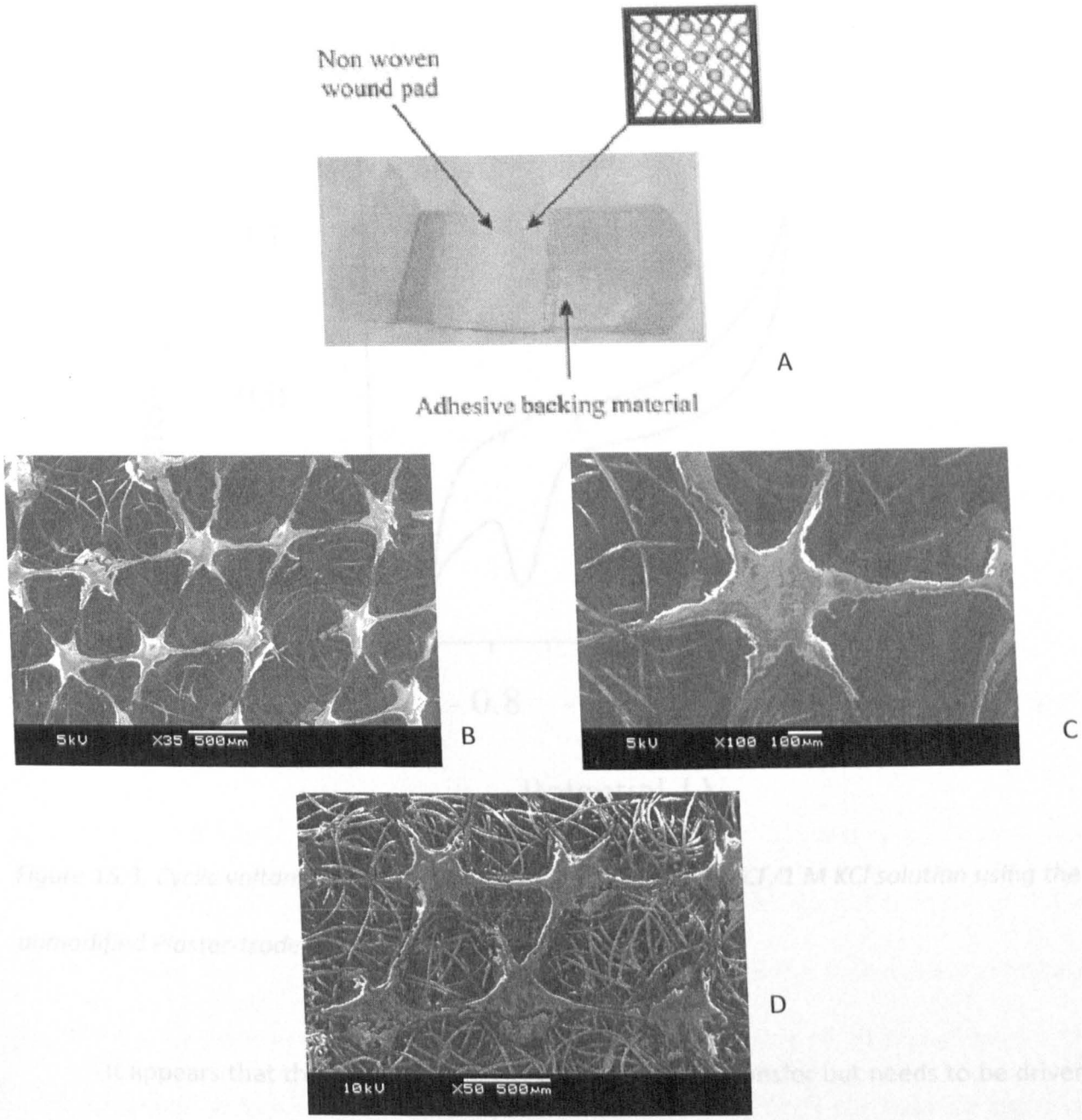

Figure 15.2. Schematic picture of the plaster (A) which is modified and used as the electrode substrate. SEM images (B) of the polyethylene net which is used as the electrode surface. SEM images of a palladium modified Plaster-trode (C and D).

The Plaster-trode was explored in a solution of 1 mM$[Ru(NH_3)_6]Cl^-$/1MKCl and as shown in Figure 15.3, where a reduction wave is observed at a high overpotential with no corresponding oxidation wave.

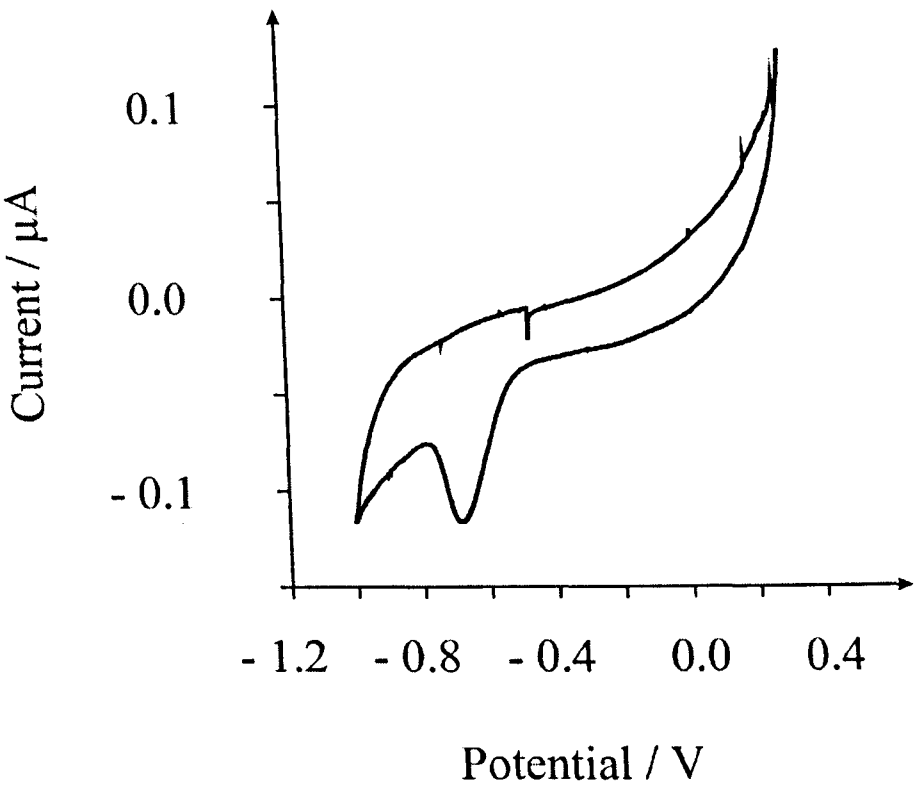

Figure 15.3. Cyclic voltammogram recorded in 1 mM $[Ru(NH_3)_6]Cl$/1 M KCl solution using the unmodified Plaster-trode. Scan rate: 5 mV s^{-1} vs. SCE.

It appears that the impregnated silver allows charge transfer but needs to be driven since the potential for the electrochemical reduction of the redox probe is at an unusually negative potential than would usually be observed on conventional electrode substrates. Further study of this observed electrochemical wave from the redox probe proved that it is under the absorption control and it is clear that the Plaster-trode is not useful 'as is'. Clearly the metallic silver which is impregnated on the polyethylene net allows it to be conductive yet the quality of the silver is not of electrochemical (purity) grade. Consequently to improve the electrochemical performance of the Plaster-trode we turn to electrolytically

modifying its surface with various electro-catalytic metals which are explored using well-known analytes to gauge the Plaster-trodes analytical usefulness.

The Plaster-trode was modified as described in the Experimental section and Figure 15.2 depicts SEM images of the unmodified polyethylene net (Figure. 15.2B) and that of a palladium modified Plaster-trode (Figure. 15.2C and D) where star-shaped microelectrodetype structures are observed, which are approximately 300 microns in diameter and are arranged in a hexagonal arrangement with centre-to-centre distances of ~1250 microns between neighbouring structures. SEM images as shown in Figure 15.2 demonstrate that some of the interlinking connections are electrochemically active and act like microbands contributing to the microelectrode array type structure and hence diffusional overlap is observed.

Next, the analytical performance of the palladium modified Plaster-trode was explored with the electro-analytical sensing of hydrazine. Figure 15.4A depicts the voltammetric profiles obtained using a bare and palladium modified Plaster-trode. Note that the voltammetric response is distinctively different from that usually observed at conventional electrodes with a no clear defined voltammetric profile which is attributable to the large surface area of the Plaster-trode. Additions of hydrazine were made into a pH 7 buffer solution with the voltammetric response monitored. Figure 15.3B depicts the analysis of the observed current recorded at + 0.55 V vs. SCE as a function of hydrazine concentration which is observed to produce a linear response over the range 50 to 500 mM ($I/A = 0.41\ AM^{-1} - 4.6x10^{-6}\ A$; $R^2 = 0.995$; $N = 10$.). In the analysis note that the response of the Plaster-trode in the absence of the analyte was subtracted from that in the presence of the analyte.

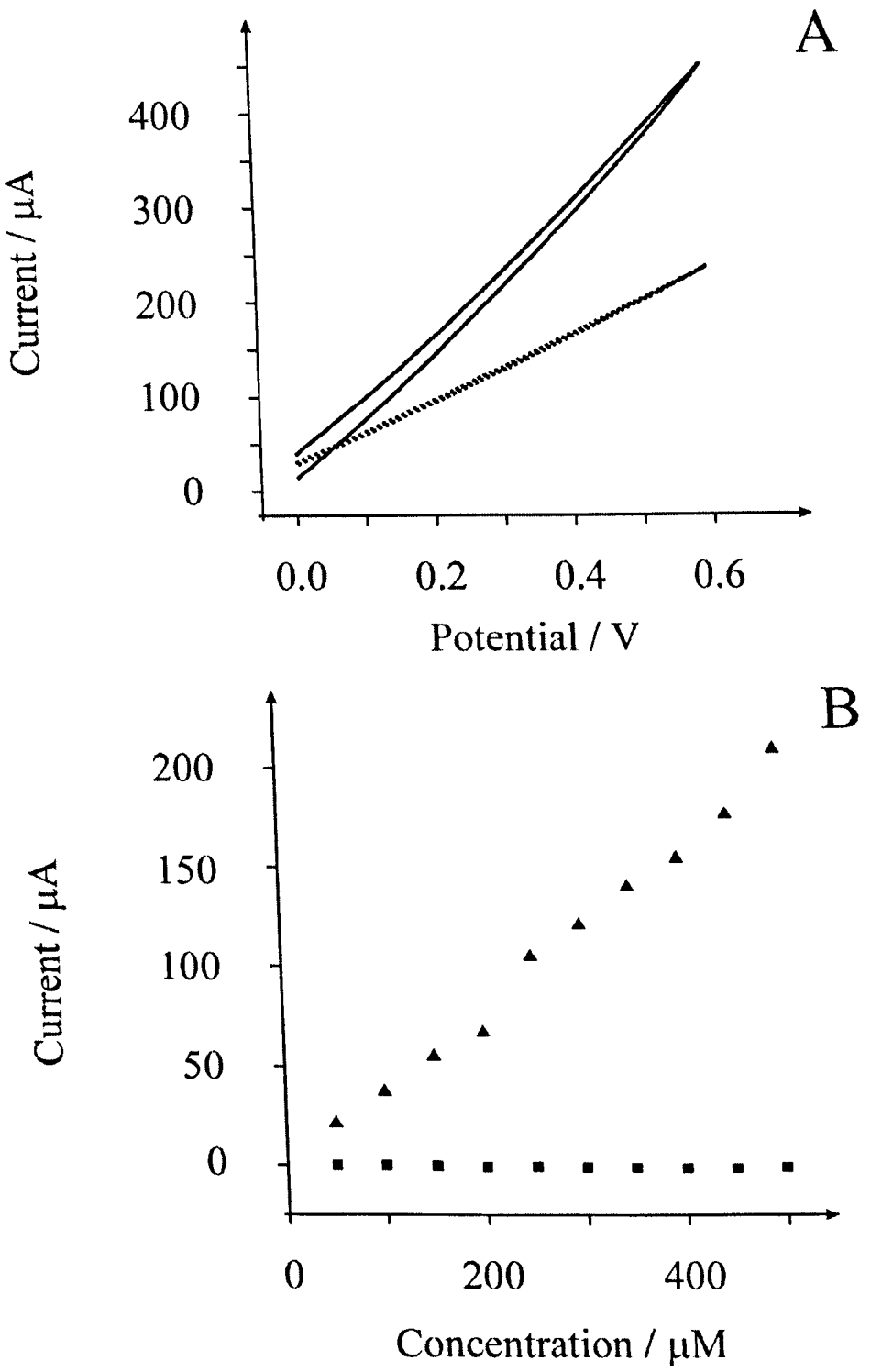

Figure 15.4. Cyclic voltammetric profiles (A) recorded using the palladium modified Plaster-trode in pH 7 in the absence (dotted line) and presence of 500 mM (solid line) hydrazine. Scan rate: 50 mVs^{-1} vs. SCE. Also shown is the calibration plot for palladium modified Plaster-trode (squares) compared with an un-modified Plaster-trode (squares) resulting from additions of hydrazine using chronoamperometry with the potential held at +0.55 V vs. SCE.

The response of the un-modified Plaster-trode is also shown in Figure 15.4B which clearly shows that the palladium surface provides an enhancement in electron transfer facilitating the analytical sensing of hydrazine. The measurement was repeated four times and the limit of detection (based on 3σ) was found to correspond to 31 mM. This detection limit is competitive to other electrochemical methodologies[9,10] but is not as low as that obtainable using palladium nanoparticles and arrays.[11] This is likely due to the heavy diffusional overlap observed on the Plaster-trode (see above) which is acting not similar to that of a microelectrode array nor a macroelectrode but somewhere in between. The benefits are that only a small fraction of metal is needed that would be required to construct the equivalent palladium film macrodisc electrode.

Next we turn to exploring the modification of the Plaster-trode with nickel. The Plaster-trode was modified by a recently reported (chapter 13) method[13] by holding the potential at -1.2 V (vs. SCE) for 500 seconds in a solution containing 1 mM nickel (II) in 0.1M acetate buffer solution (adjusted to pH 5). Figure 15.5A depicts a typical voltammetric profile in 0.1 M sodium hydroxide containing 10 mM ethanol where as observed above there is no clearly defined voltammetric profile which is attributable to the large surface area of the Plaster-trode.[13]

Additions of ethanol were made into a 0.1M NaOH solution using the nickel modified Plaster-trode via chronoamperometry employing a potential of + 0.4 V (vs. SCE) over the range of 10 mM to 70 mM. Figure. 15.5B shows typical chronoamperometric responses and Figure 5C depicts the analysis of the chronoamperometric responses as a function of added ethanol concentration.

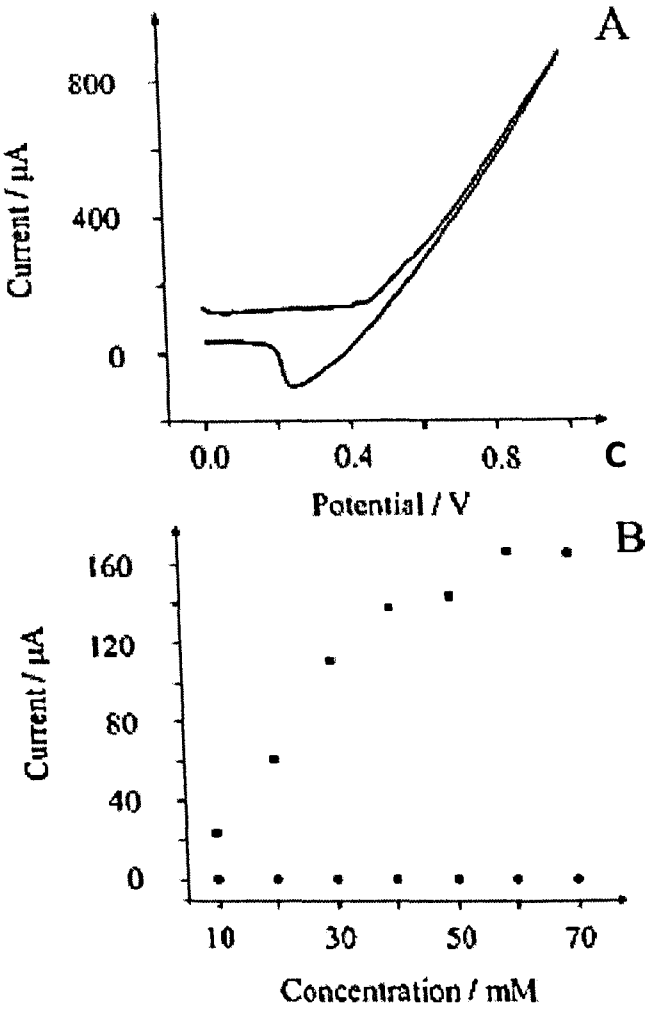

Figure 15.5. Cyclic voltammetric profiles (A) obtained at a nickel plated Plaster-trode recorded in 10 mM ethanol in 0.1 M NaOH. Part B shows a typical chronoamperometric response in the absence (dotted line) and presence of 50 mM ethanol in a 0.1 M NaOH. Part C shows the analysis of chronoamperometric experiments resulting from additions of ethanol into a 0.1 M NaOH solution using the nickel modified Plaster-trode (squares) and the response of a bare Plaster-trode (circles). The potential was held at +0.4 V (vs. SCE).

In the analysis note that the response of the Plaster-trode in the absence of the analyte was subtracted from that in the presence of the analyte. A linear range is observed from 10 mM to 40 mM with further additions resulting in a deviation from linearity. The measurement

was repeated four times and a limit of detection (based on 3σ) was found to correspond to 6.3 mM. It is well documented that the insertion of the deposited nickel into alkaline conditions results in the formation of Ni $(OH)_2$ where the Ni^{2+}/Ni^{3+} redox couple is utilised in the electro-catalysis of ethanol. While the observed linear range is shorter (at the higher end) than that of current state-of-the-art using nickel nanoparticles,[13] the limit of detection is identical. The electro-catalytic rate constant of the nickel oxide modified Plaster-trode towards the oxidation of ethanol can be deduced from the chronoamperometry experiments. The electro-catalytic rate constant can be determined from the following equation:

$$I_C / I_L = \Upsilon^{1/2}[\pi^{1/2} erf(\Upsilon^{1/2}) + \exp(-\Upsilon) / \Upsilon^{1/2}]$$

where the I_C is the catalytic current in the presence of hydroxide, I_L is the diffusion limited current in the absence of hydroxide and $\Upsilon = kc/t$ where k is the catalytic rate constant, c is the initial concentration of hydroxide and t is the time of the chronoamperometric experiment. When the value of $I_C / I_L = \Upsilon^{1/2}[\pi^{1/2} erf(\Upsilon^{1/2}) + \exp(-\Upsilon) / \Upsilon^{1/2}]$ exceeds 1.5 the error function becomes almost equal to 1 and the reaction is in a purely kinetic region and equation (1) becomes:

$$I_C / I_L = \Upsilon^{1/2} \pi^{1/2}$$

which leads to:

$$I_C / I_L = (kct)^{1/2} \pi^{1/2}$$

Experimentally, the measurement time used in the chronoamperometric experiments (100 seconds) is greater than 80 ms to avoid charging of the double layer at the electrode surface. The advantage of this chronoamperometric protocol is that the diffusion coefficient of the electro-active species and the electrode area (viz. Plaster-trodes) are not required to be known. The electro-catalytic rate constant using the above analysis (eqn (3)) was found to correspond to 2.5 M^{-1} s^{-1} which is modest compared to other chemically modified electrodes towards alcohol sensing but is a similar order of magnitude for nickel hydroxide surfaces[14] but clearly has analytical benefits as compared to current state-of-the-art methodologies.

15.5 Conclusion

We have demonstrated that an off the shelf cosmetic product, a band aid, can be used as a electrode substrate which can acts as a template for the electrolytic modification with electro-catalytic metals for a range of sensing purposes. The analytical performance of the Plaster-trode compares well to existing electrochemical methodologies indicating its potential use as a costeffective electrode.

15.6 References

1. A. Berduque, Y. H. Lanyon, V. Beni, G. Herzog, Y. E. Watson, K. Rodger, F. Stam, J. Alderman and D. W. M. Arrigan, Talanta, **71**, 1022, 2007.
2. D. W. M. Arrigan, Analyst, 2004, 129, 1157. 3 S. Fletcher and M. D. Horne, Electrochem. Commun., **1**, 502, 1999.
4. T. J. Davies and R. G. Compton, J. Electroanal. Chem., **63**, 585, 2005
5. N. A. Choudhry, R. O. Kadara and C. E. Banks, Phys. Chem. Chem. Phys., **12**, 2285, 2010.
6. N. A. Choundry, M. A. Khairy, R. O. Kadara, N. Jenkinson and C. E. Banks, Electroanalysis, **22**, 1831, 2010.
7. X. Ji, C. E. Banks, W. Xi, S. J. Wilkins and R. G. Compton, J. Phys. Chem. B, **110**, 22306, 2006.
8. S. M. Golabi and H. R. Zare, J. Electroanal. Chem., **168**, 465, 1999.
9. A. Abbaspour and M. A. Kamyabi, J. Electroanal. Chem., **73**, 576, 2005.
10. C. Batchelor-McAuley, C. E. Banks, A. O. Simm, T. G. J. Jones and R. G. Compton, Analyst, **106**, 131, 2006
11. N. R. Stradiotto, K. E. Toghill, L. Xiao, A. Moshar and R. G. Compton, Electroanalysis, **21,** 2627, 2009
12. L. Zheng and J.-F. Song, J. Solid State Electrochem., **14**, , 43, 2010.

Chapter 16 - Conclusions

16.1 Overall Conclusion

As we have discussed in this thesis, screen-printed electrodes have been widely studied and explored in different electrochemical scenarios. As discussed in chapter 7, the development of a glucose sensor has been reported using copper (II) screen-printed electrodes. This development offers an alternative in the current market which is a cost effective approach to produce a glucose sensor on a large scale.

Screen-printed electrodes were further explored in the following chapters, in particular the introduction of tailoring the electrochemical reactivity of screen-printed electrodes which allowed the electrodes to be tailored from edge-plane to basal-plane of highly ordered prycolytic graphite. This work demonstrated that the electron transfer properties of screen-printed electrodes can be tailored via the introduction of a polymeric formulation into the ink which is used to fabricate these electrochemical platforms.

In addition to this, proof of concept has been shown in the introduction of Cosmetic Electrochemistry, which is a newly formed concept that is expected to be adopted by electrochemists. This novel concept gives the chemist a cheaper, alternative to using conventional electrodes, thus making a major breakthrough in the field. Furthermore, we reported earlier the concept of 'plaster-trodes' (chapter 15) where a commercial product can be taken and used for a range of analytical purposes. In addition to this, we can explore this concept further by tailoring the diameter of the plaster mesh in order to suit the particular analyte in consideration. This in effect gives this concept further scope for development in the future.

As highlighted in the introduction of this thesis, one of the key problems in the current market is the high cost of sensors (test kits) and companies are constantly trying to reduce these costs and so to reduce the final price of the product but there are some limiting factors for this to be feasible. With screen-printed electrodes, we have demonstrated in many cases that cost-effective sensors can be easily produced which also compare well to existing literature for their limit of detection. As reported, the incorporation of chemicals in screen-printed electrodes gives this a distinct advantage over rival conventional electrodes and further highlights the dominating overtake of screen-printed electrodes in the market and in the foreseeable future for these electrodes to be household names.

16.2 Future Work

The process of fabricating screen-printed electrodes has been widely explored throughout this thesis. We have already multi-microelectrodes on screen-printed platforms and to develop this concept further would be to produce ultra multi microelectrodes.

Another exciting area for further development could be graphene. As graphene has become very popular as an electrode material recently, I believe graphene is a material for the future and can be incorporated in the area of screen-printed electrodes, in particular cosmetic electrochemistry. The study into graphene-modified (with polymeric spray – cosmetic electrochemistry) electrodes for the use as a graphene based electrochemical sensor or biosensor is a future prospective area which is anticipated to be explored.